NUMERICAL OPTIMIZATION OF A FINNED TUBE GAS TO LIQUID HEAT EXCHANGER

A Thesis Submitted to
the Graduate School of Engineering and Sciences of
İzmir Institute of Technology
in Partial Fulfillment of the Requirements for the Degree of

DOCTOR OF PHILOSOPHY

in Mechanical Engineering

by
Levent BİLİR

February 2009
İZMİR

We approve the thesis of **Levent BİLİR**

Prof. Dr. Zafer İLKEN
Supervisor

Asst. Prof. Dr. Aytunç EREK
Co-Supervisor

Prof. Dr. Barış ÖZERDEM
Committee Member

Assoc. Prof. Dr. Gamze TANOĞLU
Committee Member

Asst. Prof. Dr. Tahsin BAŞARAN
Committee Member

Asst. Prof. Dr. Moghtada MOBEDI
Committee Member

10 February 2009

Assoc. Prof. Dr. Metin TANOĞLU
Head of the Mechanical
Engineering Department

Prof. Dr. Hasan BÖKE
Dean of the Graduate School of
Engineering and Sciences

ACKNOWLEDGMENTS

The author would like to express his sincere gratitude to his supervisor Prof. Dr. Zafer İlken and to his co-supervisor Asst. Prof. Dr. Aytunç Erek, for their valuable advises and continual support through the thesis. The author would also like to thank to Asst. Prof. Dr. Moghtada Mobedi for his valuable recommendations.

The author also wishes to express his thanks to his family for their help and support during his studies.

ABSTRACT

NUMERICAL OPTIMIZATION OF A FINNED TUBE GAS TO LIQUID HEAT EXCHANGER

The optimization of the fin and protrusion dimensions and shapes of finned tube gas to liquid heat exchangers are performed numerically in this thesis. The dimensions of a commercially available heat exchanger of a combi boiler apparatus are taken as basic dimensions and various parameters about plate fin and three different protrusions, namely balcony, winglet and imprint, are examined step by step. The study is realized within the geometrical dimension range used in actual applications. The numerical analyses of several heat exchangers are performed using Fluent CFD software. The boundary conditions used in the numerical investigation are taken from the actual operating conditions of the combi boiler heater apparatus. Firstly, the best plate fin geometry is determined. Secondly, the best protrusion dimensions are obtained. Finally, the effects of three protrusion placement on plate fin surface are examined. The fin I5B2W3 is determined as the best among the investigated fins. The use of actual operating conditions as boundary conditions and the investigation of the individual and cumulative effects of three different protrusions are the novelties of the study. In order to validate the numerical models, a comparison with a computational and experimental study performed by Wu and Tao is also made. The results of the models created for comparison purpose show good agreement with the results given by Wu and Tao. It is also observed that results obtained from the two alternatives for the modeling, one with symmetrical and the other with periodic boundary condition, are very close. According to these results, it is concluded that the numerical outcomes obtained in the present study are reliable.

ÖZET

KANATLI BORULU GAZDAN SIVIYA ISI DEĞİŞTİRGECİNİN SAYISAL OPTİMİZASYONU

Bu tezde kanatlı borulu gazdan sıvıya ısı değiştirgecinin kanat ve kanat üzerindeki çıkıntılarının boyut ve şekillerinin optimizasyonu gerçekleştirilmiştir. Bir kombi cihazının ısı değiştirgeci ölçüleri temel alınarak düz kanat ve üzerinde yer alan farklı şekillerdeki üç değişik çıkıntı ile ilgili pek çok parametre incelenmiştir. İncelenmekte olan çıkıntılar balkon, kanatçık ve baskı tipi çıkıntı yüzeylerdir. Parametrik çalışmada kullanılan geometrik ölçüler gerçek uygulama değerleri içerisinde kalacak şekilde seçilmiştir. Çeşitli ısı değiştirgeci modelleri Fluent isimli bir HAD programı vasıtasıyla analiz edilmiştir. Analizlerde sınır koşulları olarak kombi cihazının gerçek çalışma koşulları kullanılmıştır. İlk olarak, en iyi düz kanat geometrisi belirlenmiş, daha sonra çıkıntı yüzeylerin en iyi geometrik ölçüleri ve kanat üzeri yerleşimleri tespit edilmiş, son olarak da düz kanat üzerinde her üç çıkıntı tipinin bir arada bulunduğu durumun etkileri incelenmiştir. Sonuç olarak, incelenen kanat modelleri içerisinde en iyi kanatın I5B2W3 ismi verilen kanat olduğu tespit edilmiştir. Sınır koşulu olarak gerçek çalışma koşullarının uygulanması ve üç değişik çıkıntının hem tek tek hem de birlikte kullanılmaları durumundaki etkilerinin incelenmesi bu çalışmanın getirdiği yeniliklerdir. Çalışmada kullanılan sayısal modellerin sınanması amacıyla, Wu ve Tao tarafından gerçekleştirilmiş bir sayısal ve deneysel çalışmanın sonuçlarıyla karşılaştırma gerçekleştirilmiştir. Karşılaştırma amacıyla oluşturulan modellerden elde edilen sonuçlar Wu ve Tao tarafından verilmiş olan sonuçlarla iyi bir uyum göstermektedir. Isı değiştirgecinin modellenmesinde kullanılabilecek iki alternatif de değerlendirilmiştir. Simetri sınır koşulu kullanılan alternatif model ile periyodik sınır koşulu kullanılan diğer alternatif modellerden elde edilen sonuçlar birbirleriyle çok büyük bir yakınlık göstermektedir. Bu sonuçlar göz önüne alınarak elde edilen sayısal sonuçların güvenilir olduğu görülmektedir.

TABLE OF CONTENTS

LIST OF FIGURES

LIST OF TABLES

LIST OF SYMBOLS

a	Greater radius of fin tube ellipse	mm
A	Cross sectional area	m^2
b	Smaller radius of fin tube ellipse	mm
c_p	Specific heat	j/kg.K
d	Wave height	mm
D_h	Hydraulic diameter	mm
f	Friction factor	
F	External force vector	N
Gr	Grashof number	
h	Balcony type protrusion height	mm
h	Convective heat transfer coefficient	W/m^2K
i	Unit vector in x direction	
j	Unit vector in y direction	
k	Unit vector in z direction	
k	Thermal conductivity	W/mK
L	Fin height	mm
L_l	Fin tube location on fin	mm
L_b	Balcony type protrusion length	mm
L_w	Winglet type protrusion length	mm
L_i	Imprint type protrusion length	mm
$\dot{m}$	Mass flow rate	kg/s
Nu	Nusselt number	
P	Pressure	Pa
P	Perimeter	m
Pr	Prandtl number	
Q	Heat transfer rate	W
r	Imprint type protrusion radius	mm
R	Residual	
Re	Reynolds number	
t	Fin tube thickness	mm
t	Time	s

T	Temperature	K
U	Perimeter of tubecover outer surface	mm
V	Velocity	m/s
V	Velocity vector	m/s
w	Winglet type protrusion width	mm
x	x coordinate	
y	y coordinate	
z	x coordinate	

Subscripts

air	for air
copper	for copper
flue gas	for flue gas
water	for water
x	in x direction
y	in y direction
z	in z direction

Greek

α	Under-relaxation factor	
θ	Angle of attack for winglet type protrusion	^{0}
β	Thermal expansion coefficient	1/K
Δ	Difference	
μ	Dynamic viscosity	kg/ms
ρ	Density	kg/m^3
τ	Stress tensor	Pa
Φ	General variable	
∇	The vector differential operator	

CHAPTER 1

INTRODUCTION

1.1. Heat Exchangers

Heat exchangers are devices that enable thermal energy flow between two or more fluids at different temperatures. They are used in several applications such as power production, electronics, waste heat recovery, manufacturing industry, air conditioning and refrigeration applications (Kakaç and Liu 2002).

In general, no external heat and work interactions are present between the heat exchanger and the environment. The fluids are in direct contact in a few applications. Mostly, the fluids are separated with a wall through which heat is transferred. In some cases the fluids contact with a wall in a transient manner. In many heat exchangers, the fluids are separated by a heat transfer surface, and ideally they do not mix or leak. Such exchangers are referred to as direct transfer type, or simply recuperators. Exchangers in which there is intermittent heat exchange between the hot and cold fluids are referred to as indirect transfer type or simply regenerators. Common examples of heat exchangers are shell-and-tube type heat exchangers, fin and tube heat exchangers, plate type heat exchangers and cooling towers (Shah and Sekulic 2003).

1.2. Classification of Heat Exchangers

There are several classification methods for heat exchangers, depending on the transfer process, number of fluids, surface compactness, geometry of construction, flow arrangements etc. The heat exchangers can be classified as indirect and direct contact type according to transfer process, as compact or noncompact according to surface compactness, as single-pass or multipass according to flow arrangement.

The classification according to geometry of construction is given in detail in Figure 1.1 and brief description of each type will be presented.

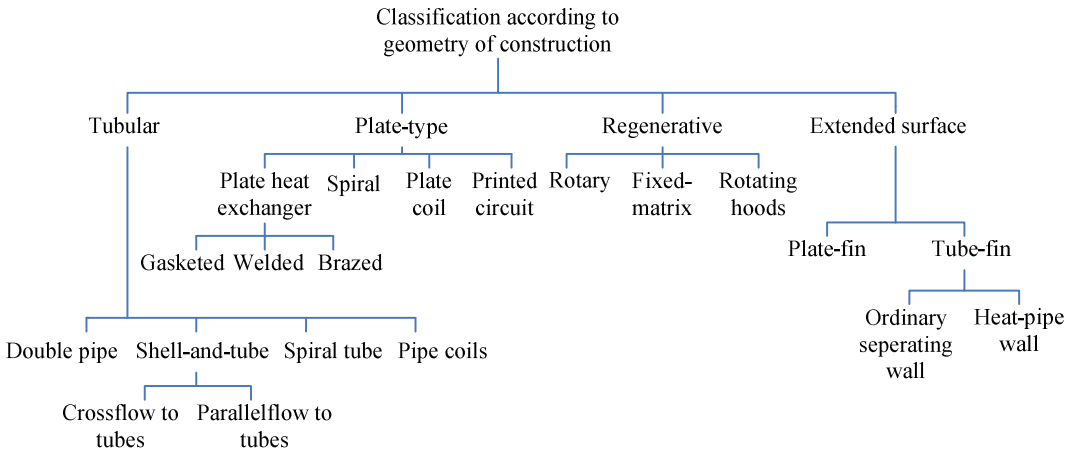

Figure 1.1. Classification of heat exchangers according to geometry of construction. (Source: Shah and Sekulic 2003)

1.2.1. Tubular Heat Exchangers

This type of heat exchangers generally consists of circular tubes. They can endure high pressures and they are convenient for the cases where high pressure difference between the two fluids exists. They are generally used for liquid to liquid heat transfer applications. The most frequently used heat exchanger in this type is shell and tube heat exchanger which is shown in Figure 1.2.

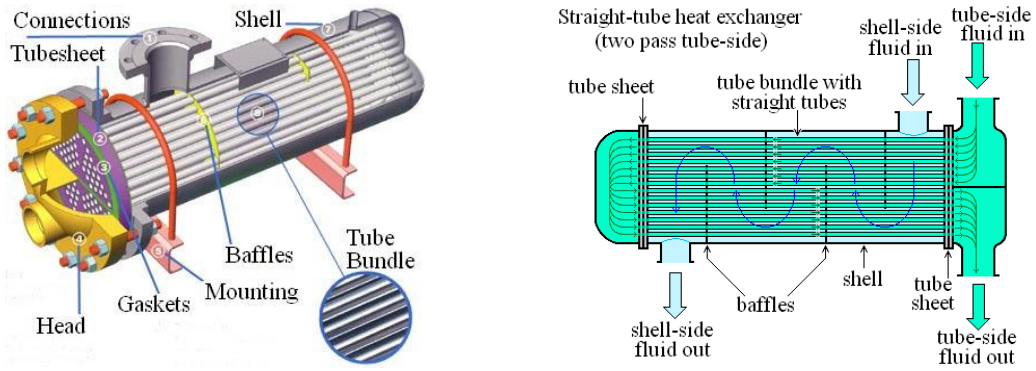

Figure 1.2. Shell-and-tube heat exchanger. (Sources: SEC Heat Exchangers 2008 and Wikimedia 2008a)

1.2.2. Plate-Type Heat Exchangers

Plate-type heat exchangers are formed with thin plates. The plates can be smooth or corrugated (Figure 1.3 (a)). This type heat exchangers are not appropriate for the cases where high pressure or high temperature differences are present between two fluids. A plate heat exchanger is shown in Figure 1.3 (b). Hot and cold fluids flows separately through the gaps between plates as seen in Figure 1.3 (b) and since the heat transfer area is very great, they can provide very high heat transfer capacities at small dimensions.

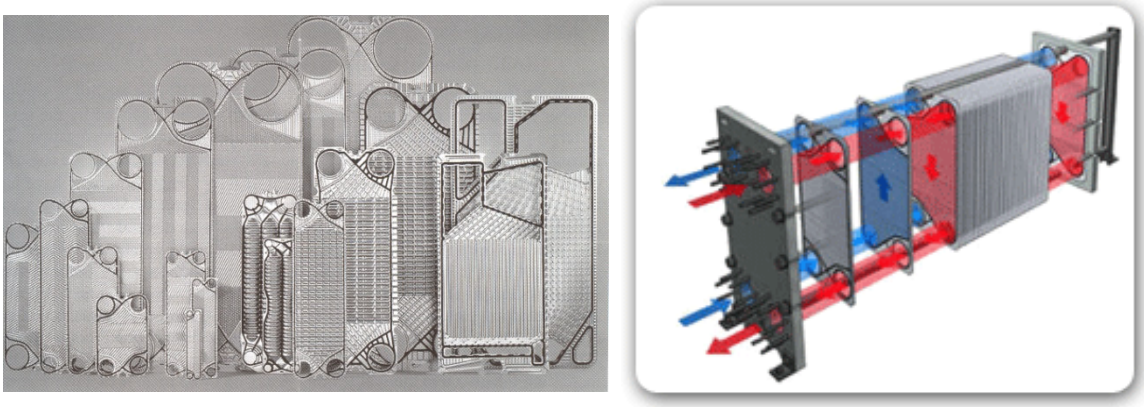

(a) (b)

Figure 1.3. Plate type heat exchanger (a) Typical range of plate forms (Source: Hesselgreaves 2001) (b) Schematical view of a plate type heat exchanger (Source: Alpha Heat Transfer & Allied Services 2008).

1.2.3. Regenerative Heat Exchangers

Regenerative heat exchangers are storage type heat exchangers. The heat transfer element rotates while it contacts with hot and cold fluids successively, as in rotary regenerator. However, in fixed matrix regenerators, hot and cold fluid streams are passed through the heat transfer element successively. The rotary type heat exchanger can be seen in Figure 1.4.

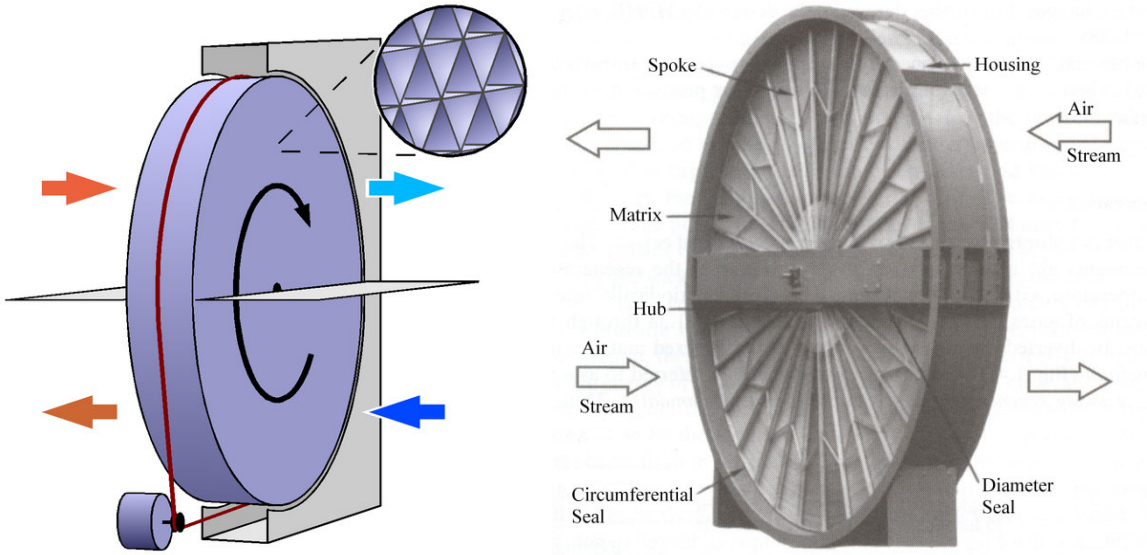

Figure 1.4. Rotary regenerator.
(Sources: Wikimedia 2008b and Shah and Sekulic 2003)

1.2.4. Extended Surface Heat Exchangers

Extended surface heat exchangers are one of the most used exchanger types for gas-to-fluid heat transfer applications. The unique characteristics of extended surface exchangers compared to conventional shell and tube type exchangers are (Shah and Sekulic 2003);

- Availability of numerous surfaces having different orders of magnitude of surface area density.
- Flexibility in distributing surface area on the hot and cold sides.
- Generally, substantial cost, weight or volume savings.

However, the extended surface exchangers have also some drawbacks as follows (Shah and Sekulic 2003);

- Fluids must be clean and relatively non-corrosive because of narrow flow passages and no easy techniques for cleaning.
- The fluid pumping power (and hence the pressure drop) is often an important parameter.
- Operating parameters and temperatures are somewhat limited compared to shell-and-tube exchangers, due to joining of the fins to plates or tubes by brazing, mechanical expansion and so on.

● With the use of highly compact surfaces, the resulting shape of the exchanger is one having a large frontal area and a short flow length; the header design of a compact heat exchanger is thus important for achieving uniform flow distribution among very large numbers of small flow passages.

The finned tube gas to liquid heat exchangers, which are investigated in this thesis, are also included in this category. The liquid flowing inside the tubes of the heat exchanger is heated or cooled by transferring heat from or to the gas flowing through the gaps between fins via the fin and tube surfaces. Since the gas side of the heat exchanger has considerably higher thermal resistance, the fins provide extra heat transfer surface at the gas side and enhance the heat transfer.

The fins are attached to the circular, elliptical or rectangular tubes by a tight mechanical fit, tension winding, adhesive bonding, welding or extrusion. This type heat exchangers are used extensively as condensers or evaporators in air-conditioning and refrigeration applications, as air-cooled exchangers in process and power industries. Another usage area of fin and tube heat exchangers is the domestic water heater appliances such as combi boiler apparatus. The fin shape can be plate as well as corrugated (wavy) or interrupted such as louvered. The schematic view of a plate fin and tube heat exchanger is given in Figure 1.5.

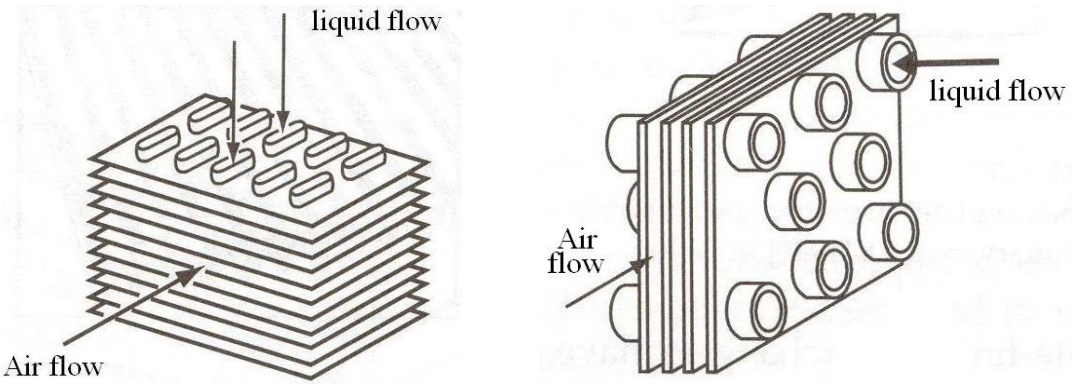

Figure 1.5. Schematic view of plate fin and tube heat exchanger.
(Source: Kays and London 1964)

The louvered and corrugated fins are also presented in Figure 1.6 and Figure 1.7, respectively. The louvers shown in Figure 1.6 disturb the flow and the thermal boundary layer. Similarly, the wavy fin illustrated in Figure 1.7 lengthens the gasflow path and

improve the gas mixing. Consequently, higher heat transfer rate can be obtained compared to plate fin.

Figure 1.6. Louvered fin.
(Source: Burr Oak Tool Incorporation 2008)

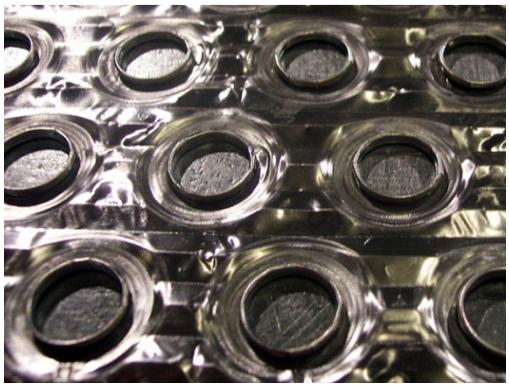

Figure 1.7. Wavy fin.
(Source: GB Coil Incorporation 2008)

In order to improve thermal performance of fins, some type of additional protrusions on fins such as winglets, wings, imprints etc. can be applied. These are embossed, stamped, punched or attached on the fin surface. These protrusions also disturb the boundary layers and create vortices which provide better flow mixing. However, during heat enhancement process, these additional surfaces can cause excessive pressure drop because of block effect created against gas flow. The vortices occurred around the protrusions and flow separation can also cause a large pressure loss. Consequently, appropriate placement of these protrusions on the fin surface should be taken into account in order to obtain satisfactory results. The schematic views of various protrusions are presented in Figure 1.8.

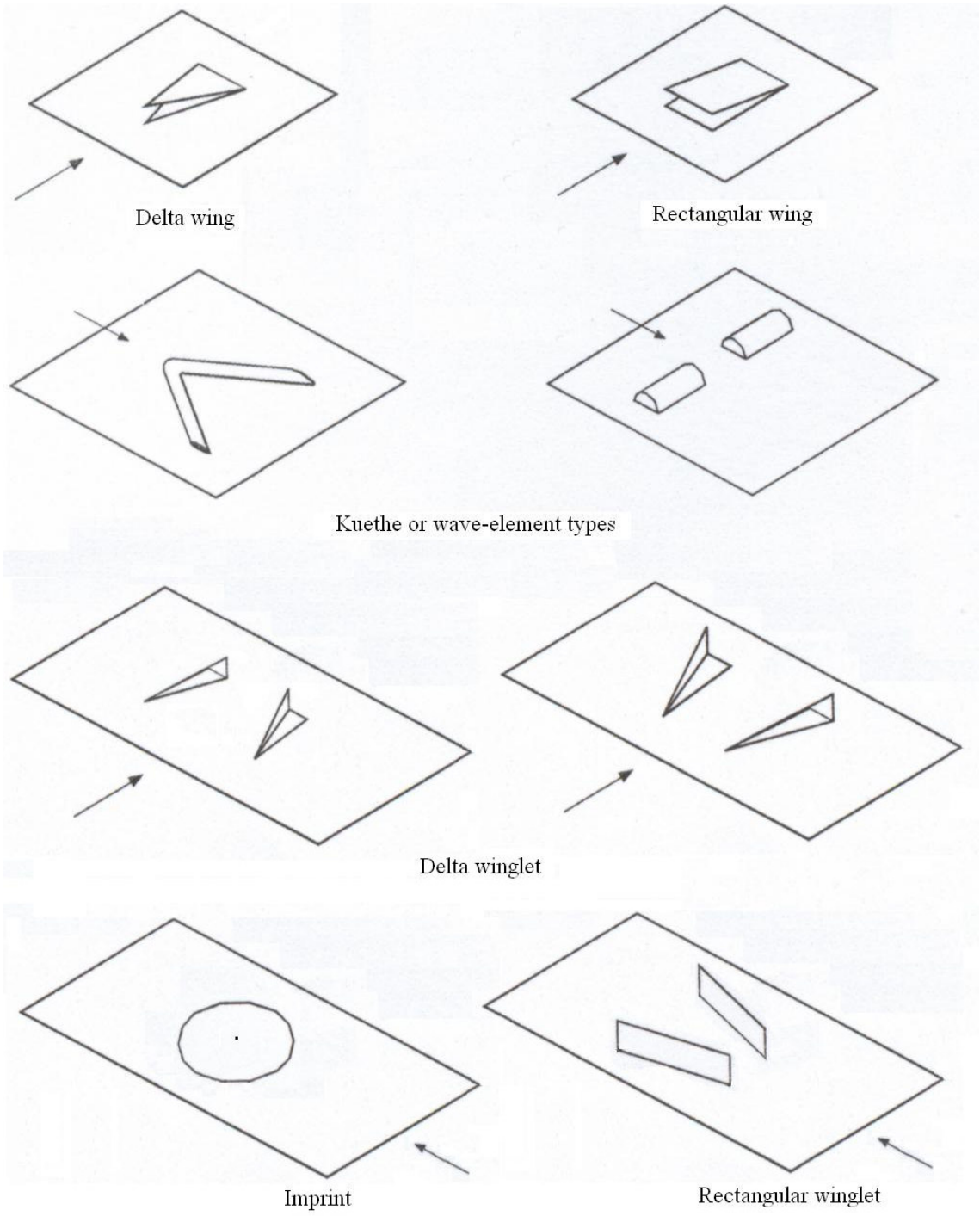

Figure 1.8. Schematic view of some protrusions.
(Source: Wang, et al. 2002a)

1.3. Unique Contribution and the Parts of the Study

Heat exchangers of fin-tube type have been applied to a wide variety of thermal engineering fields for many years and the most popular fin pattern in heat exchanger applications is plate fin configuration due to its simplicity and rigidity. However, since the convection coefficient on the gas side of these heat exchangers is significantly low compared to the liquid side, extensive studies investigating the influence of fin (corrugated and interrupted fins) and tube (circular, elliptical, etc.) shapes, and protrusions on heat exchanger characteristics were performed by many researchers. However, it is noticed that the performed studies did not take into consideration the actual operating conditions. In this thesis, a finned tube gas to liquid heat exchanger which is used in a combi boiler apparatus is investigated and the actual operating conditions are taken into account and used as boundary conditions in the numerical analyses. Furthermore, it is also realized that the effects of only one type protrusion were investigated in the studies made up until now. However in the present study, three types of protrusions are evaluated and the individual as well as the cumulative influences of these protrusions on heat transfer and pressure drop values of a fin and tube heat exchanger are examined as a novelty.

Various studies about the finned tube heat exchangers are summarized in chapter 2 of this thesis.

In chapter 3, the considered problem is explained in detail and the investigated parameters about the plate fin and protrusions are summarized.

In chapter 4, some information about the computational fluid dynamics (CFD) basics and the CFD program (Fluent) used in the present study for the analysis of different fin and tube configurations is given.

The governing equations for the investigated heat transfer and fluid flow problem are derived in chapter 5 according to the assumptions which are valid for the considered cases.

In chapter 6, the numerical modeling of the finned tube heat exchangers is explained and the boundary conditions used in the models are given.

In chapter 7, the generated meshes for the numerical models are presented and computational details are given.

The numerical results of heat transfer and total pressure drop values obtained from the numerical solutions of Fluent program are presented in chapter 8.

Finally, the results are concluded in chapter 9.

CHAPTER 2

LITERATURE SURVEY

In this thesis, a fin and tube gas to liquid heat exchanger is under investigation. Several geometrical parameters of fin and tube are examined as well as three different protrusions on fin, namely winglet, balcony and imprint type protrusions, are evaluated in order to determine their influence on the heat transfer and pressure drop characteristics of the heat exchanger. Various similar studies about plate fin and tube geometry, different fin shapes and protrusion effects are available in the literature and they will be summarized in this chapter. Firstly, the investigations about the effects of plate fin and tube geometries are presented as follows;

Rocha et al. (1997) made a two dimensional heat transfer analysis in order to reveal if the elliptical tubes are more feasible than the circular tubes for plate fin heat exchangers. They analyzed heat exchangers with one and two row tubes. They used the heat transfer coefficients obtained from a heat and mass transfer analogy presented in an earlier work. They examined two different eccentricity values, namely 0.5 and 0.65, for the tubes besides the circular tube. Two different fin and tube materials, iron and aluminum, were also taken into consideration. It was found that the heat exchanger made from aluminum is more efficient than the one made from iron as aluminum has better thermal properties. The heat transfer performance with the use of two tube rows was superior than the use of on tube row. Lastly, they concluded that as the tube eccentricity value is increased the efficiency of the heat exchanger is improved.

Kundu and Das (1997) determined the dimensions of a plate fin which provides the maximum heat transfer for a constant volume and different circular tube arrangements. They examined rectangular and equilateral triangular arrays for the circular tubes. They assumed constant convective heat transfer coefficient and fluid temperature in their analysis. They obtained heat transfer curves for different constant volume values and Biot numbers for both rectangular and triangular tube arrays. They also presented two design curves, one for rectangular and the other for equilateral triangular tube array, which give the optimum fin thickness for different constant volume and Biot number values. Their calculations revealed that equilateral triangular tube arrangement results in better heat transfer performance.

Mendez et al. (2000) investigated the fin spacing effect on heat transfer and pressure drop values of a plate fin and circular tube heat exchanger numerically. They also performed flow visualization experiments in a water tunnel in order to investigate the horseshoe vortex system formed by the tube and to visualize the tube wake zone. For small fin spacing values no horseshoe vortex was formed while for larger fin spacings one or two vortices were observed. From the visualization of the tube wake zone, it is observed that for small fin spacing values the contact of fluid and the tube is not interrupted while for large values of fin spacing the flow recirculates in the wake zone. They found no local Nusselt number increase before the tube for small fin spacing. However, when the fin spacing was increased a high local Nusselt number was observed in front of the tube because of the horseshoe vortex. They reported that as the fin spacing is increased larger Nusselt number values are obtained while there is a reduction in pressure drop values.

Wang and Chi (2000) carried out an experimental study investigating the tube row number, fin pitch and tube diameter influence on a plate fin and tube exchanger performance. They tested 18 different configurations in a wind tunnel. For a heat exchanger with four tube rows they found that the fin pitch does not have an effect on heat transfer. Nevertheless better heat transfer performance was observed when smaller fin pitch value is used in one and two rows tube configurations for a Reynolds number lower than 5000. For greater Reynolds number values this effect was not apparent. They observed smaller Colburn j factor values when the number of tube rows is increased. This effect was also clear for Reynolds number lower than 3000 and became ambiguous for higher Reynolds number values. The friction factor was found approximately the same for all heat exchangers with different number of tube rows. They also found that the tube diameter value does not have a significant influence on heat transfer while greater tubes causes a considerable pressure drop increase compared to smaller tubes.

Wang et al. (2000) developed correlations of Colburn j factor and friction factor using 74 plate fin samples obtained from previous investigations of the authors and other related previous studies. They used multiple regression technique in order to derive correlations. The presented correlations includes the effects of Reynolds number, transverse and longitudinal tube pitches as well as fin pitch, tube and hydraulic diameters. The application range of their correlation was 1 – 6 tube row numbers, tube outside diameter of 6.35 – 12.7 mm, fin pitch of 1.19 – 8.7 mm, transverse tube pitch of 17.7 – 31.75 mm and longitudinal fin pitch of 12.4 – 27.5 mm. They reported that the

proposed Colburn j factor correlation represents 88.6 % of the investigated data within ± 15 % while the presented friction factor correlation represents 85.1 % of the data within ± 15 %.

Matos et al. (2001) realized a two dimensional numerical heat transfer analysis using finite element method for plate fin heat exchangers with staggered circular and elliptic tubes. The ellipticity values for the tubes were 0.65 and 0.8. They performed an optimization study in order to determine the geometry which provides maximum heat transfer for a constant volume. Their results indicated that as ellipticity value of the tube is decreased a heat transfer performance improvement is observed. A 13 % higher heat transfer rate compared to the case with circular tubes eventuated when an elliptic tube with ellipticity value of 0.65 is used. They also presented the graphs of heat transfer values according to the distance between tube rows for different Reynolds numbers and tube ellipticity values. The optimum tube spacing values between tube rows were determined from the presented graphs.

Saboya and Saboya (2001) used naphthalene sublimation technique to calculate the average mass transfer coefficient for a plate fin and elliptic tube heat exchanger. The average convective heat transfer coefficient was determined by using heat and mass transfer analogy. They performed experiments in a wind tunnel in which naphthalene plates simulating isothermal fins were placed. One and two rows of tubes were used in the analysis and the ellipticity values of the tubes were taken as 0.5 and 0.65. They reported that the use of elliptical tubes does not have a negative effect on average convective heat transfer coefficient. Since the pressure drop created by the elliptical tubes is lower than circular tubes, it was concluded that elliptical tubes provide better overall performance. They also determined that the average transfer coefficients take smaller values for larger tube distances. The increase in Reynolds number was found to have a positive effect on average transfer coefficients. Finally, they developed 7 different average Sherwood number correlations for the investigated cases.

Kim and Song (2002) made naphthalene sublimation experiments in order to examine the effects of the gap between two fins, Reynolds number and tube location on heat transfer of a plate fin and circular tube heat exchanger. They also made flow visualization experiments to investigate the flow at different Reynolds numbers. The wake zone of the tube was observed to grow when the Reynolds number is increased. The naphthalene sublimation experiments realized in a wind tunnel reveal that when the tube is placed in a downstream position, better Sherwood number and consequently

better heat transfer is accomplished. They stated that since the local mass and heat transfer coefficient around the horseshoe vortex which arises in front of the tube is not location dependent, heat transfer enhancement can be obtained when the tube is placed at downstream where the heat transfer coefficient is low. They also observed that the heat transfer improves with an increasing Reynolds number. The mass and heat transfer for a fixed air volumetric flow rate was determined to increase when the gap between the fins is decreased.

Ay et al. (2002) used an infrared thermovision in order to visualize the temperature distribution on the plate fin of a plate fin and three row tube heat exchanger. They also determined the local heat transfer coefficients using the obtained temperature distribution and a control volume formulation. They examined heat exchangers with in-line and staggered tube arrangements for several air velocity values in a wind tunnel. The fin spacing was also varied between 10 mm and 20 mm. The experimental findings indicate that higher convection coefficient values are formed at the leading edge of the fin. Higher temperature gradients were observed in front of the first two tube rows and smaller temperature gradients were formed behind the tube which is the wake zone. Another outcome was that the wake region of the staggered tubes is smaller than that of in line tubes for small fin spacing. Similar local convection coefficient variation was observed on the fin up to an air velocity of 2 m/s. However for greater air velocity values the similarity was not maintained after the first tube row. They also reported that for an air velocity of 1 m/s the average heat transfer coefficient is found 14 – 32 % higher for staggered arrangement than in line arrangement for Reynolds number range of 543 – 2172.

Tutar and Akcakoca (2004) made a three dimensional numerical simulation of single and multi row heat exchangers. They investigated unsteady laminar flow, the horseshoe vortex occurrence and heat transfer for a Reynolds number range of 600 – 2000 for one row and 60 – 1500 for multi row heat exchangers. The influences of tube configuration (in line and staggered) was also examined. They assumed constant temperature values for aluminum fin and copper tube surfaces and defined an unsteady sinusoidal air inlet velocity. For one tube row case they found that higher convective heat transfer coefficient values are encountered in front of the tube as time goes by. The horseshoe vortex development was determined to be the main reason of the increase at this region. The average convective heat transfer coefficient showed a decreasing trend as the tube row number is increased. The reason of this finding was explained with the

longer boundary developing zone for low tube row configuration and with the creation of more wake zones, which do not contribute to heat transfer effectively, by the tubes for multi row tube configuration. Another outcome of the study was that the pressure drop value increases as the tube row number is increased both in in line and staggered tube arrangements. The average heat transfer and pressured drop values also increased with the increase in Reynolds number, but the augmentation of both values was found to be higher for staggered tube arrangement.

Chen et al. (2005) determined the convective heat transfer coefficient of a plate fin and tube heat exchanger numerically for several air velocities and ambient – tube temperature difference values. They used the experimental temperature distribution on the fin for their numerical study. They also conducted experiment in a wind tunnel for different air velocities. They divided the fin surface into 6 regions and calculated the average convective heat transfer coefficient for these regions. They found that for greater ambient – tube temperature difference value more heat transfer takes place. 33 % increase in average convection coefficient and 61 % increase in heat transfer were observed for a 43^{o}C temperature difference compared to a 34^{o}C temperature difference. They correlated the average convection coefficient and fin efficiency in terms of air velocity for two temperature difference values. Increased heat transfer values were obtained for greater air velocity for both two temperature difference values. However fin efficiency showed a decrease with increasing air velocity and it was found to be lower for greater ambient – tube temperature difference value.

Erek et al. (2005) performed a numerical study and investigated the effect of the changes in fin geometry on heat transfer and pressure drop of a plate fin heat exchanger with one row tube configuration. The parameters investigated in the numerical study were the distance between two fins (2.6 and 2.7 mm), tube center location (12.5, 15.5 and18.5 mm away from the fin bottom), fin height (35 and 38 mm), tube thickness (0.6, 0.8 and 1.2 mm) and tube ellipticity (0.4064, 0.7345 and 1). They used a computational fluid dynamics software “Fluent” for their numerical analyses. They modeled a commercially available heat exchanger and took the actual operation conditions as boundary conditions. They found that for a fixed flue gas mass flow rate lower heat transfer as well as lower pressure drop across the heat exchanger takes place for a greater distance between fins. They observed a heat transfer enhancement as the fin tube is shifted to downsteam region. Greater heat transfer and pressure drop values were obtained when the fin height is increased. Thinner fin tubes were found to cause less

pressure drop and to provide greater heat transfer rate. Finally, they determined that elliptic tubes perform better than circular ones in terms of both heat transfer and pressure drop. Furthermore, as the ellipticity of the tube is increased, heat transfer enhancement is stronger and pressure drop decrease is higher because of the better aerodynamic shape.

The studies given above investigated only the geometry of plate fin and tube. The fin shape is also an important parameter which can influence the flow and hence the heat transfer and pressure drop values of a heat exchanger as explained in chapter 1. The studies investigating different fin shapes can be summarized as the following;

Wang et al. (1997) examined 18 different fin and tube heat exchangers with wavy fin pattern. They conducted experiments in a wind tunnel to study the effects of tube row number, fin pitch and flow arrangement on heat transfer and pressure drop characteristics for Reynolds numbers varied from 400 to 8000. Lower Colburn j factor and friction factor resulted from higher Reynolds numbers both for in line and staggered tube arrangements. The friction factor took almost the same values for two, three and four tube rows in staggered arrangement. One row tube arrangement had 10 – 20 % smaller friction factor value depending on Reynolds number. A small heat transfer enhancement was observed as the number of staggered tubes is decreased from 4 to 2. However this trend was valid for a Reynolds number up to 900. Afterwards larger Colburn j factors were determined as the tube row number is increased. The heat transfer performance was found to be almost independent from the fin pitch value for staggered fin tubes. They also derived Colburn j factor and friction factor correlations using the data obtained for staggered tube arrangement. For in line tube arrangement the tube row number had also minor effect on friction factor. Nevertheless unlike staggered arrangement the increase in tube row number resulted in lower heat transfer until Reynolds number reaches to a value of 2000. After this value the heat transfer performance became independent of tube row number. The change in fin pitch had also no effect on heat transfer for in line tube arrangement. They also reported that the thermal performance of wavy fin is 55 – 70 % higher than a plate fin with similar geometry. However the friction factor rises by 66 – 140 % with the use of wavy fin.

Abu Madi et al. (1998) tested plate and corrugated fins in a wind tunnel for a velocity range of 1 – 20 m/s. They investigated the influence of tube the influence of tube row number, fin thickness, the distance between fins, tubes and tube rows. The experimental study was conducted for 28 different heat exchangers with staggered tube

arrangement. One, two and four tube rows were investigated while fin spacing ranged from 1.587 mm to 4.233 mm. Three different row spacing values (16, 16.5 and 22 mm) and two different tube spacing values (19 and 25.4 mm) were taken in the study. The fin thickness was also varied from 0.12 mm to 0.2 mm. First of the findings of the study was that corrugated fins lead to higher heat transfer and pressure drop than plate fins. They observed that higher Colburn j factor values are obtained for thinner fins while friction factor is not affected from fin thickness. Both Colburn j factor and friction factors became higher for higher fin spacing values. The tube row number effect showed a dependency on fin and tube geometry and negligible effect on friction factor. They also derived correlations for Colburn j and friction factors including all the variables investigated in their study. Separate correlations are obtained for two different fin types.

Yan and Sheen (2000) compared plate, wavy and louvered fin performances in their experimental study. 12 fins from each type were tested in a wind tunnel for a Reynolds number range of 300 -2000. The effects of tube row number and fin pitch (1.4, 1.6 and 2 mm) were observed in the study. Increasing Reynolds number resulted in a decrease in both Colburn j and friction factors. Additionally j and friction factors were greater for louvered fin compared to plate fin. For the plate fin case higher heat transfer and friction penalty were observed when fin pitch is decreased. However for the louver fin case the effect of fin pitch could not be determined clearly. Greater pressure drop value was found when the tube row number is increased. They compared the performances of three fin types by area goodness factor and volume goodness factor. As a result wavy fin was found as the best in terms of area goodness factor. However louver fin heat exchanger showed the highest performance for a constant heat exchanger volume.

Lozza and Merlo (2001) carried out an experimental study on the heat transfer and pressure drop performances of 15 different heat exchangers with diverse fin types (plate, wavy, louvered and with winglet). The geometrical dimensions of fins and staggered tubes and fin pitch value were the same for all investigated cases. They conducted the tests in a wind tunnel with air velocity of 1 – 3 m/s. The comparison of wavy and corrugated fins indicated that the wavy fin provides better performance. Another finding was that louvered fins show higher heat transfer performance than wavy fins especially at low Reynolds numbers along with an excessive pressure drop. Additionally it was observed that when the louver height is increased from 0.75 mm to

0.9 mm no heat transfer enhancement is obtained, but more pressure drop is encountered. The extended louver fin was determined to have the highest heat transfer performance. They reported that the plate fin with winglet could not provide significant performance improvement and the louvered fin with winglet provides higher Colburn j factor but also higher friction factor compared to the similar louver fin.

Kim and Bullard (2002) analyzed multi louvered fin and tube heat exchangers with various louver angles (15^o – 29^o), fin pitches (1, 1.2 and 1.4 mm) and flow depths (16, 20 and 24 mm) experimentally. They conducted the tests for different Reynolds numbers (100 – 600) in a wind tunnel. A total of 45 different heat exchangers were investigated. The thermal analysis was made using effectiveness-NTU method. One of the outcomes of the study was that the increase in air velocity leads to an exponential increase in heat transfer coefficient while the flow depth affects the heat transfer coefficient negatively. Higher pressure drop values were observed for the cases with higher air velocity and larger flow depth. Another observation was that as the louver angle is increased higher pressured drop values are obtained. However, the louver angle effect on heat transfer was found to be dependent on the flow depth, fin spacing and Reynolds number. Fin pitch effect on heat transfer was found to be very small for the investigated cases, but increasing fin pitch affected pressure drop positively. It was also reported that the effect of fin pitch diminishes for larger louver angles.

Pirompugd et al. (2006) performed the tests of 18 wavy fin and tube heat exchangers in a wind tunnel for dehumidifying conditions and investigated the effects of air inlet relative humidity, fin spacing, wave height and tube row number on the heat and mass transfer characteristics. They detected that heat transfer increases as the fin spacing value gets smaller. This effect was observed to be more evident at small Reynolds numbers but becomes unapparent for Reynolds numbers above 3000. Additionally, both heat and mass transfer performance almost became unaffected from the fin spacing for tube row number greater than 2. The influence of wave height on heat transfer was found as insignificant for large fin spacings. However for a small fin spacing value better heat transfer performance was observed with greater wave height. Similarly for large fin spacing case air inlet relative humidity showed no effect on mass transfer performance, but they observed an increase in mass transfer coefficient with the decrease in relative humidity for small fin spacings. Another important result of the study was that when the tube row number is increased the effects of geometrical

variations and inlet relative humidity become less apparent. Finally, they derived correlations for Colburn j factors of both heat and mass transfer.

As mentioned in chapter 1, the protrusions placed on fin surface can provide significant heat transfer enhancement for a fin and tube heat exchanger. However, they also cause some pressure drop penalty which can reach at excessive levels in some cases. So, the investigation of protrusions effects also attracted many researches and the exploitation of the protrusions in heat exchangers has received a lot of attention. As a result extensive studies have been performed. Various different protrusion types such as wing, winglet, wave, imprint (dimple) etc. are examined and the summary of the studies about this subject are given as follows;

Gentry and Jacobi (1997) determined heat and mass transfer enhancement for a plate fin with the use of delta wing located at the leading edge. Flow visualization experiments were carried out in a wind tunnel and the effect of delta wing on the flow is observed. Different delta wing aspect ratio (0.5 – 2), angle of attack (10^o – 55^o) and Reynolds number values (600 – 1000) are used in the study and vortex location and strength are examined. In order to determine the effect on heat transfer, mass transfer experiments were performed using naphthalene sublimation technique. They reported a 50 – 60 % heat transfer increase compared to plate fin. They also showed that for a constant Reynolds number and aspect ratio, an optimum angle of attack is encountered. The reason of this finding is reported to stem from the vortex and boundary layer interaction.

Chen et al. (1998) made a numerical analysis in order to explore the influence of delta winglet pairs which are punched in in-line arrangement on a fin and oval tube heat exchanger. The numerical study was performed for a constant Reynolds number of 300. The fins and tube are assumed to be at different constant temperatures and air was chosen as the fluid. They mentioned that the use of only one winglet pair was found to be insufficient as at downstream region of the winglet the Nusselt number decreases. Thus they investigated fins with one, two and three winglet pairs in their study. They examined two different fins with two winglet pairs. In one of these fins the gap between the first and second winglet pairs was 1/3 of the distance from the first winglet to the exit while in the other fin the second winglet pair was placed at the middle of this distance. They reported that the vortices formed after the second winglets are stronger than the ones formed after the first winglets. A similar result was also obtained for the vortices behind the third and second winglets, the former being stronger than the latter.

They found that the second configuration among the fins with two winglet pairs shows a better heat transfer performance. Another outcome was that the heat transfer enhancement provided by the first and second winglet pairs are determined to be the same while the third winglet pair resulted only 66.7 % enhancement compared to these two winglet pairs. The pressure drop penalty of the second winglet pair was found to be the greatest, followed by the third and then the first winglet pairs.

Chen et al. (2000) investigated the effect of winglet pairs in staggered and in line arrangements on heat transfer and pressure drop of a fin-oval tube heat exchanger numerically. They used finite volume method in their three dimensional analysis. Five different winglet configurations, one in line and four staggered, are analyzed in the study. One of their findings is that the heat exchanger with staggered winglet pairs is better in terms of both heat transfer and pressure drop than the one with in line winglets. They also found that the winglet away from the tube enhances heat transfer more than the one near the tube in a staggered arrangement.

Ligrani et al. (2001) investigated a channel with a dimpled wall. Two cases were taken into consideration for the other wall of the channel; a plate surface and a surface with protrusions which have the same shape as dimples. They realized an experimental study in a wind tunnel for a Reynolds number range of 380 – 30000. 13 staggered rows, each of which contains 9 dimples in transverse direction, were present on a surface of the channel. The same arrangement was also valid for the protrusions on the other surface. However the dimples and protrusions were aligned for one case while for other cases they were misaligned by 0.953, 1.27 and 4.11 cm. They observed that the protrusions provide stronger secondary flow and flow mixing even at low Reynolds numbers. The flow mixing was found to be higher as the misalignment of the dimples and protrusions is increased. As a result of the flow mixing enhanced heat transfer characteristics were observed for the channels with protrusions. They also observed higher local Nusselt number values in front of each dimple. They determined that the friction factor of the channels with dimples and protrusions are 2 – 2.7 times higher than the one of the channel with only dimples on one surface.

Wang et al. (2002a) conducted flow visualization observations for fin-and-tube heat exchangers with plain fin and fins having two different wave type vortex generators. They used dye-injection technique for flow visualization in a water tunnel. They performed flow visualization experiments for 3 different Reynolds number values which are 500, 1500 and 3300. They observed that the mixing of fluid is enhanced when

vortex generator is present. About 25 – 55 % higher pressure drop values for the fins with vortex generators are reported in the study compared to the plain fin. In additon, they observed that the pressure drop ratio of the fins with different vortex generators and the plain fin is almost constant for different Reynold numbers.

Wang et al. (2002b) performed flow visualization experiments in a water tunnel in order to observe the effects of annular and delta winlet vortex generators. They used dye-injection technique for flow visualization. They also determine the pressure drop values in their experiments. Better flow mixing is encountered for the delta winlet while the delta winlet causes lower pressure drop than the annular winlet with the same height at the same Reynolds number. They observed 10-65 % higher pressure drop values than the plain fin for the investigated cases with winlets. However they reported that the ratio of the pressure drop value of the fins with winlet to the pressure drop value of the plain fin is not affected remarkably from the change in Reynolds number.

Mahmood and Ligrani (2002) examined the flow and local Nusselt number distribution of a dimpled channel. They investigated the effects of different channel height to dimple diameter ratios (0.20, 0.25, 0.5 and 1) and air inlet stagnation temperature to surface temperature ratios (0.78 – 0.94) for a Reynolds number range of 600 – 11000. The geometrical dimensions of the dimpled wall were the same as the one used in their previous study (Ligrani et al. 2001). The other wall of the channel was plain. An electrical heater was present on the dimpled wall to supply heat. They determined the temperature distribution on the dimpled wall using infrared imaging and they used smoke wires for flow visualization. They observed that stronger vortex pairs, formed by the dimples, are encountered for smaller channel height to dimple diameter ratios. Consequently, higher local Nusselt number values were seen as this ratio is decreased. They determined that higher local Nusselt number values are formed in close vicinity of dimple cavity downstream region. However, inside the dimple cavity very low local Nusselt number values were present. The transport of colder fluid near to the heated dimpled surface by the vortices also affected the heat transfer positively and this effect was found to be stronger as the air inlet stagnation temperature to surface temperature ratio is decreased.

Kim and Yang (2002) conducted an experimental investigation on the effect of winglet vortex generator angle of attack on the flow and heat transfer. The values used for angle of attack were between 20^{o} and 45^{o}. They examined both common flow up and common flow down configuration for delta winglets used as vortex generator. They

determined surface temperature distribution using thermo-chromatic liquid crystal and calculated convective heat transfer coefficient. The experiments were conducted in a wind tunnel. They determined that for the common flow down configuration maximum heat transfer value is obtained by the use of a winglet pair with a 45^o angle of attack. The maximum local heat transfer value for 45^o angle of attack case was observed as 7 % and 3 % higher than for the cases of 20^o and 30^o angles of attack, respectively. They observed two maximum local heat transfer values for the common flow down winglets while they encountered only one maximum local heat transfer value for common flow up configuration. The angle of attack which provides the maximum local heat transfer value was also found as 45^o for common flow up configuration. This value for 45^o angle of attack was determined as 10.5 % higher than both the cases of 20^o and 30^o angles of attack. Finally, they reported that common flow down configuration is better than common flow up configuration in terms of heat transfer performance.

Torii et al. (2002) realized an experimental study in order to reveal delta winglet type vortex generator's effect on heat transfer and pressure drop of a 3 row fin-and-circular tube heat exchanger. They used common flow up configuration for the delta winglets placed at the first row of the heat exchanger. A wind tunnel was used in order to perform experiments at a Reynolds number range of 350 to 2100. They analyzed both staggered and in line tube arrangements of 3 row tubes. They compare their results with a similar previous work which used common flow down winglets placed at each 3 row of tubes. They reported that this configuration shows a better performance for heat transfer than the plain fin but also causes a pressure drop increase. However, their findings revealed that the configuration they proposed leads to a heat transfer increase while causes a lower pressure drop values compared to the plain fin without winglet. They stated that the winglet they used in their study creates flow acceleration and has a positive effect on the tube wake zone. They also mentioned that the flow acceleration provides a delay of separation of air from the tube and a reduction of drag across the tube.

Kwak et al. (2003) made an experimental study investigating heat transfer and pressure drop values of fin and tube heat exchangers with different number of staggered tube rows. They placed a common flow up winglet pair at the first row in their experiments. They investigated the effects of two, three, four and five rows of tubes. They performed experiments in a wind tunnel. They found that heat transfer does not depend on the tube row number for plain fin; however pressure drop shows a slight

dependency. Another observation was that the heat transfer enhancement ratio does not change considerably when the tube row number is changed except for two rows for which the heat transfer is the highest. The pressure drop value is found to be largest for the fin with three row tubes.

Tiwari et al. (2003) investigated heat transfer and laminar flow characteristics of air in a channel with oval tube and delta winglets. They realized a three dimensional study by using finite volume method and solved Navier-Stokes equations and energy equation to obtain heat transfer results and fluid flow field. They used common flow up and common flow down configurations for the winglets. They investigated the effects of the axial location of winglets, the winglet angle of attack, the number of winglet pairs and the Reynolds number. They assumed that the fins and the tube are at a constant temperature and the delta winglets are non-conductor of heat. They used different axial positions for one winglet pair with common flow down configuration and a constant 40^{o}. They reported that this type of winglet provides better heat transfer when placed near the leading edge of the oval tube. Three different angles of attack (30^{o}, 35^{o}, 40^{o}) are investigated for a fin with two winglet pairs (one common flow down and one common flow up). They observed that greater Nusselt number values are achieved for larger angle of attack since winglets with larger angle of attack create stronger vortices. They observed the effect of winglet pair numbers by investigating fins with one, two and three winglet pairs. As a result they found that adding an additional winglet pair increases heat transfer significantly. They also observed the effect of three different Reynolds numbers (500, 1000 and 1500) for a fin with one winglet pair. The results showed that an increase in Nusselt number is obtained as the Reynolds number is increased.

Chen and Shu (2004) determined the effects of delta-wing vortex generator on the uniform and fan flows as well as on the heat transfer. They performed experiments for various Reynolds numbers in a wind tunnel in which a heated plate with a delta wing is placed. They found that the presence of delta wing creates vertical flow and the heat transfer values for both uniform and fan flow with the use of delta wing are higher than the ones of plain fin. Another outcome is that as Reynolds number is increased higher Nusselt numbers are encountered. The Nusselt numbers for fan flow are determined higher than the ones for uniform flow. However, the effect of delta wing on heat transfer performance is found to be larger for uniform flow since the fan flow is already vertical without delta wing.

Leu et al. (2004) analyzed heat transfer and flow of a 3 row fin and tube heat exchanger with rectangular winglet vortex generators. Their study includes numerical and experimental investigation of three different winglet angles (30^o, 45^o and 60^o) for different Reynolds numbers. They conducted experiments in a water tunnel in order to obtain flow pattern by using dye injection technique. They also determined temperature distribution on the fin placed in a wind tunnel using an infrared thermovision. The best winglet angle is reported as 45^o among the investigated cases and it is found that this configuration provides up to 25 % fin area reduction. Another conclusion was that the overall heat transfer coefficients found from numerical solutions are always lower than the ones obtained from the experimental studies.

Kwak et al. (2005) examined pressure loss and heat transfer values of plate fin and tube heat exchangers with common flow up winglet configuration and three tube rows. The winglets were mounted on the first tube row and on the first two tube rows for the heat exchangers under investigation. They evaluated heat transfer and pressure drop performances experimentally in a wind tunnel for a Reynolds number range of 350 – 2100. They also investigated the effect of in-line and staggered tube arrangements. They compared the investigated fins with a plate fin without winglet and a fin with single row common flow down type winglets proposed by other studies. They obtained a 10 – 30 % heat transfer augmentation for the fin with single winglet row evaluated experimentally in the study, while the fin with single row common flow down type winglet provided only 5 – 15 % heat transfer enhancement. They also reported that their fin shows a 34 – 55 % pressure drop decrease compared to plate fin. However, for the same Reynolds number range the fin proposed by other studies showed a 2 – 10 % pressure drop increase. They concluded that the common flow up configuration is better for winglets. They also found that for staggered tube configuration the fins with two row winglets provides 6 – 15 % more heat transfer and causes 61 – 117 % more pressure drop compared to the fin with one row winglet. These values are determined as 7 – 9 % heat transfer increase and 3 – 9 % pressure drop increase for in-line tube arrangement.

Sommers and Jacobi (2005) examined the effect of delta wing vortex generator on the performance of a heat exchanger operating under frosting and dry conditions. They investigated a fin spacing value of 8.5 mm which is on the range used for frosting applications. They performed experiments in a wind tunnel with various airflow rates. The angle of attack for winglets used in the study was set as 55^o. The results for dry

operating conditions showed a 17 – 67 % pressure drop increase for Reynolds numbers between 430 - 2270. For frosting conditions, they found a considerable reduction of 35 - 42 % for airside thermal resistance with the use of delta wings for the Reynolds number range of 500 – 1300. This reduction was also described with a 60 – 93 % increase in convective heat transfer coefficient. The convection coefficient was found as 18 – 26 W/m^2K for plain fin while for the fins with delta wings, the convection coefficient values are determined as 33 – 53 W/m^2K. Another finding of the study was that higher air side heat transfer coefficient is encountered as the frost layer thickens. They explained the reason of this outcome with the fact that the frost layer causes an increase in surface roughness and consequently the flow becomes turbulent. The decrease of the gap between fins which accelerates the air was also mentioned as the other factor.

Joardar and Jacobi (2005) undertook an experimental investigation in order to evaluate the thermal performance of louvered fins with delta wings. They conducted their tests under dry and wet conditions in a wind tunnel. Their tests included a parametric study for angle of attack and aspect ratio. An angle of attack of 45^o and an aspect ratio of 0.8 are found as the best values among the examined cases. Early vortex breakdown at higher angles of attack and stability problem at lower angles of attack were encountered. For higher aspect ratios, the vortices were not strong enough and for lower aspect ratios unstable vortices were observed. An average of 21 % heat transfer coefficient increase compared to the case without wings was observed for the investigated air velocities in dry conditions. They also found that the delta wings do not generate a significant pressure drop increase. A 28 % increase in Colburn j factor and a 6.6 % increase in friction factor were determined in average. The experiments for wet conditions are conducted for dehumidifying operation of the heat exchanger. Similar heat transfer increase (23.4 % for Colburn j factor) was obtained. Pressure drop values were higher than the ones for dry conditions since the liquid blocks the flow. The friction factor increase for wet conditions was found as 6.6 %.

Pesteei et al. (2005) accomplished an experimental study in order to determine the effects of delta winglet location on heat transfer and pressure drop values of a fin and tube heat exchanger. Their experimental set up consisted of 24 aluminum fins, with a 12 mm fin spacing, which are placed in a wind tunnel. They performed the experimental study with a constant Reynolds number of 2250. The delta winglet with constant geometrical dimensions and a 45^o angle of attack is placed at 5 different locations on the fin. The heat transfer and pressure drop values for the 5 different cases

and for the plate fin are determined while a constant heat flux is given by a heater element placed inside the heat exchanger tube. They determined local convective heat transfer coefficient at different locations on the fin and the average Nusselt number for all cases. They observed that the presence of delta winglet increases the heat transfer compared to plate fin for all cases. In addition, it was also found that the placement of delta winglet at downstream locations provides more heat transfer increase than the placement at upstream location. The use of delta winglet also caused more pressure drop than the plate fin. As a conclusion, they found that when the delta winglet is placed at a location of half tube diameter away from the tube both in vertical and horizontal axis, maximum heat is transferred to the flowing air. They reported a 46.64 % increase in average Nusselt number with a 18.07 % increase in pressure drop compared to the plate fin for this optimum case.

Hiravennavar et al. (2007) made a numerical simulation of an unsteady, three dimensional laminar flow through a channel with delta winglets. They took three cases into consideration; a channel without winglet, with only one winglet and with a winglet pair. They also investigated the effects of Reynolds number and winglet thickness for the case with winglet pair. Their results revealed that higher average Nusselt number is possible as Reynolds number is increased. The use of single winglet showed a positive effect on heat transfer compared to plane channel. Furthermore, it is determined that heat transfer value of the case with a winglet pair approximately doubles the one for the case with only one winglet. Another outcome was that the increase in winglet thickness leads to an enhancement in overall heat transfer.

Sohankar (2007) performed a simulation of an unsteady flow through a channel with a pair of vee-shaped vortex generator. He changed the angle of the vortex generators between 10^o and 30^o and the investigation was performed for a Reynolds number range of 200 – 2000. The channel walls and vortex generators were assumed to be at a constant temperature. They reported that the flow and heat transfer becomes unsteady for high Reynolds number values (Re>1000). They observed that the pressure at the front region of the vortex generators is higher than the back region which indicates that vortices are formed due to the presence of vortex generators. The maximum local Nusselt value was obtained upstream of the vortex generators. Higher Nusselt number values were also observed as Reynolds number is increased. However, the Colburn j factor was found to be lower for higher Reynolds numbers. When the angle of vortex generator was gradually increased from 10^o to 30^o, both Nusselt number

and Colburn j factor values showed an increasing trend. Nevertheless, the friction factor also increased with the increase in Reynolds number and vortex generator angle. The thermal performance parameter was always found greater than 1 for all Reynolds numbers used in the study except for the Reynolds number value of 200. The thermal performance parameter for Reynolds number of 200 was found as 0.93. The reason of this outcome was that at lower Reynolds numbers weaker vortices are formed and at high Reynolds numbers (Re>1000) the flow becomes unsteady and heat transfer enhancement is stronger due to this unsteady flow characteristic.

Allison and Dally (2007) presented the delta winglet vortex generator effects on a fin and tube radiator. They conducted flow visualization experiments using dye injection technique in a water tunnel in order to investigate the flow and vortex generation for flow up and flow down configurations of the winglet. Delta winglet pairs with a 30^{o} angle of attack were placed before the tubes in the experimental study. They concluded that both configurations provide vortices which increase the heat transfer. However, they also reported that the flow up configuration shows more promising flow characteristic as it directs and accelerates the flow towards the tube. As a result they decided to use flow up configuration for the heat transfer and pressure drop analysis part of their study. They conducted numerous experiments varying Reynolds number between 2500 and 7500. They supplied air at a constant inlet temperature of 40^{o}C to the heat exchanger tubes and water at a constant inlet temperature of 11.5^{o}C to the water tunnel. They compared their experimental results with the ones of a louvered fin having the same dimensions as the investigated fins. They observed that the heat transfer coefficient for the fin with winglet is approximately 70 % compared to that of louvered fin for the investigated Reynolds number range. However, they also found that the friction factor of the fin with winglet is about 53 % relative to that of louvered fin. Finally, they reported that the energy consumed by the fan is reduced by 46 % when the fins with delta winglets are used.

Kim and Shin (2007) analyzed turbulent flow (with a Reynolds number of 22500) through a channel with a plane and a staggered dimpled wall numerically. They tried to find optimum dimensions of the dimples using Kriging model. The considered parameters were dimple depth to dimple print diameter ratio, channel height to dimple print ratio and dimple print diameter to distance between dimples ratio. They assumed a constant heat flux at the dimpled wall in their calculations while the plane wall was assumed as adiabatic. The heat transfer and friction coefficient were affected mostly

from dimple depth to dimple print diameter and were insensitive to channel height to dimple print diameter ratio. They observed a heat transfer enhancement downstream edge of the dimple and a decrease in front of the dimple because of flow separation. They also presented a graph of optimum parameter values versus weighting factor which defines the emphasis on friction factor. The optimum values of dimple depth to dimple print diameter ratio and dimple print diameter to distance between dimples showed a decreasing trend as the weighting factor increases and the reduction of friction is more emphasized, however the channel height to dimple print diameter ratio increased at the same time.

An experimental inquiry was performed by Joardar and Jacobi (2008) in order to determine the heat transfer and pressure drop performance of a plate fin and tube heat exchanger with winglet type vortex generator. Common flow up configuration is selected for the delta winglets. The experiments were realized in a wind tunnel with a Reynolds number range of 280 to 960. Two types of heat exchanger are investigated. One type had winglets at only the first row of tubes while the other type had winglets at first, third and fifth row of tubes. Heat transfer coefficient is reported to show an 11.7 – 32.7 % increase and about 38 % increase for the former and the latter type, respectively. The coincident reduction for air side thermal resistance was found as 13 – 20 % for the first and 21.4 – 28.3 % for the second case. Nevertheless the pressure drop values showed an increasing trend with the use of winglet type vortex generator. A pressure drop increase of less than 12 % for the first type and 26 - 87.5 % for the second type heat exchanger was observed. The pressure drop for the heat exchanger with three row winglet increased with the decrease in Reynolds number. However, the extra fan power need to overcome the core pressure drop is reported to be less than 0.8 W. They also evaluated the performance of the heat exchangers using area goodness and volume goodness factors. They found that for the case of one row winglet, area goodness factor increases between 35.7 % and 50.8 % compared to plate fin. They also reported that the area goodness factor for the case of three row winglet is lower than that of the plate fin for low Reynolds numbers, but they observed a 43 % increase in area goodness factor for the maximum Reynolds number. They mentioned that according to volume goodness factor the fin with three row winglet showed a better performance at high Reynolds numbers, while the two types showed similar performances for low Reynolds number values.

Lienhart et al. (2008) investigated both numerically and experimentally whether the use of dimples can result in less skin friction drag for a turbulent channel flow or not. They examined three different channel types; a channel with one plane and one dimpled wall, a channel with two dimpled walls and a plane channel. They also considered two different dimple geometry, one of which with a dimple diameter of 15 mm and a depth of 0.75 mm (small dimple) while the other with a dimple diameter of 47 mm and a depth of 2 mm (big dimple). The tests of the plane channel and the channel with on small dimpled wall revealed that the friction coefficient for both cases is more or less the same. Nonetheless the channel with one big dimpled wall resulted in a noteworthy pressure drop increase. Finally they determined that a channel with two dimpled walls causes even more pressure drop. They found a 2 % and 3.8 % increase in friction coefficient for the channel with one big dimpled wall and the channel with two dimpled walls, respectively. They concluded that drag reduction is not possible for the investigated cases. However they also pointed out that the pressure drop increase because of dimple usage is not at an enormous level.

Wu and Tao (2008a) performed a numerical investigation of a laminar flow in a rectangular channel which has a punched rectangular winglet pair on one of its walls. They examined the effect of punched hole and winglet thickness on heat transfer. Different Reynolds numbers and winglet angles of attack (15^o, 30^o, 45^o, 60^o and 90^o) were used in their study. They found that the punched hole increases the local Nusselt number around the hole. As a result the average Nusselt number was found as 1.1 % higher than the case without punched hole. In addition, the average friction factor for the case with punched hole was reported to be 1.2 % lower than the case without hole. Another finding of the study was that when the thickness of the winglet is taken into account it affects the local Nusselt number in the near region of winglet. A 4.1 % lower average Nusselt number is encountered when the winglet thickness is taken into consideration. They also reported that the higher the Reynolds number, the larger the heat transfer and Nusselt number. Additionally, their results indicated that the highest heat can be extracted when the winglets have a 45^o angle of attack. The second best value was 60^o and the followings were 30^o, 90^o and 15^o. They also compared the cases with winglets and without winglets in terms of average synergy angle. The synergy angle for the case with a winglet pair which has a 45^o angle of attack was found as the minimum among the investigated angles of attack. The same order as the heat transfer (60^o, 30^o, 90^o, and 15^o) was also found to be valid for the other cases for the synergy

angle. The largest synergy angle was found for plate fin. They concluded that these results are consistent with the field synergy principle.

Wu and Tao (2008b) continued their numerical study and investigated the winglet pair effect on heat transfer and pressure drop for a laminar flow in a channel. They evaluated different locations on the fin for winglet pair as well as different winglet geometric sizes and winglet shapes using the field synergy principle. The results for rectangular winglet pairs indicated that as the winglet pair is located downstream region, an increase occurs in the channel average synergy angle and the heat transfer enhancement compared to plate fin decreases. The reason was explained with the larger occurrence of streamwise vortices and consequently improvement of the synergy between velocity and temperature fields when the winglet pair is placed at upstream region. Another outcome was that when the space between the rectangular winglets constituting a winglet pair increases, the heat transfer enhancement weakens due to the increase in the average synergy angle. They reported that as the height of the rectangular winglet is increased more heat transfer values are obtained with a decrease in synergy angle. However this situation also leads to a maximum 88.7 % pressure drop increase compared to plain channel. Additionally, longer winglets are found to have a positive effect on heat transfer, but also to cause higher pressure drop values. Two different delta winglets are also evaluated in the study. One with a height equal to the channel height and the other with a half channel height. They found that delta winglets are more effective than the rectangular ones. They also made an experimental study in order to compare their numerical results with the experimental ones.

Lawson and Thole (2008) simulated a louvered fin heat exchanger with delta winglets which is generally used in automotive industry. They used a 20:1 scale model of an actual heat exchanger. The influence of the variations in winglet and piercing geometries on only tube wall heat transfer and pressured drop were observed in their experimental work conducted in a wind tunnel. The winglet aspect ratio value was changed from 1.5 to 3. The values of the distance between tube wall and winglet were 4.185 mm, 6.138 mm and 8.091 mm. Two different winglet thickness values (0.066 mm and 2.2 mm) were also taken into consideration. They used 16 or 28 winglets on the louvered fins in their experiments for Reynolds numbers of 216, 577 and 955. They also investigated the case of winglets without piercing. Their study revealed that the lack of modeling the flat landing causes a serious error in determining the Nusselt number when they compare their experimental results with a previous numerical study. They

examined mirrored and non-mirrored winglet configurations as well. The Nusselt number increase compared to baseline geometry was found as 47 %, 30 % and 1 % for non-mirrored configuration and 33 %, 14 % and -5 % for mirrored configuration for Reynolds numbers of 955, 577 and 216, respectively. Mirrored configuration was also found to result in slightly more friction factor. They determined that the enhancement in Nusselt number increases as the winglet aspect ratio is decreased. However they also found that decreasing winglet aspect ratio leads to a friction factor increase. The Nusselt number enhancement showed a slight increasing trend as the winglets are nearer to the tubes while friction factor values are almost the same. Their experimental results indicated that the winglet thickness is not an affecting variable. The Nusselt number increase and friction factor values for the cases with 16 and 28 winglets were found almost the same. The last finding of the study was that piercings have a negative effect on heat transfer while they lower pressure drop values.

Elyyan et al. (2008) realized direct and large eddy simulations of fin with staggered dimples and protrusions, which are aligned to each other. Two different fin pitch values, one doubling the other, were investigated. They assumed a constant heat flux boundary condition for both fins. They reported that the pressure drop because of the presence of protrusion is small at low Reynolds numbers. Similarly, the pressure values before and after the dimple showed a minor change when Reynolds number is small. However, when the Reynolds number is increased higher pressure drop occurred due to the wake formation and flow separation on the protrusion and separation and reattachment inside the dimple. Their results for the case of greater fin pitch indicated that at a Reynolds number of 250, maximum local Nusselt number is observed at the middle of the protrusion since airflow velocity reaches its maximum at this point. Nevertheless for smaller fin pitch case maximum local Nusselt number was shifted to the sides of the protrusion middle point and higher Nusselt number values than the case with great fin pitch were encountered. For the dimple side, it was also observed that higher heat transfer is accomplished for smaller fin pitch case. They found that the fin with smaller fin pitch provides higher heat transfer enhancement up to a Reynolds number of 2000. However the difference between two cases vanished after this value and they both showed almost the same heat transfer performance.

Chu et al. (2008) accomplished a numerical study investigating the effects of the winglet location, angle of attack (15^o, 30^o, 45^o and 60^o) and tube row number (2, 3, 4 and 5) on the heat transfer and pressure drop performances of a fin and oval tube heat

exchanger. The comparison of a heat exchanger with three tube rows and delta winglets placed at downstream of the tubes and a similar heat exchanger with plate fins showed that there is a 13.6 – 32.9 % increase in average Nusselt number and a 29.2 – 40.6 % increase in friction factor in the investigated Reynolds number range (500 -2500) for the case with winglets. It is also seen that the winglets provide a reduction in tube wake zone and accelerate the fluid which contribute to the heat transfer enhancement. They also showed that the average intersection angle of the case with winglets is always smaller than the case without winglet. Thus the synergy effect of the case with winglets was determined as better. They also revealed that the downstream placement of winglets provides more heat transfer and bigger friction factor than the upstream placement. Furthermore the intersection angle of downstream placement is found to be smaller for all the investigated Reynolds numbers. They determined that maximum average Nusselt number is accomplished at an angle of attack of 30^{o}. However, the friction factor showed an increase with the increasing angle of attack. The maximum heat transfer value among the investigated heat exchangers with different tube row numbers was reached for the heat exchanger with two tube rows and the friction factor showed a decreasing trend with increasing tube row number. They concluded that as the tube row number gets smaller the field synergy gets better.

CHAPTER 3

THE CONSIDERED PROBLEM

3.1. The Considered Heat Exchanger

In this thesis, a finned tube gas to liquid heat exchanger used in a combi boiler apparatus is investigated numerically and it is aimed to determine the best fin, tube and protrusion geometries. The dimensions of the heat exchanger (such as fin height, tube dimensions etc.) are kept in the practical application range. The heat exchanger under analysis is shown in Figure 3.1.

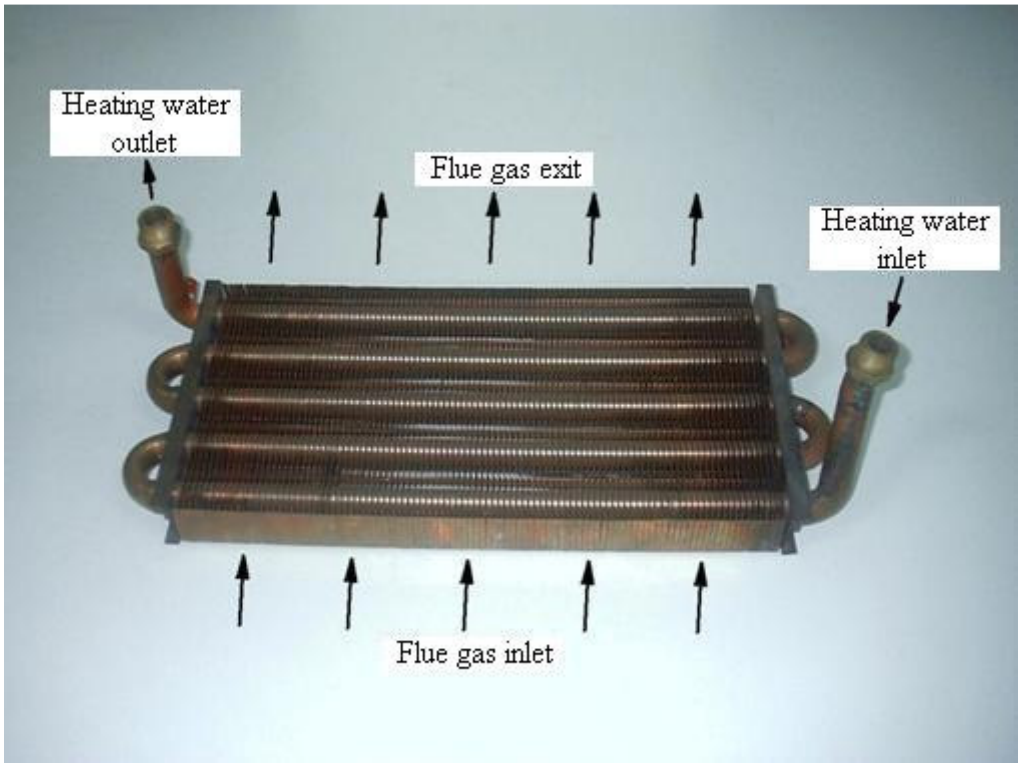

Figure 3.1. View of the heat exchanger under analysis.

As it can be seen from Figure 3.1, the cold heating water enters the tube of the heat exchanger, heated by the flue gas passing through the fins and leaves the heat exchanger from the exit of the tube. The reference fin used in the heat exchanger is illustrated in Figure 3.2.

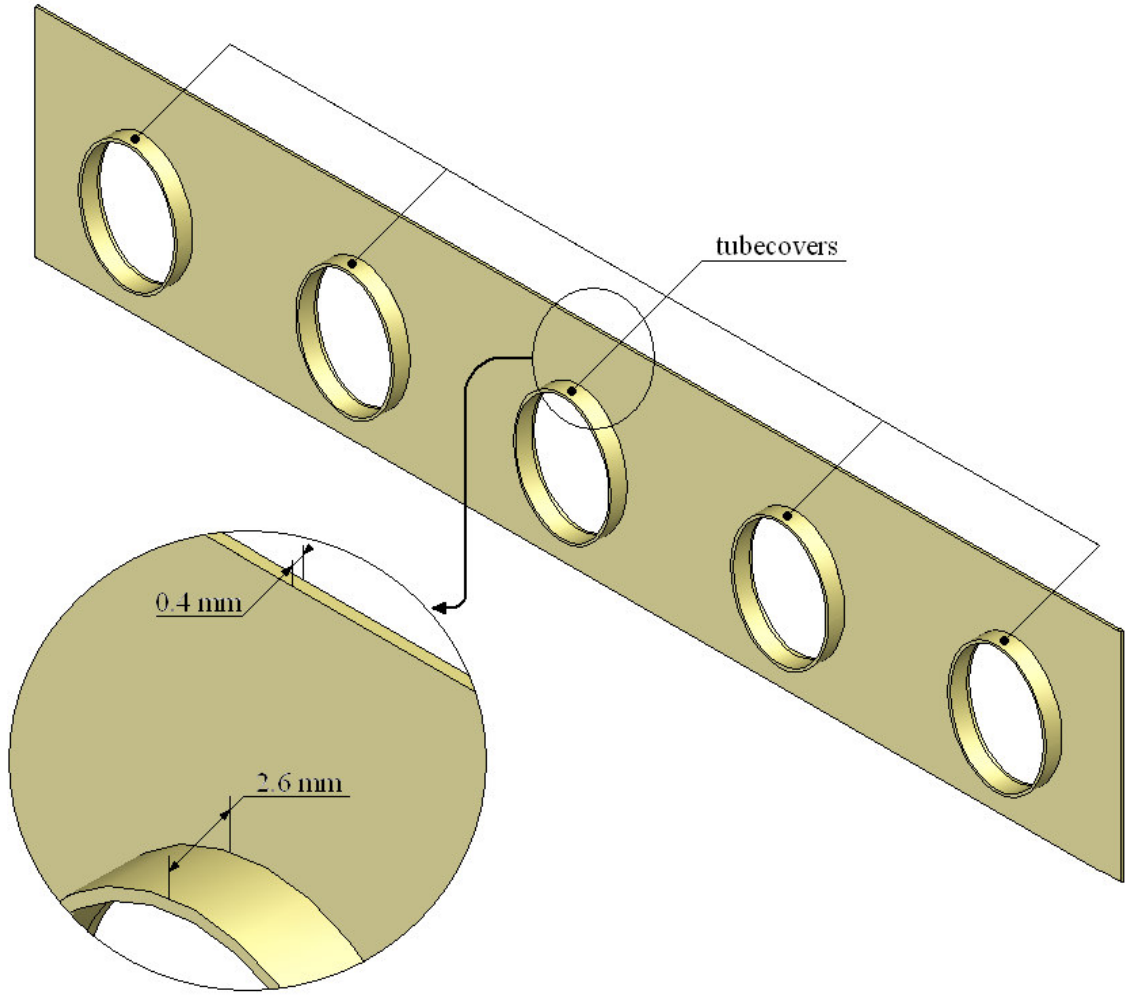

Figure 3.2. The reference fin used in the heat exchanger.

3.2. Specifications of the Investigated Heat Exchangers

The heat exchanger consists of 101 plate fins with a fin width of 175 mm and the gap between two fins is 2.6 mm. The thickness of the fins is 0.4 mm (so, the tubecover thickness is also 0.4 mm). These three values are kept constant in the numerical calculations as they are the ones used in practical application and several other parameters of the fins are changed in order to determine the optimum fin geometry of the finned tube gas to liquid heat exchanger. The dimensions of the reference fin, with which the study is started, are given in Figures 3.2 and 3.3.

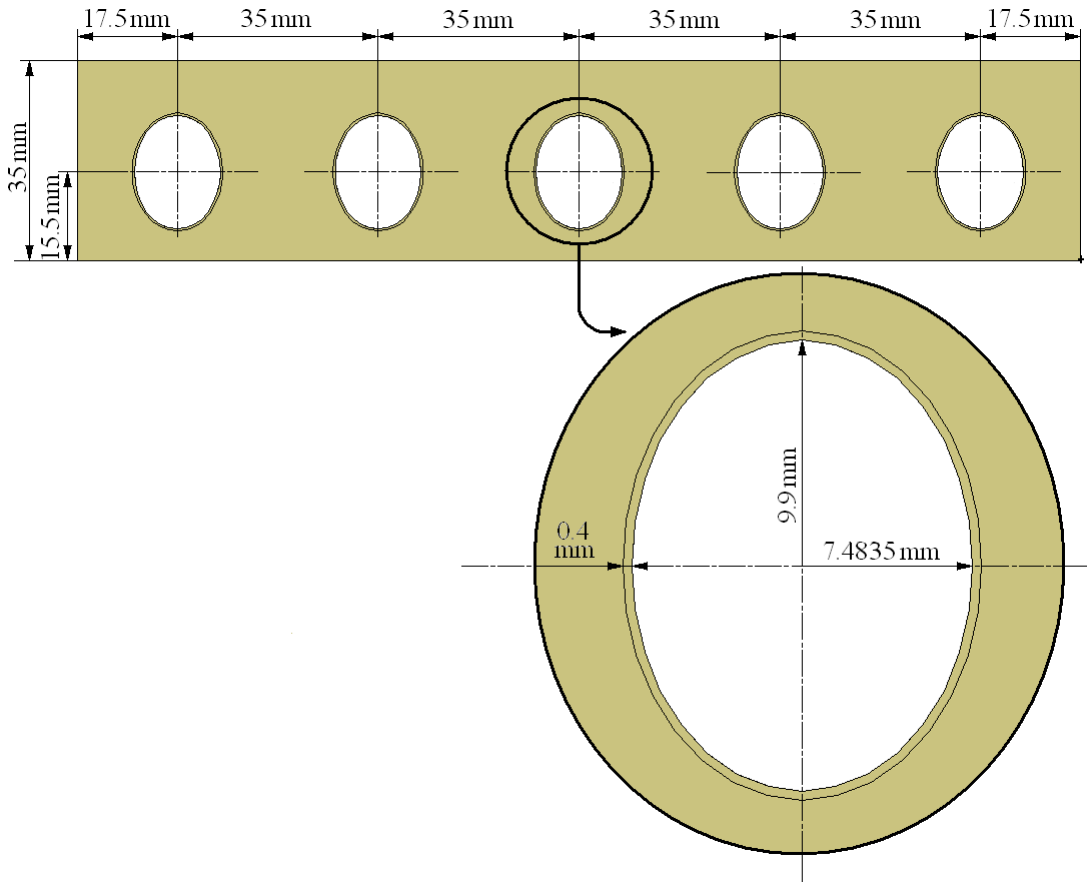

Figure 3.3. Dimensions of the reference fin used in the heat exchanger.

Because of the symmetrical conditions only one tenth segment of the actual fins are used in the numerical analyses. Thus, the schematic view of the investigated fins which are presented in Figures 3.4, 3.5 and 3.6 represent the one tenth segment of an actual fin. Firstly, the following parameters about the plate fin geometry, which are illustrated in Figure 3.4, are examined;

- Fin height (L) and fin tube thickness (t)

The fin height is varied between 35 and 40 mm, the fin tube thickness is changed between 0.6 and 1.2 mm.

- Fin tube location (L_1) and ellipticity (b/a)

Four different fin tube locations are examined. These are 12.5, 15.5, 18.5 and 21.5 mm. In addition, four different ellipticity values for the fin tube, which are 0.45, 0.55, 0.7345 and 1, are investigated.

- Fin shape (Wave height: d)

The wave height is changed between 1 and 5 mm.

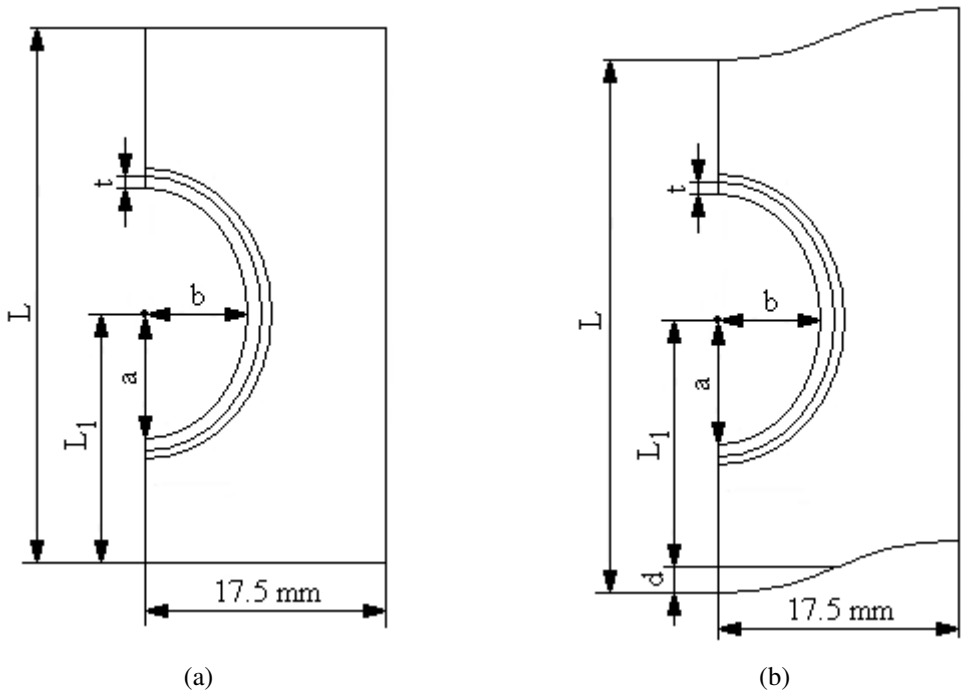

(a) (b)

Figure 3.4. Investigated parameters for (a) Rectangular plate fin (b) Wavy plate fin.

After the determination of the best plate fin geometrical dimensions, some protrusions, placed on the plate fin, are also investigated in order to reveal their effect on heat transfer between the flue gas and heating water and pressure drop of the flue gas across the heat exchanger. The protrusions analyzed in this study are balcony, winglet and imprint type protrusions. Balcony type and imprint type protrusions are placed at the middle point between two fin tube centers while the winglet type protrusion is placed at the one third and two third of the distance between two fin tube centers. The geometrical dimensions and positions of the protrusions on the plate fin are varied and the effects of these variations are observed. The parameters about the protrusions, which are illustrated in Figures 3.5, can be summarized as follows;

- Protrusion height (h), width (w) and radius (r)

The balcony height (h), winglet width (w) and imprint radius (r) are varied between 2 - 8 mm, 2 - 6 mm and 4 – 8 mm, respectively. For this part of the study the protrusion length is maintained as 2.425 mm. The angle of attack for winglets used in the present study is $\theta = 45^0$.

- Protrusion length between two fins (Lb, Lw, Li)

The balcony (Lb), winglet (Lw) and imprint length (Li) are changed in the range of 1 – 2.425 mm, 1.3 – 2.425 mm and 1.3 – 2.425 mm, respectively.

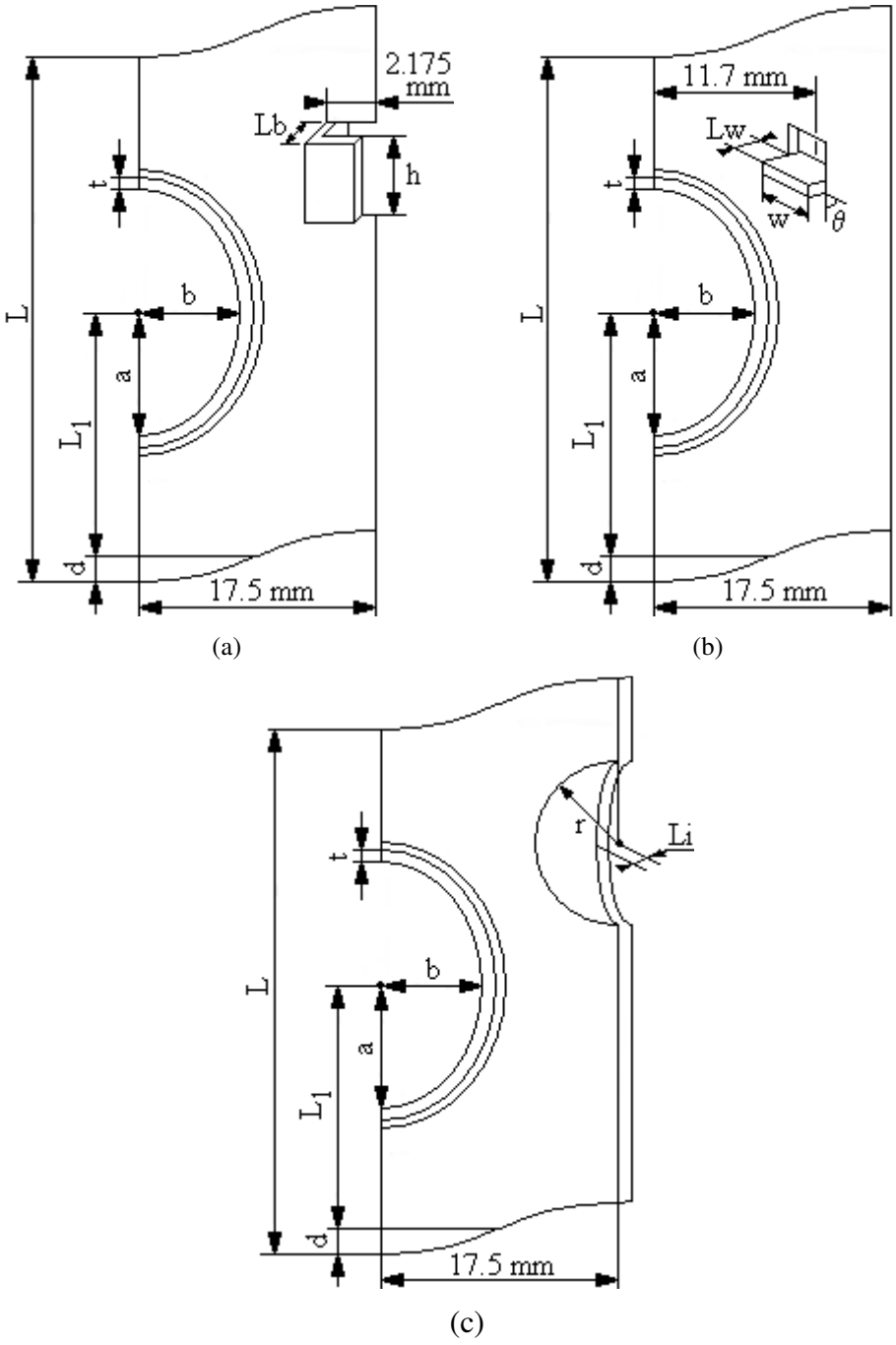

Figure 3.5. Investigated parameters for (a) Fin with balcony (b) Fin with winglet (c) Fin with imprint.

- Protrusion location on fin

For the protrusion height, width and radius study and protrusion length between two fins study, the protrusions are always located at location 5. However, in this part balcony and winglet type protrusions are placed at locations 1, 2, 3, 4, 5, 6 and 7, while imprint type protrusion is placed at locations 2, 3, 4, 5 and 6. These locations are illustrated in Figure 3.6.

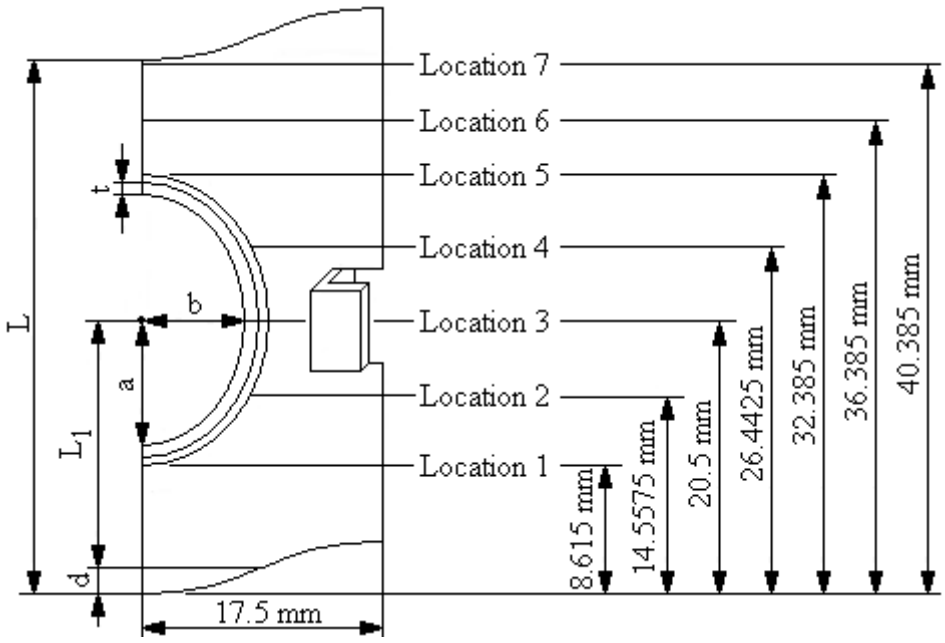

Figure 3.6. Investigated locations for protrusions.

Finally, the use of three different type protrusions together on the plate fin is also investigated in order to find whether in this situation better performance is obtained or not. Detailed analysis results are presented in chapter 8.

3.3. Material Properties

3.3.1. Thermophysical Properties of Copper

The fins and fin tube of the heat exchanger are made of copper because of the fine thermo physical characteristics of copper. Following constant thermo physical properties of copper which are present in Fluent software database are used in the numerical calculations;

$$\rho_{copper}=8978\ kg/m^3 \tag{3.1}$$

$$c_{p\,copper} = 381\ j/kg.K \tag{3.2}$$

$$k_{copper} = 387.6\ W/m.K \tag{3.3}$$

3.3.2. Thermophsical Properties of Flue Gas

Flue gas is the combustion products of the fuel burned in the burner of a domestic water heater appliance. It is a mixture of CO_2, CO, NO_x, air and unburned fuel (if there is any). The thermo physical properties of the flue gas used in the present study are also taken from an actual combi boiler apparatus application. Since the density value of the flue gas is not available, the density value of air is used instead. The inlet temperature of the flue gas is 1500 K and it was found that the exit temperature of flue gas at the outflow boundary is in the range of 400-500 K. So, the density value for flue gas is taken as 0.3482 kg/m^3, which is the air density at 1000 K. Since in this study, the comparison of the different heat exchangers operating under the same conditions is made, the density value is selected as constant. The other thermo physical properties of the flue gas as functions of flue gas temperature are as follows;

$$c_{p\,flue\,gas} = 977.7 + 0.2932 \times T - 3.97 \times 10^{-5} \times T^2 \tag{3.4}$$

$$k_{flue\,gas} = 0.005774 + 6.409 \times 10^{-5} \times T \tag{3.5}$$

$$\mu_{flue\,gas} = 5.054 \times 10^{-6} + 4.267 \times 10^{-8} \times T - 6.534 \times 10^{-12} \times T^2 \tag{3.6}$$

where, T is flue gas temperature in K.

3.4. Type of Flue Gas Flow

In order to determine whether the flue gas flow is laminar or turbulent the Reynolds number of the flow is calculated as follows;

$$Re = \frac{\rho V D_h}{\mu} \tag{3.7}$$

Since the fins form small channels for the flue gas flow, the hydraulic diameter of these channels should be calculated in order to determine the Reynols number.

$$D_h = \frac{4 \times A}{P} \tag{3.8}$$

A is the cross sectional area and P is the perimeter of the channel and they are calculated as 4.55×10^{-4} m^2 and 0.3552 m, respectively. As a result the hydraulic diameter for a channel is found as 5.1239×10^{-3} m.

The dynamic viscosity of flue gas is taken as 4.119×10^{-5} kg/m.s. This value is calculated from Equation 3.6 for 1000 K, which is the approximate average of the flue gas inlet and exit temperatures for the investigated heat exchangers. The velocity of flue gas is selected as 3.85 m/s, which is the highest velocity value encountered inside the channel formed by two fins. As a result the maximum Reynolds number that can be obtained for the investigated cases is calculated as follows;

$$Re = \frac{0.3482 \times 3.85 \times 5.1239 \times 10^{-3}}{4.119 \times 10^{-5}} = 166.76 \tag{3.9}$$

Since the Reynolds number of flue gas flow is found smaller than the critical Reynolds number for the channel flows, which is 2300, it is concluded that the flue gas flow can be accepted as laminar.

However, the effect of buoyancy on the heat transfer should also be investigated in order to determine if mixed convection flow occurs or not. The importance of buoyancy forces in a mixed convection flow can be measured by the ratio of the Grashof and Reynolds numbers as the following (Fluent 6.3 User's Guide 2006);

$$\frac{Gr}{Re^2} = \frac{g\beta\Delta T D_h}{V^2} \tag{3.10}$$

If the value obtained from Equation 3.10 approaches or exceeds unity, strong buoyancy contribution to the flow is expected. However, if this value is very small, buoyancy forces may be ignored. The gravitational acceleration, g, is 9.81 m/s^2, β is the thermal expansion coefficient and it can be accepted as $\frac{1}{1000}$ K^{-1} as the average flue gas temperature can be assumed as 1000 K and ΔT is the temperature difference between

flue gas and fin surface. The minimum average fin surface temperature among the investigated cases is determined to be approximately 450 K and the maximum flue gas temperature is 1500 K, so ΔT value can be taken as 1050 K. The flue gas velocity value is taken as 1 m/s, which is the lowest average flue gas velocity value that can be encountered inside the channel. So, for the considered problems, the following result is obtained;

$$\frac{Gr}{Re^2} = \frac{9.81 \times \frac{1}{1000} \times 1050 \times 5.1239 \times 10^{-3}}{1^2} = 5.2779 \times 10^{-2} \quad (3.11)$$

As the calculated value for the considered problems is very lower than 1, the buoyancy effect on the flow is found to be negligible and it is found that the mixed convection flow condition does not occur. Finally, it is concluded that the flow type for the present conditions is laminar flow.

3.5. Negligence of Radiative Heat Transfer

The heat from the flue gas to the heating water which flows inside the fin tubes is transferred from the fins and tube surfaces by convection and conduction. The flue gas is assumed to be radiatively non-participating fluid. The fins have hotter parts on their bottom region which firstly contact with the flue gas entering the channel between two fins. Since the flue gas becomes colder while it reaches to the upper region of the channel, the fins also have colder parts on their upper region. So, there is a temperature difference between the upper and bottom regions of the fins which are parallel to each other. In this case, radiative heat transfer can take place between two parallel fins. However, since the two fins are very close to each other (2.6 mm apart from each other), the view factor of the hotter parts of a fin and colder parts of the other fin will be very small. Hence, in this study the radiative heat transfer is neglected and the heat transfer is assumed to be only by convection and conduction.

CHAPTER 4

COMPUTATIONAL FLUID DYNAMICS BASICS

4.1. Introduction to Computational Fluid Dynamics (CFD)

Computational Fluid Dynamics (CFD) can be described as the use of computers to produce information about the ways in which fluids flow in given situations. CFD uses various science disciplines such as mathematics, computer science, engineering and physics to provide the means of modeling fluid flows. Such modeling is used in many fields of science and engineering but, if it is to be useful, the models should represent a realistic simulation of a fluid in motion. At present this depends on the problem being simulated, the software being used and the skill of the user (Shaw 1992).

CFD is concerned with numerical solution of differential equations governing transport of mass, momentum, and energy in moving fluids. For a long time, design of engineering equipment was dependent on generated empirical information. Correlations, tables and nomograms were the examples of the empirical information. However, the empirical information was applicable only for the conditions for which it is generated. The information applicable to bigger scales had to be generated via laboratory-scale models. So, scaling laws, which maintain geometric, kinematic and dynamics similarities between the model and the full-scale equipment, were used. Some flow visualization studies and simple analytical solutions also needed to ensure the reliability of the results. Because of these difficulties a design tool that is scale neutral is strongly needed. This scale neutral information can be obtained using the fundamental laws of mass, momentum, and energy. However, for most cases, the analytical solution of these fundamental equations cannot be obtained and only numerical solutions are possible. So, the use of this potential (the ability to solve the relevant differential equations) has been made possible only with the availability of computers (Date 2005). So, the development of modern CFD began with the advent of the digital computer in the early 1950s (Chung 2002).

A variety of reasons can be cited for the increased importance that simulation techniques have achieved in recent years (Löhner 2008);

- The need to forecast performance. The inability to forecast accurately the performance of a new product can have a devastating effect on companies. The only way to minimize the risk of unexpected performance is through insight information. Simulation techniques such as CFD can provide this information.
- Cost of experiments. Experiments, the only other alternative to simulations, are very costly.
- Impossibility of experiments. In some instances, experiments are impossible to conduct. Examples are atmospheric nuclear explosions or biomedical situations that would endanger the patient's life.
- Insight. Most large-scale simulations offer more insight than experiments. A mesh of 1×10^6 grid points is equivalent to an experiment with 1×10^6 probes or measuring devices. Moreover, many derived properties (e.g. vorticity, shear, residence time, etc.) can easily be obtained in a simulation, but may be unobtainable in experiments.
- Computer speed and memory. Computer speed and memory capacity continue to double every 18 months. At the same time, algorithm development continues to improve accuracy and performance. So, more realistic simulations can be performed.

4.2. Governing Equations in Fluid Flow and Heat Transfer

In order to determine the flow characteristics (the velocity, temperature and pressure field of the flow), the following governing equations should be solved (Bird, et al. 1960);

- Continuity equation which defines that the mass of the fluid is conserved (Scalar equation).

$$\frac{\partial \rho}{\partial t} + (\nabla . \rho \mathbf{V}) = 0 \tag{4.1}$$

- Momentum equations which state that the rate of change of momentum equals to the sum of the forces on a fluid particle (Newton's second law) (Vectoral equations).

$$\frac{\partial}{\partial t}(\rho \mathbf{V}) + [\nabla . \rho \mathbf{V}\mathbf{V}] = -\nabla P - [\nabla . \tau] + \rho \mathbf{g} + \mathbf{F} \tag{4.2}$$

- Energy equation which represents that the rate of change of energy is equal to the sum of the rate of heat addition to and the rate of work done on a fluid particle (First law of thermodynamics) (Scalar equation).

$$\frac{\partial}{\partial t}\left(\rho c_p T\right) + \left(\nabla . \rho c_p T \mathbf{V}\right) = \nabla . (k \nabla T) - (\tau : \nabla \mathbf{V}) + \left(\frac{\partial \ln V}{\partial \ln T}\right)_p \frac{DP}{Dt} + \rho T \frac{Dc_p}{Dt} \tag{4.3}$$

These are the general form of the governing equations and they can take simplified forms according to the assumptions made for the fluid and flow (Incompressible flow, incompressible fluid etc.). Equations 4.2 are also known as Navier-Stokes equations. If the flow is turbulent some additional equations depending on the turbulence model used for the solution are required. In these equations, ρ represent the density of the fluid, P represents the pressure, τ represents the stress tensor, $\mathbf{g}$ represents the gravitational acceleration, $\mathbf{F}$ represents the external forces, c_P represents the specific heat of the fluid, k represents the thermal conductivity of the fluid. $\mathbf{V}$ is the velocity vector of the fluid and it has three components, one in x direction (V_x), one in y direction (V_y) and one in z direction (V_z). So $\mathbf{V}$ can also be written as;

$$\mathbf{V} = V_x \mathbf{i} + V_y \mathbf{j} + V_z \mathbf{k} \tag{4.4}$$

The term $(\tau : \nabla \mathbf{V})$ in Equation 4.3 can also be represented as follows;

$$\begin{aligned}(\tau : \nabla \mathbf{V}) = {} & \tau_{xx}\left(\frac{\partial V_x}{\partial x}\right) + \tau_{yy}\left(\frac{\partial V_y}{\partial y}\right) + \tau_{zz}\left(\frac{\partial V_z}{\partial z}\right) + \tau_{xy}\left(\frac{\partial V_x}{\partial y} + \frac{\partial V_y}{\partial x}\right) \\ & + \tau_{yz}\left(\frac{\partial V_y}{\partial z} + \frac{\partial V_z}{\partial y}\right) + \tau_{zx}\left(\frac{\partial V_z}{\partial x} + \frac{\partial V_x}{\partial z}\right)\end{aligned} \tag{4.5}$$

4.3. Numerical Solution of the Governing Equations

The governing equations of fluid flow and heat transfer given by Equations 4.1, 4.2 and 4.3 cannot be solved analytically and they are to be solved numerically for the investigated fluid flow problems. Three different numerical solution techniques can be used for the solution: finite difference (and volume), finite element and spectral methods.

In finite difference method, the unknowns of the flow problem are calculated at node points of a grid of coordinate lines. Truncated Taylor series expansions are used to represent the derivatives of unknowns. So, the derivatives in the governing equations are replaced by finite differences and algebraic equations are obtained to determine the values of unknowns at each node (Versteeg and Malalasekera 1995).

The finite volume method is a special finite difference formulation. Fluent CFD software, which is used in this thesis for the analysis of finned tube heat exchangers, also uses this technique in order to solve the relevant governing equations. The numerical algorithm consists of the following steps (Versteeg and Malalasekera 1995);

- Formal integration of the governing equations of fluid flow over all the finite control volumes of the solution domain.
- Discretization involves the substitution of a variety of finite difference type approximation for the terms in the integrated equation representing flow processes such as convection, diffusion and sources. This converts the integral equations into a system of algebraic equations.
- Solution of algebraic equations by an iterative method.

Piecewise functions (linear or quadratic) which are valid on elements are used in finite element method in order to define the local variations of unknowns.

Truncated Fourier series or series of Chebyshev polynomials are used to approximate the unknowns in spectral methods.

The finite volume method has become popular among the others in CFD as a result of primarily two advantages. First, it ensures that the discretization is conservative, mass, momentum and energy are conserved in a discrete sense. Second, finite volume method do not require a coordinate transformation in order to be applied

on irregular meshes. This increased flexibility can be used to great advantage in generating grids about arbitrary geometries (Lomax, et al. 1999).

With the use of finite control volume technique, the discrete values of scalars at cell centers are stored and the face values of the scalars needed for the convection terms are computed by interpolating the cell center values. The realization of this interpolation is made by using an upwind scheme. There are mainly four different upwinding schemes; first order upwinding scheme, second order upwinding scheme, power law and QUICK. The details of these schemes can be found in many computational fluids dynamics books.

There is a point which needs to be taken into consideration for the numerical solution. Solution of the Navier-Stokes equations is complicated because of the lack of an independent equation for the pressure, whose gradient contributes to each of three momentum equations. For this reason some pressure-velocity linkage algorithms (SIMPLE, SIMPLER, SIMPLEC, PISO) are used in order to resolve this problem.

SIMPLE (Semi Implicit Method for Pressure Linked Equations) is mainly a guess and correct procedure for the calculations of pressure. It can be summarized as (Versteeeg and Malalasekera 1995);

- An approximation of the velocity field is obtained by solving the momentum equation. The pressure gradient term is calculated using the pressure distribution from the previous iteration or an initial guess.
- The pressure equation is formulated and solved in order to obtain the new pressure distribution.
- Velocities are corrected and a new set of conservative fluxes is calculated.

SIMPLER (SIMPLE Revised) is an improved version of SIMPLE. In this algorithm the discretized continuity equation is used to derive a discretized equation for pressure, instead of a pressure correction equation as in SIMPLE (Versteeeg and Malalasekera 1995).

SIMPLEC (SIMPLE Consistent) algorithm follows the same steps as the SIMPLE algorithm with the difference that the momentum equations are manipulated so that the SIMPLEC velocity correction equations omit terms that are less significant than those omitted in SIMPLE (Versteeeg and Malalasekera 1995).

PISO (Pressure Implicit with Splitting of Operators) is a pressure-velocity calculation procedure which involves one predictor step with two corrector steps and

may be seen as an extension of SIMPLE with a further corrector step to enhance it (Versteeeg and Malalasekera 1995).

4.4. Boundary Conditions

In order to perform numerical calculations, information about the boundaries of the computational domain should be supplied. Boundary conditions specify the flow and thermal variables on the boundaries of the physical model. They are, therefore, a critical component of numerical simulations and it is important that they are specified appropriately. The values of the unknowns at the inner region of the computational domain are calculated using the boundary conditions. The boundary conditions depend on the physical model under investigation.

4.4.1. Flow Inlet and Outlet Boundary Conditions

The following boundary condition types define the flow conditions at the inlet and at the exit of the flow on the computational domain (Fluent 6.3 User's Guide 2006).

- Velocity inlet boundary condition: It is used to define the flow velocity, along with all relevant scalar properties of the flow, at flow inlets. The total (or stagnation) properties of the flow are not fixed, so they take whatever value is necessary to provide the prescribed velocity distribution.
- Mass flow inlet boundary condition: It is used to provide a prescribed mass flow rate or mass flux distribution at an inlet. A mass flow inlet is often used when it is more important to match a prescribed mass flow rate than to match the total pressure of the inflow stream.
- Pressure inlet boundary condition: It is used to define the fluid pressure at flow inlets, along with all other scalar properties of the flow. It suitable for both incompressible and compressible flow calculations. Pressure inlet boundary conditions can be used when the inlet pressure is known but the flow rate and/or velocity is not known.
- Outflow boundary condition: It is used to model flow exits where the details of the flow velocity and pressure are not known prior to solution of the flow problem.

- Pressure outlet boundary condition: It requires the specification of a static (gauge) pressure at the outlet boundary. So, it is used in the cases where the exit static pressure value is known.

4.4.2. Wall Boundary Condition

This type boundary condition defines the borders of solid and fluid regions. Walls can be stationary or moving depending on the problem. For a stationary wall, all velocity component values are zero. Several heat transfer conditions can be defined at wall boundaries such as heat flux, constant temperature, convective heat transfer coefficient and free stream temperature etc. (Fluent 6.3 User's Guide 2006).

4.4.3. Symmetry Boundary Condition

Symmetry boundary conditions are used when the physical geometry of interest, and the expected pattern of the solution, has symmetry. A zero flux of all quantities across a symmetry boundary is defined, so no input is required at symmetry boundaries (Fluent 6.3 User's Guide 2006).

4.4.4. Periodic Boundary Condition

Periodic boundary conditions are used when the physical geometry of interest and the expected pattern of the solution have a periodically repeating nature (Fluent 6.3 User's Guide 2006).

4.5. Main Elements of a CFD Code

With the developments in the CFD area commercial software packages became available since the early 1970s. Each software package has to assist the user in carrying out the tasks that form the analysis process. This is done by providing, typically, three main pieces of software: a pre-processor, a solver and a post-processor.

4.5.1. Pre-Processor

All the tasks that take place before the numerical solution process is started are called pre-processing. In this part, inputs of a flow problem are determined using an interface and these inputs are used by the solver. At the pre-processor stage, the following activities are performed by the user (Versteeg and Malalasekera 1995);

- Definition of the geometry of the region of interest: the computational domain.
- Grid-generation – the subdivision of the domain into a number of smaller, non-overlapping sub-domains: a grid (or mesh) of cells (or control volumes or elements).
- Selection of the physical and chemical phenomena that need to be modeled.
- Definition of fluid properties.
- Specification of appropriate boundary conditions at cells which coincide with or touch the domain boundary.

The number of control volumes is the key factor in the accuracy of a CFD solution. The control volumes should be generated at sufficient level in order to obtain physically realistic results. Generally, as the control volume number is increased better solution is obtained. However, more control volumes also lead to a longer computational time which is already very long for complicated flow problems. Therefore, optimal control volume number which provides satisfactory results should be used for this type flow problems.

4.5.2. Solver

Each package has a program that solves the numerical equations for the problem under consideration with one of the solution techniques explained before. All the relevant data defined in the pre-processor must be given to the solver. The pre-processor writes out data files to transfer the data between the pre-processor and the solver. Once the data files are in place, the solver program is activated and the required solution process carried out (Shaw 1992).

4.5.3. Post-Processor

The results acquired from the CFD software for the flow problem under consideration can be investigated in detail in this stage. For example, the heat transfer, pressure drop values as well as temperature or velocity value at a specific location can be determined. In the post-processor stage, data visualization can also be accomplished such as (Versteeg and Malalasekera 1995);

- Domain geometry and grid display.
- Vector plots.
- Line and shaded contour plots.
- Particle tracking.
- View manipulations (translation, rotation, scaling etc.)
- Colour postscript output.

4.6. Fluent CFD Software Package

In this study, the numerical optimization of finned tube gas to liquid heat exchangers is focused on. For this purpose, a commercial CFD software, Fluent is used. Fluent is a computer program written in the C computer language for modeling fluid flow and heat transfer in complex geometries. It provides complete mesh flexibility, including the ability to solve flow problems using unstructured meshes that can be generated about complex geometries with relative ease. Supported mesh types include 2D triangular/quadrilateral, 3D tetrahedral/hexahedral/pyramid/wedge/polyhedral, and mixed (hybrid) meshes (Fluent 6.3 User's Guide 2006).

Fluent package consists of the following two programs;

- Gambit, the pre-processor for geometry modeling and mesh generation.
- Fluent, the solver. The post-processing is also accomplished with Fluent software.

4.6.1. The Pre-Processor Program: Gambit

As mentioned before, flow problems involve the solution of governing equations which are nonlinear partial differential equations. The numerical solution of these governing equations is accomplished by dividing the computational domain into sub domains and solving the algebraic form of these partial differential equations for these small sub domains which are also called as meshes. Gambit program can generate different structured or unstructured meshes for the geometrical model of the considered problem, which can also be created with Gambit software. The mesh types available for two and three dimensional cases are shown in Figure 4.1.

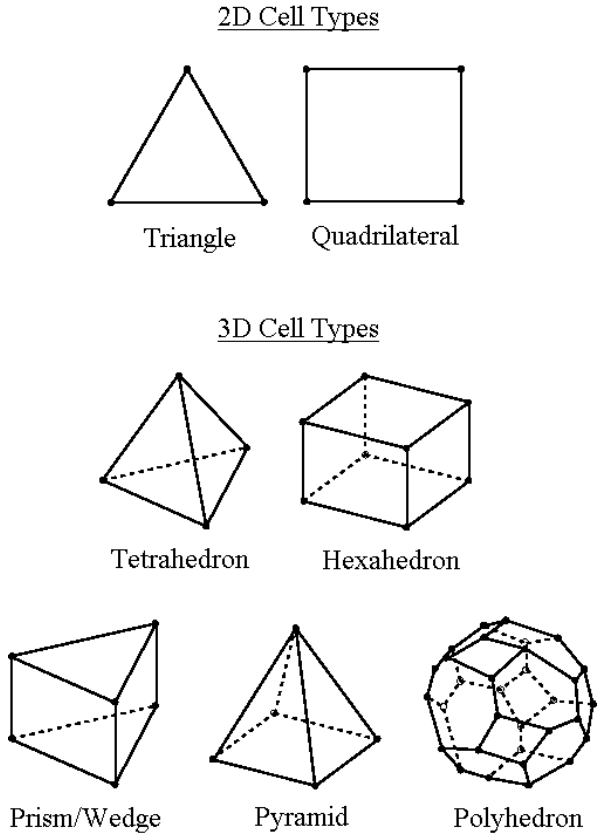

Figure 4.1. Different two and three dimensional mesh types.
(Source: Fluent 6.3 User's Guide 2006).

4.6.2. The Solver and Post-Processing Program: Fluent

The numerical solution of the flow problem under consideration is obtained with the solver program Fluent. Fluent allows two numerical methods:

- pressure-based solver
- density-based solver

The pressure-based approach is used for low-speed incompressible flows, while the density-based approach is mainly used for high-speed compressible flows. In both methods the velocity field is obtained from the momentum equations. In the density-based approach, the continuity equation is used to obtain the density field while the pressure field is determined from the equation of state. On the other hand, in the pressure-based approach, the pressure field is extracted by solving a pressure or pressure correction equation which is obtained by manipulating continuity and momentum equations. Fluent solves the governing integral equations for the conservation of mass and momentum, and (when appropriate) for energy and other scalars such as turbulence in both cases using a control-volume-based technique (Fluent 6.3 User's Guide 2006).

4.6.2.1. Pressure-Based Solver

The pressure equation is derived from the continuity and the momentum equations in such a way that the velocity field, corrected by the pressure, satisfies the continuity. The governing equations are nonlinear and coupled to one another. For this reason iterations for the solution of the governing equations are performed until convergence criteria are satisfied.

Two pressure-based solver algorithms are available in Fluent. A segregated and a coupled algorithm. In the segregated algorithm, the individual governing equations for the solution variables are solved one after another. Each governing equation is decoupled (or segregated) from other equations, while being solved. This algorithm requires relatively low memory, because only one discretized equation needs to be stored. Nevertheless, relatively slow solution convergence is encountered. The steps of each iteration can be summarized as (Fluent 6.3 User's Guide 2006);

- Update fluid properties based on the current solution (or initialized solution).
- Solve the momentum equations, one after another, using the recently updated values of pressure and face mass fluxes.
- Solve the pressure correction equation using the recently obtained velocity field and the mass-flux.
- Correct face mass fluxes, pressure, and the velocity field using the pressure correction obtained from Step 3.
- Solve the equations for additional scalars, if any, such as turbulent quantities, energy, and radiation intensity using the current values of the solution variables.
- Update the source terms arising from the interactions among different phases
- Check for the convergence of the equations.

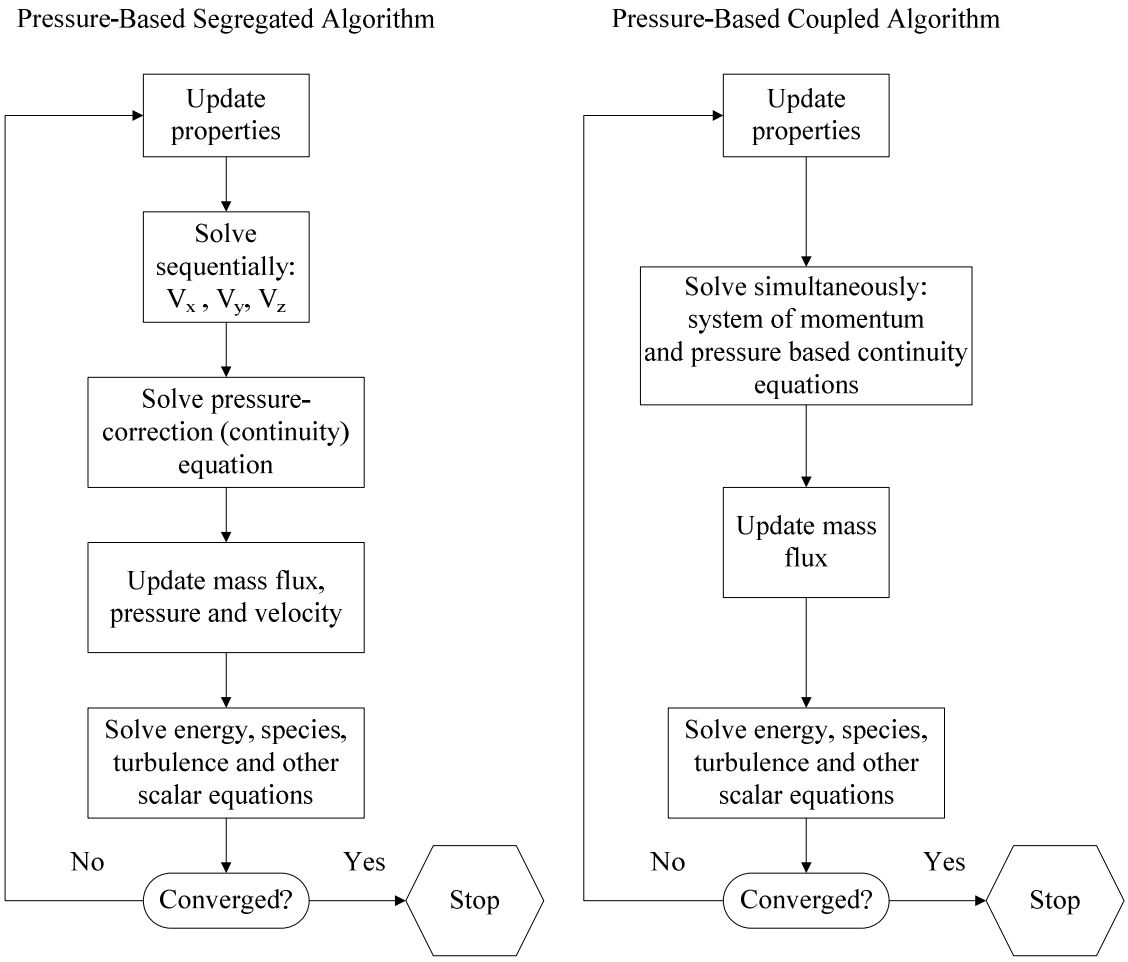

Figure 4.2. Overwiew of the pressure-based solution methods.
(Source: Fluent 6.3 User's Guide 2006)

The pressure-based coupled algorithm solves a coupled system of momentum and continuity equations Thus, in the coupled algorithm, Steps 2 and 3 of the segregated solution algorithm are replaced by a single step in which the coupled system of equations are solved. The other equations are solved as in the segregated algorithm. The convergence is faster than the segregated algorithm, but as momentum and continuity equations are stored at the same time, higher memory requirement arises when coupled algorithm is used. The steps of segregated and coupled algorithms are illustrated in Figure 4.2.

4.6.2.2. Density-Based Solver

The governing equations of continuity, momentum, and (where appropriate) energy and species transport are solved simultaneously when density-based solver is used. Governing equations for additional scalars will be solved afterward and sequentially. Several iterations must also be performed before a converged solution, for which all convergence criteria are met, is obtained. The steps of each iteration of density-based solver are (Fluent 6.3 User's Guide 2006);

- Update the fluid properties based on the current solution (or the initialized solution).
- Solve the continuity, momentum, and (where appropriate) energy and species equations simultaneously.
- Where appropriate, solve equations for scalars such as turbulence and radiation using the previously updated values of the other variables.
- When interphase coupling is to be included, update the source terms in the appropriate continuous phase equations with a discrete phase trajectory calculation.
- Check for convergence of the equation set.

4.6.2.3. Convergence

At the end of each iteration, the residual sum for each of the conserved variables is computed and stored. On a computer with infinite precision, these residuals will go to zero as the solution converges but on an actual computer, the residuals decay to some small value (round-off) and then stop changing. Residual definitions that are useful for

one class of problem are sometimes not appropriate for other classes of problems. Therefore, it is convenient to judge convergence not only by examining residual levels, but also by monitoring relevant quantities.

After discretization, the conservation equation for a general variable Φ at a cell P can be written as (Fluent 6.3 User's Guide 2006);

$$a_P \Phi_P = \sum_{nb} a_{nb} \Phi_{nb} + b \tag{4.6}$$

where, a_P is the center coefficient, a_{nb} are the influence coefficients for the neighboring cells, and b is the contribution of the constant part of the source term and of the boundary conditions.

The residual is defined as the imbalance in Equation 4.6 summed over all the computational cells. In this way unscaled residuals are calculated as (Fluent 6.3 User's Guide 2006);

$$R^{\Phi} = \sum_{\text{cells P}} \left| \sum_{nb} a_{nb} \Phi_{nb} + b - a_P \Phi_P \right| \tag{4.7}$$

Since the unscaled residual is difficult to be used for the judgement of the convergence, the scaled residuals are used instead. The scaled residuals are defined as (Fluent 6.3 User's Guide 2006);

$$R^{\Phi}_{\text{scaled}} = \frac{\sum_{\text{cells P}} \left| \sum_{nb} a_{nb} \Phi_{nb} + b - a_P \Phi_P \right|}{\sum_{\text{cells P}} |a_P \Phi_P|} \tag{4.8}$$

For the momentum equations the denominator term $a_P \Phi_P$ is replaced by $a_P V_P$, where V_P is the magnitude of the velocity at cell.

For the continuity equation, the unscaled form and scaled form of residual are defined by Equations 4.9 and 4.10, respectively (Fluent 6.3 User's Guide 2006);

$$\text{Unscaled form: } R^c = \sum_{\text{cells P}} |\text{rate of mass creation in cell P}| \tag{4.9}$$

$$\text{Scaled form: } R^c_{\text{scaled}} = \frac{R^c_{\text{iteration N}}}{R^c_{\text{iteration 5}}} \tag{4.10}$$

In Equation 4.10, $R^{c}_{\text{iteration N}}$ represents the residual at the N^{th} iteration while $R^{c}_{\text{iteration 5}}$ is the largest absolute value of the continuity residual in the first five iterations.

4.6.2.4. Under-Relaxation Factors

The under-relaxation of equations is used in the pressure-based solver to stabilize the convergence behavior of the nonlinear iterations by introducing selective amounts of Φ in the system of discretized equations (Fluent 6.3 User's Guide 2006).

$$\frac{a_P \Phi}{\alpha} = \sum_{nb} a_{nb} \Phi_{nb} + b + \frac{1-\alpha}{\alpha} a_P \Phi_{old} \qquad (4.11)$$

where, α is the under-relaxation factor.

CHAPTER 5

GOVERNING EQUATIONS FOR THE CONSIDERED PROBLEM

The general form of the governing equations, which is valid for any fluid flow and heat transfer problem, was described in chapter 4 by Equations 4.1, 4.2 and 4.3. However, for the cases investigated in this thesis, some assumptions for the fluid and for the flow can be made and the governing equations can take simplified forms according to these assumptions. In this chapter the governing equations valid for the considered problems are derived.

For the considered problems, the following assumptions can be made;

- The flow is considered as steady, so the time dependent terms in Equations 4.1, 4.2 and 4.3 are canceled.
- The flow can be assumed as incompressible. This assumption can be made when the Mach number of the flow is lower than 0.3. As a result of this assumption, the following condition can be written (White 1999);

$$\boldsymbol{\nabla}.\rho\mathbf{V} = \rho\boldsymbol{\nabla}.\mathbf{V} \tag{5.1}$$

Additionally, the assumption of incompressible flow leads to the omission of the compression work term $\frac{\mathrm{DP}}{\mathrm{Dt}}$.

- The density of the flue gas is taken as constant (ρ:constant). Consequently, the fluid is incompressible.
- The fluid is assumed to be Newtonian. For Newtonian fluids the stress terms can be written as (Bird, et al. 1960);

$$\tau_{xx} = -2\mu\frac{\partial \mathrm{V_x}}{\partial \mathrm{x}} + \frac{2}{3}\mu(\boldsymbol{\nabla}.\mathbf{V}) \tag{5.2}$$

$$\tau_{yy} = -2\mu\frac{\partial \mathrm{V_y}}{\partial \mathrm{y}} + \frac{2}{3}\mu(\boldsymbol{\nabla}.\mathbf{V}) \tag{5.3}$$

$$\tau_{zz} = -2\mu\frac{\partial \mathrm{V_z}}{\partial \mathrm{z}} + \frac{2}{3}\mu(\boldsymbol{\nabla}.\mathbf{V}) \tag{5.4}$$

$$\tau_{xy} = \tau_{yx} = -\mu\left(\frac{\partial V_x}{\partial y} + \frac{\partial V_y}{\partial x}\right) \tag{5.5}$$

$$\tau_{yz} = \tau_{zy} = -\mu\left(\frac{\partial V_y}{\partial z} + \frac{\partial V_z}{\partial y}\right) \tag{5.6}$$

$$\tau_{xz} = \tau_{zx} = -\mu\left(\frac{\partial V_z}{\partial x} + \frac{\partial V_x}{\partial z}\right) \tag{5.7}$$

Additionally, the following condition is valid for Newtonian fluids;

$$(-\tau : \boldsymbol{\nabla}\mathbf{V}) = \mu\Phi_v = \frac{1}{2}\mu\sum_i\sum_j\left[\left(\frac{\partial V_i}{\partial x_j} + \frac{\partial V_j}{\partial x_i}\right) - \frac{2}{3}(\boldsymbol{\nabla}.\mathbf{V})\delta_{ij}\right]^2 \tag{5.8}$$

$$\text{where, } \delta_{ij} = \begin{cases} 1 \text{ for } i = j \\ 0 \text{ for } i \neq j \end{cases}$$

Φ_v is known as dissipation and the term $\mu\Phi_v$ represents viscous heating. The viscous heating is not taken into account for the considered problems as the flow velocity is very low.

According to the mentioned assumptions made for the present fluid flow and heat transfer problems, the governing equations take the following forms;

$$\boldsymbol{\nabla}.\mathbf{V} = 0 \tag{5.9}$$

$$\rho(\boldsymbol{\nabla}.\mathbf{V}\mathbf{V}) = -\boldsymbol{\nabla}P - [\boldsymbol{\nabla}.\tau] \tag{5.10}$$

$$\rho\left(\boldsymbol{\nabla}.\left(c_pT\mathbf{V}\right)\right) = \boldsymbol{\nabla}(k\boldsymbol{\nabla}T) \tag{5.11}$$

The unknowns for the investigated problems are T, **V**, P. SIMPLE algorithm is used for the pressure-velocity coupling in the numerical solution.

The closed form of governing equations given by Equations 5.9, 5.10 and 5.11 can also be written in Cartesian coordinates as;

$$\frac{\partial V_x}{\partial x} + \frac{\partial V_y}{\partial y} + \frac{\partial V_z}{\partial z} = 0 \tag{5.12}$$

$$\rho\left(V_x\frac{\partial V_x}{\partial x} + V_y\frac{\partial V_x}{\partial y} + V_z\frac{\partial V_x}{\partial z}\right) = -\frac{\partial P}{\partial x} + \frac{\partial}{\partial x}\left(2\mu\frac{\partial V_x}{\partial x}\right) + \frac{\partial}{\partial y}\left(\mu\left(\frac{\partial V_x}{\partial y} + \frac{\partial V_y}{\partial x}\right)\right) + \frac{\partial}{\partial z}\left(\mu\left(\frac{\partial V_x}{\partial z} + \frac{\partial V_z}{\partial x}\right)\right) \tag{5.13}$$

$$\rho\left(V_x\frac{\partial V_y}{\partial x}+V_y\frac{\partial V_y}{\partial y}+V_z\frac{\partial V_y}{\partial z}\right)=-\frac{\partial P}{\partial y}+\frac{\partial}{\partial x}\left(\mu\left(\frac{\partial V_y}{\partial x}+\frac{\partial V_x}{\partial y}\right)\right)+\frac{\partial}{\partial y}\left(2\mu\frac{\partial V_y}{\partial y}\right)+\frac{\partial}{\partial z}\left(\mu\left(\frac{\partial V_y}{\partial z}+\frac{\partial V_z}{\partial y}\right)\right) \quad (5.14)$$

$$\rho\left(V_x\frac{\partial V_z}{\partial x}+V_y\frac{\partial V_z}{\partial y}+V_z\frac{\partial V_z}{\partial z}\right)=-\frac{\partial P}{\partial z}+\frac{\partial}{\partial x}\left(\mu\left(\frac{\partial V_z}{\partial x}+\frac{\partial V_x}{\partial z}\right)\right)+\frac{\partial}{\partial y}\left(\mu\left(\frac{\partial V_z}{\partial y}+\frac{\partial V_y}{\partial z}\right)\right)+\frac{\partial}{\partial z}\left(2\mu\frac{\partial V_z}{\partial z}\right) \quad (5.15)$$

$$\rho\left(V_x\frac{\partial(c_pT)}{\partial x}+V_y\frac{\partial(c_pT)}{\partial y}+V_z\frac{\partial(c_pT)}{\partial z}\right)=\frac{\partial}{\partial x}\left(k\frac{\partial T}{\partial x}\right)+\frac{\partial}{\partial y}\left(k\frac{\partial T}{\partial y}\right)+\frac{\partial}{\partial z}\left(k\frac{\partial T}{\partial z}\right) \quad (5.16)$$

The above set of equations is coupled and nonlinear. They are valid for the fluid side of the considered problems and the density, dynamic viscosity and thermal conduction values should be taken for flue gas. There are five unknowns as V_x, V_y, V_z, T, P and solution of the above set of equations provides the distributions of these unknowns in the computational domain. These equations are suitable for the computational domain, given in Figure 5.1, investigated in this thesis. The details of the computational domain are explained in chapter 6. For solid side of the considered problem, only the Equation 5.16 is valid without the terms with velocities. For the solid side, the thermo physical properties should be taken for copper.

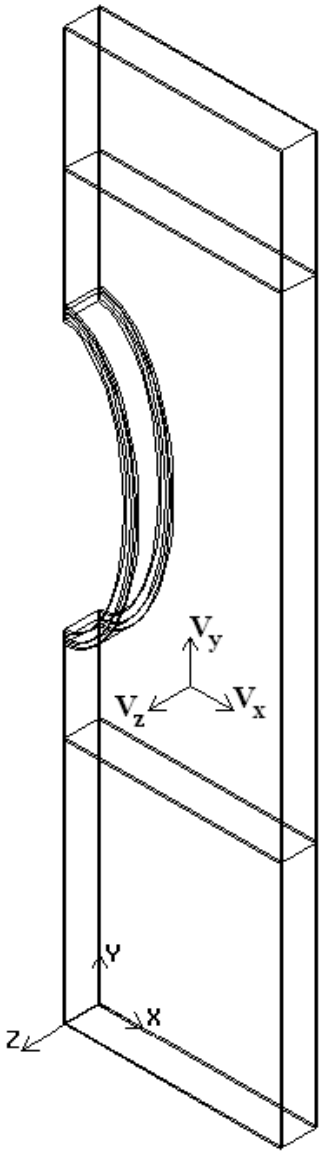

Figure 5.1. The computational domain investigated in the thesis.

CHAPTER 6

NUMERICAL MODELING OF THE CONSIDERED FINNED TUBE GAS TO LIQUID HEAT EXCHANGERS AND BOUNDARY CONDITIONS USED IN MODELS

Two different numerical models can be created for the finned tube heat exchangers investigated in this thesis. In the first one, symmetry boundary condition while in the second one, periodic boundary condition is used for the front and back surfaces of the model. These two cases are explained in detail in the following sections.

6.1. Numerical Modeling with Symmetry Boundary Condition

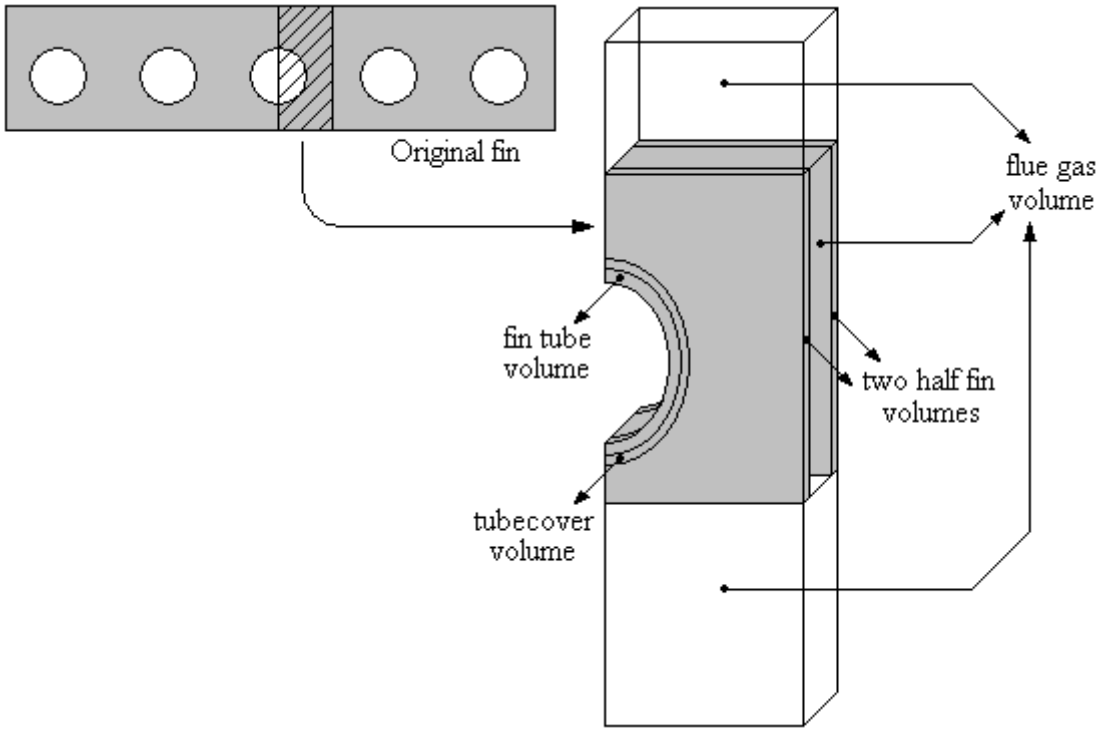

Figure 6.1. Schematic view of a heat exchanger model with symmetry boundary condition.

Since the whole heat exchanger cannot be modeled numerically due to the computer source limitation, only the middle fin (the 51st fin) of the heat exchanger is taken into consideration in the numerical investigations. Furthermore, because of the

symmetrical conditions, only one tenth segment of the actual fin is modeled and used in the numerical calculations.

As a result, the model of a heat exchanger consists of two fin volumes with half fin thickness, a fin tube volume, a tubecover volume and a flue gas volume. The schematic view of a heat exchanger model is given in Figure 6.1.

The volume representing the flue gas which is passing through the gap between two fins is extended beyond the inlet and exit of the gap between two fins in order to enable more accurate boundary condition application.

6.1.1. Boundary Conditions for the Models with Symmetry Boundary Condition

The boundary conditions used for the models with symmetry boundary condition are summarized in this section as follows;

6.1.1.1. Mass Flow Inlet Boundary Condition

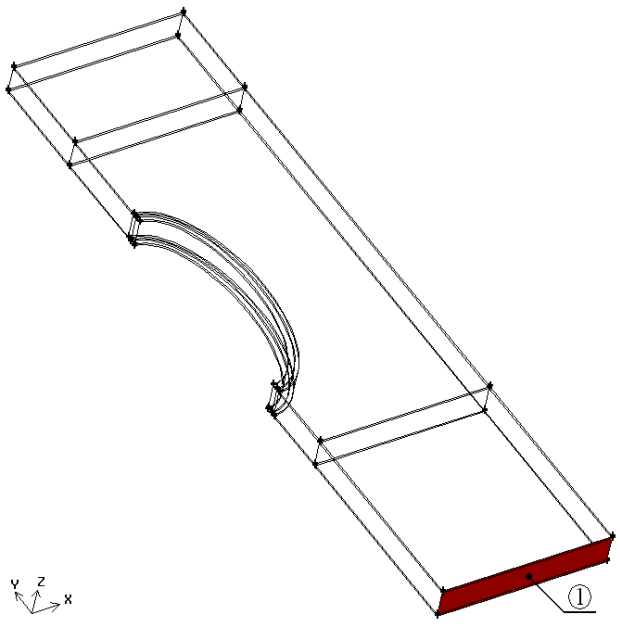

Figure 6.2. Inlet boundary condition surface.

Mass flow inlet boundary condition is defined for the surface which is indicated as (1) in Figure 6.2, since flue gas enters at a constant mass flow rate from that cross section. The mass flow rate used in the analyses of all heat exchanger models is 1.904×10^{-5} kg/s. The uniform flue gas velocity is calculated using the mass flow rate and flue gas density value at this inlet surface. Temperature value of the flue gas at the inlet is also defined for this surface as 1500 K. These values are taken from a combi boiler apparatus application results. For this inlet surface, the boundary conditions can be listed as;

$$\dot{m} = 1.904 \times 10^{-5} \text{ kg/s (corresponding } V_x=0,\ V_z=0,\ V_y = 1.0415 \text{ m/s)} \quad (6.1)$$

$$T = 1500 \text{ K} \quad (6.2)$$

$$P_{gauge} = 0 \text{ Pa} \quad (6.3)$$

6.1.1.2. Outflow Boundary Condition

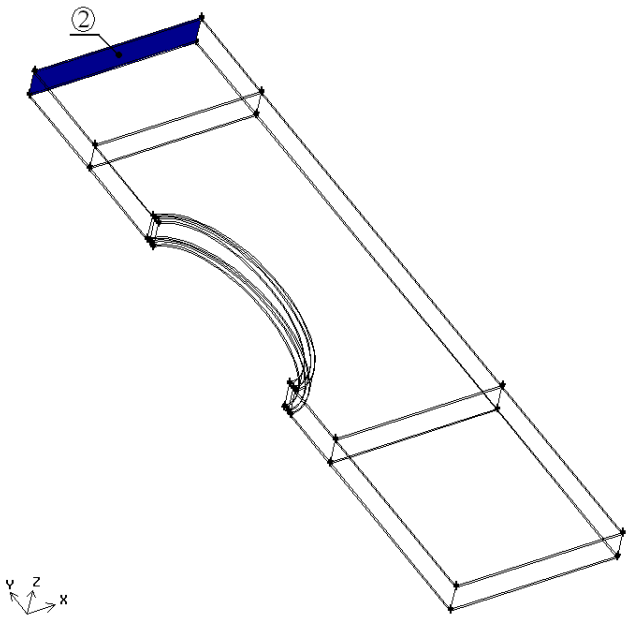

Figure 6.3. Outflow boundary condition surface.

The flue gas is exhausted from the top side of the heat exchanger which is indicated as (2) in Figure 6.3 and the pressure value and velocity of the flue gas at the exit surface is not known at the beginning of the calculations. In Fluent, outflow boundary condition is used to model flow exits where the details of the flow velocity

and pressure are not known prior to solution of the flow problem. Fluent extrapolates the required information for the outlet surface from the interior (Fluent 6.3 User's Guide 2006). So, outflow boundary condition is given to this surface, and the conditions are as follows;

$$\frac{\partial T}{\partial y} = 0 \tag{6.4}$$

$$\frac{\partial V_x}{\partial y} = 0 \tag{6.5}$$

$$\frac{\partial V_z}{\partial y} = 0 \tag{6.6}$$

The derivatives of V_x and V_z with respect to y are taken equal to zero in Equations 6.5 and 6.6. However, special care should be taken for the V_y. Firstly, V_y values are also calculated by the following Equation 6.7 (Versteeg and Malalasekera 1995);

$$\frac{\partial V_y}{\partial y} = 0 \tag{6.7}$$

If the total number of nodes in y direction is N, according to the Equation 6.7, the velocity in y direction at the outflow surface will be;

$$V_y(i,N,k) = V_y(i,N-1,k) \tag{6.8}$$

However, during the iterations of SIMPLE algorithm, these velocities cannot conserve mass over the computational domain as a whole. In order to satisfy the continuity, the mass flow rate leaving the domain ($\dot{m}_{out}$) is calculated by using the velocity values calculated according to Equation 6.8 and the velocity values in y direction are multiplied with the ratio of the mass flow rate entering the domain ($\dot{m}_{in}$) and the mass flow rate leaving the domain. So, the velocities in y direction for the outflow boundary are calculated as (Versteeg and Malalasekera 1995);

$$V_y(i, N, k) = V_y(i, N-1, k) \times \frac{\dot{m}_{in}}{\dot{m}_{out}} \tag{6.9}$$

The velocity at the outflow boundary is not corrected with pressure correction equation, so the relevant coefficients in the pressure correction equations are set to zero.

6.1.1.3. Symmetry Boundary Condition

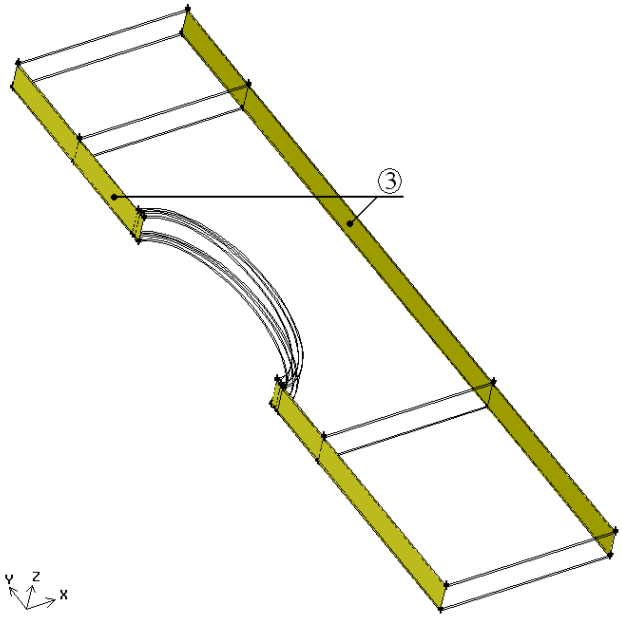

Figure 6.4. Side surfaces of the model.

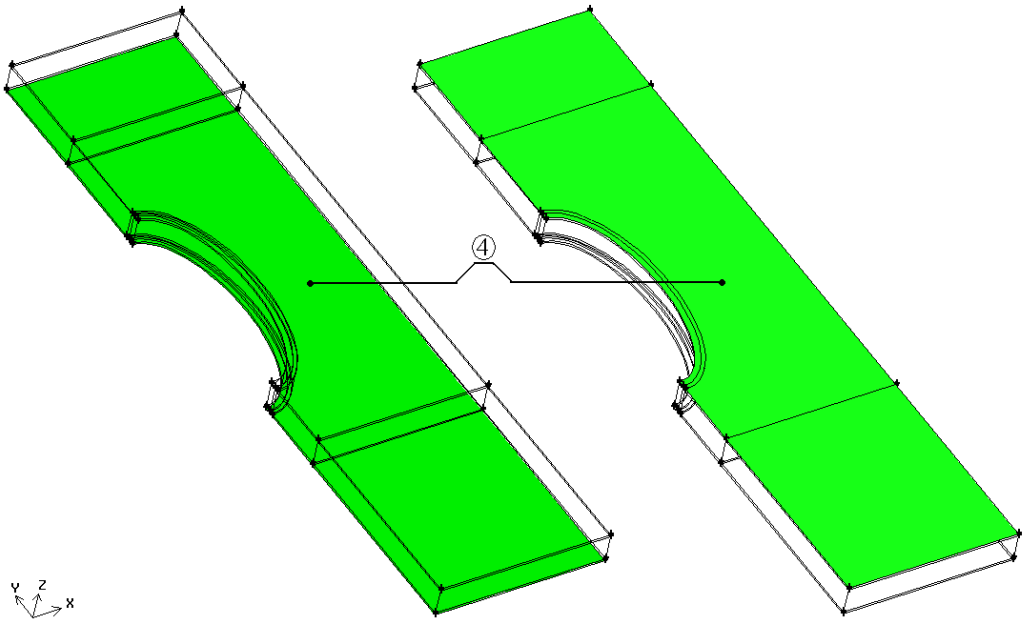

Figure 6.5. Front and back surfaces of the model.

Symmetry boundary condition is applied to the side, indicated as (3) in Figure 6.4, and front and back surfaces, indicated as (4) in Figure 6.5, of the model due to the symmetry.

The conditions for the surfaces (3) are;

$$\frac{\partial T}{\partial x} = 0 \tag{6.10}$$

$$V_x = 0 \tag{6.11}$$

$$\frac{\partial V_y}{\partial x} = 0 \tag{6.12}$$

$$\frac{\partial V_z}{\partial x} = 0 \tag{6.13}$$

The conditions for the surfaces (4) are;

$$\frac{\partial T}{\partial z} = 0 \tag{6.14}$$

$$V_z = 0 \tag{6.15}$$

$$\frac{\partial V_x}{\partial z} = 0 \tag{6.16}$$

$$\frac{\partial V_y}{\partial z} = 0 \tag{6.17}$$

For the symmetry boundary, the appropriate coefficients in pressure correction equation are set to zero in order to cut the link of pressure correction equation and the symmetry boundary and no further modifications are necessary (Versteeg and Malalasekera 1995).

6.1.1.4. Wall Boundary Condition

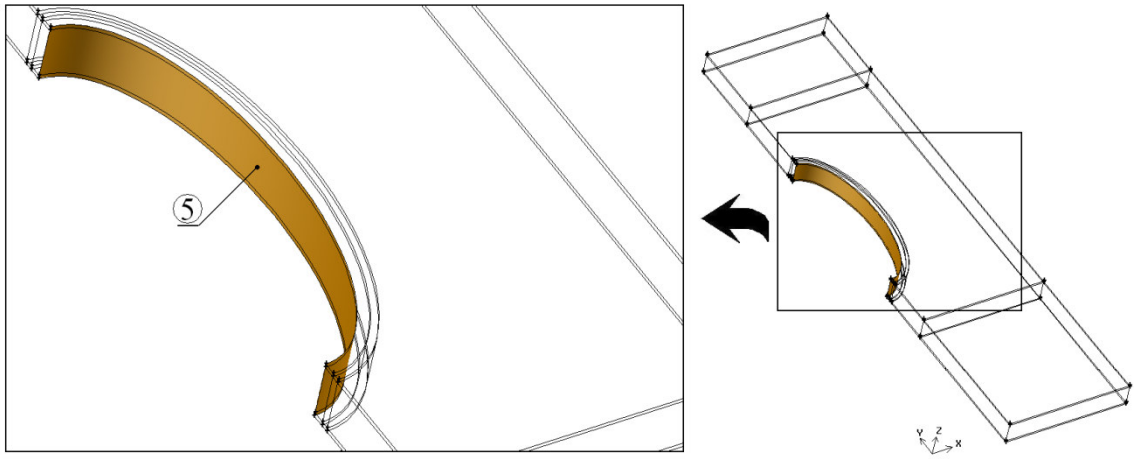

Figure 6.6. Fin tube inner wall.

For the fin tube inner wall, indicated as (5) in Figure 6.6, wall boundary condition is applied. The heating water flows inside the tubes in the actual process, however in order not to model the heating water, convective heat transfer is defined for this wall. The boundary condition for this stationary solid wall is as follows;

$$-k_{copper}\left.\frac{\partial T}{\partial n}\right|_{solid} = h_{water}(T_{wall} - T_{water}) \tag{6.18}$$

where, n is the surface normal direction.

The convection coefficients between the water flowing inside the tubes and the fin tube inner wall (h_{water}) are calculated by using the Gnielinski correlation given by Equation 6.19 for fully developed turbulent forced convection through a duct (Kakaç and Yener 1995).

$$Nu = \frac{(f/2)\times(Re-1000)\times Pr}{1+12.7\times(f/2)^{1/2}\times(Pr^{2/3}-1)} \tag{6.19}$$

where, $f = (1.58 \times \ln Re - 3.28)^{-2}$

Free stream temperature of water (T_{water}) is also defined for the fin tube wall. The middle section of fin is taken into consideration and free stream temperature is assumed as 343 K. The heating water enters the heat exchanger at 333 K and leaves at 353 K. Since the 51st fin is taken into consideration and as the third fin tube is used in the modeling of the heat exchangers, the free stream temperature of water is selected as 343 K.

6.1.1.5. Interface Surfaces

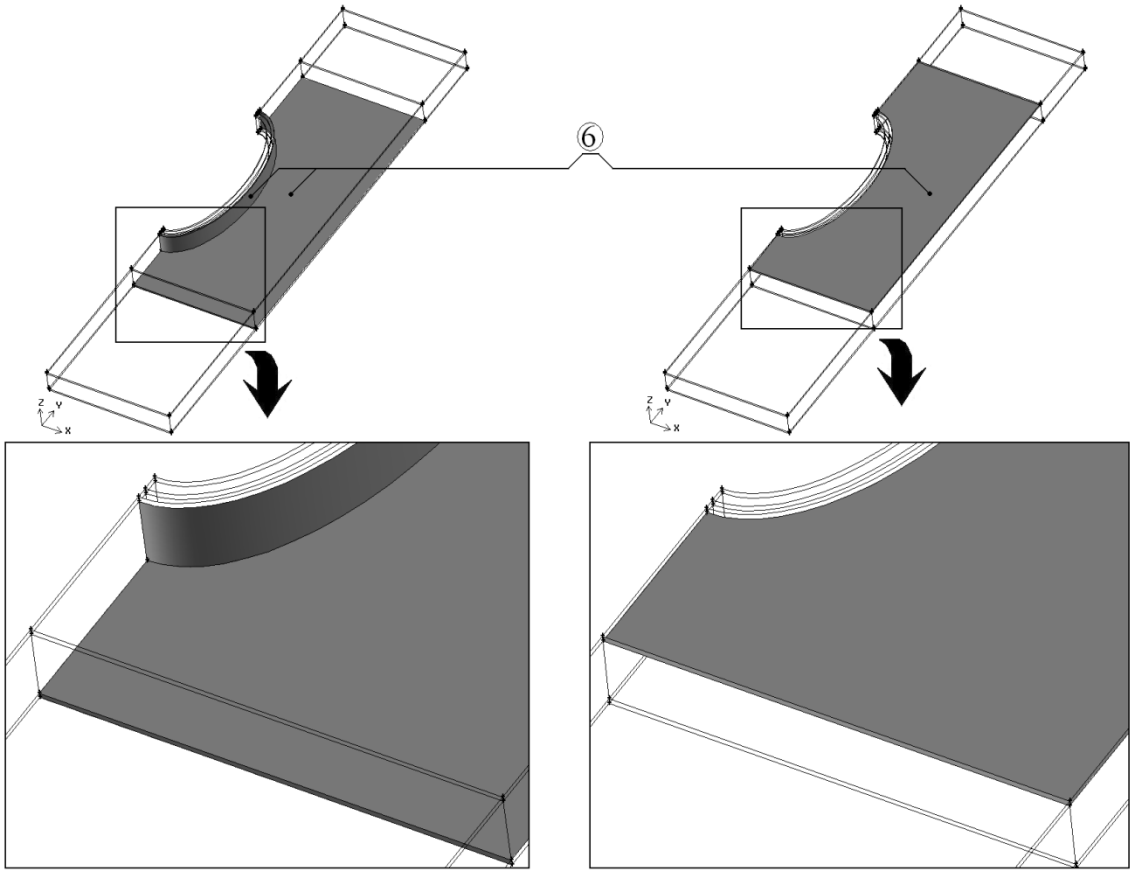

Figure 6.7. Interface surfaces.

The surfaces of solid regions which are in contact with the fluid flow are called interface surfaces. These surfaces are indicated as (6) in Figure 6.7. The following conditions can be written for these interface surfaces;

$$V_x = V_y = V_z = 0 \tag{6.20}$$

$$-k_{copper}\left.\frac{\partial T}{\partial n}\right|_{solid} = -k_{flue\ gas}\left.\frac{\partial T}{\partial n}\right|_{fluid} \quad (6.21)$$

where, n is the surface normal direction.

The pressure values at these interface surfaces are calculated since the wall velocities are known.

6.2. Numerical Modeling with Periodic Boundary Condition

The one tenth segment of a fin could also be modeled by modeling the fin with whole fin thickness and the surrounding flue gas volumes on two sides of the fin. In this case, the front and back surfaces should be defined as periodic boundaries while side surfaces remain as symmetry boundaries. The schematic view of such a model is illustrated in Figure 6.8.

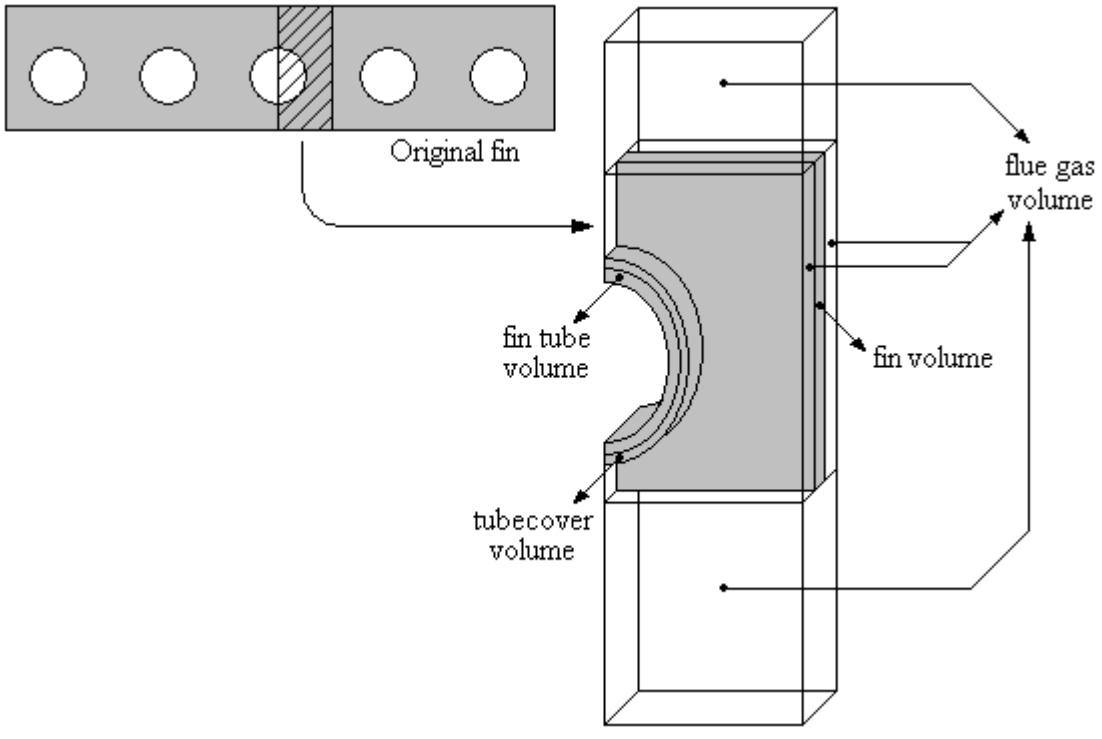

Figure 6.8. Schematic view of a heat exchanger model with periodic boundary condition.

6.2.1. Boundary Conditions for the Models with Periodic Boundary Condition

All the boundary conditions for the model with periodic boundary condition are the same as the model with symmetry boundary condition except the front and back surfaces of the model. Periodic boundary conditions instead of symmetry boundary conditions are used for the front and back surfaces of the model.

6.2.1.1. Periodic Boundary Condition

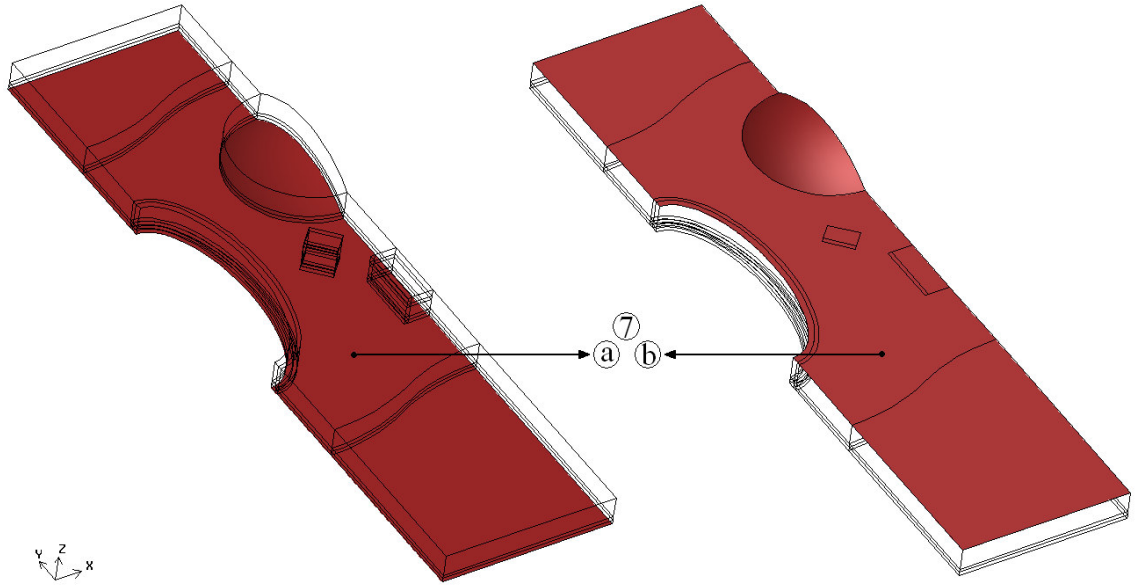

Figure 6.9. Periodic front and back surfaces of the model.

The periodic boundaries are the surfaces indicated as (7) in Figure 6.9. The cells of a periodic boundary surface are treated as the direct neighbor of the cells of the other periodic boundary surface and the flow conditions of the two periodic boundaries are taken as the same. The conditions valid for periodic boundaries can be summarized as follows;

$$V_{x,7a} = V_{x,7b} \tag{6.22}$$

$$V_{y,7a} = V_{y,7b} \tag{6.23}$$

$$V_{z,7a} = V_{z,7b} \tag{6.24}$$

$$T_{7a} = T_{7b} \tag{6.25}$$

$$P_{7a} = P_{7b} \tag{6.26}$$

CHAPTER 7

MESH GENERATION AND COMPUTATIONAL DETAILS

As it was explained before, in order to perform numerical calculations, the geometry of the considered problem should be divided into several small sub domains which are called as meshes. The meshing operation for the considered heat exchanger models is accomplished using Gambit program.

7.1. Meshing of the Models with Symmetry Boundary Condition

Since the vicinity of fin tube and protrusions is subjected to higher gradients, finer meshes are employed for these regions. The meshes created for a fin with three different protrusions is given in Figure 7.1 and the complete meshed geometry is shown in Figure 7.2.

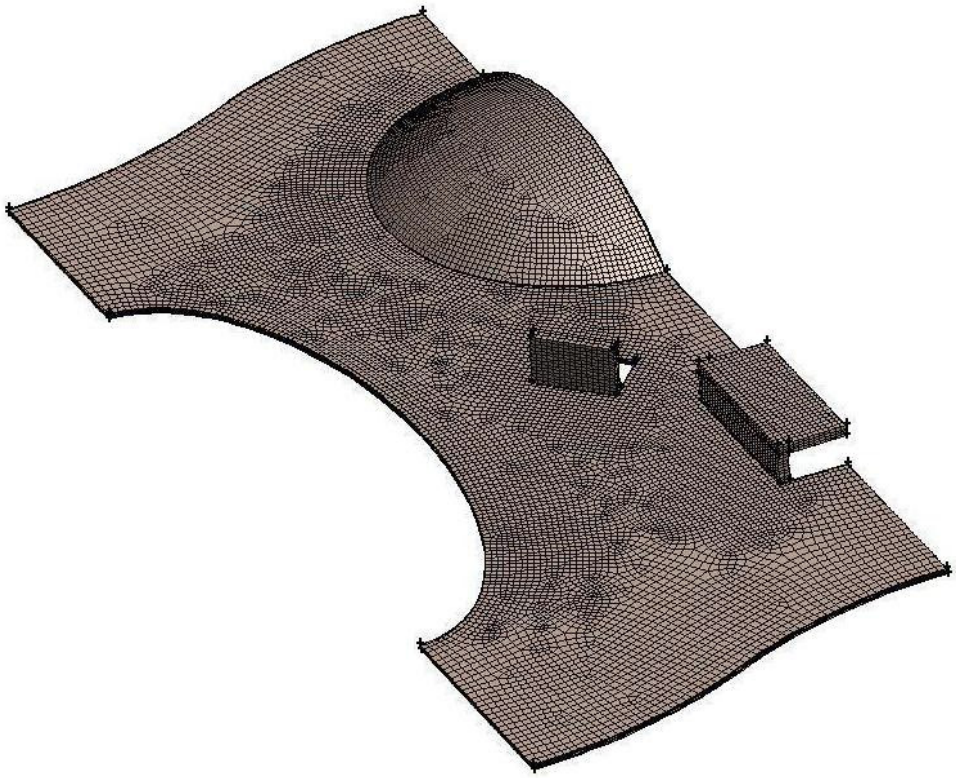

Figure 7.1. Meshes created on a fin surface.

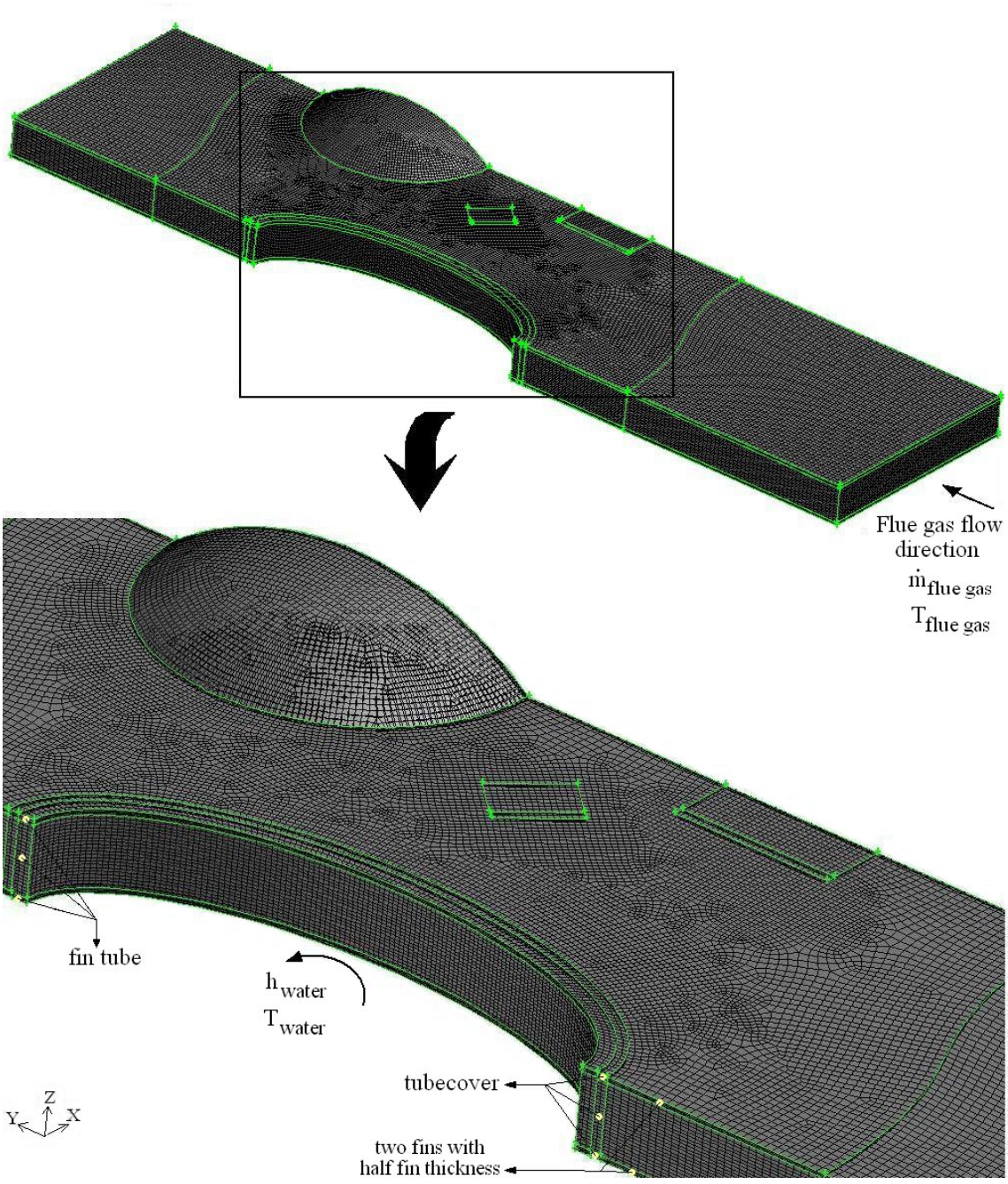

Figure 7.2. Meshes created for a heat exchanger model with symmetry boundary condition.

Four hexahedral finite volume elements along the thickness of the half fin and twenty to twenty three (depending on the model geometry) of the same elements along the gap between two fins are used. Hexahedral meshes are generated for each heat exchanger model. As a result, up to 600,000 (approximately) hexahedral volume elements are generated for the heat exchanger models depending on the investigated geometry. In order to create the volume meshes, face meshes are created firstly. The volume meshes are then generated using cooper algorithm, which projects the face meshes to the opposite face of the volume. The interval size values used to create the face meshes are summarized in Figure 7.3.

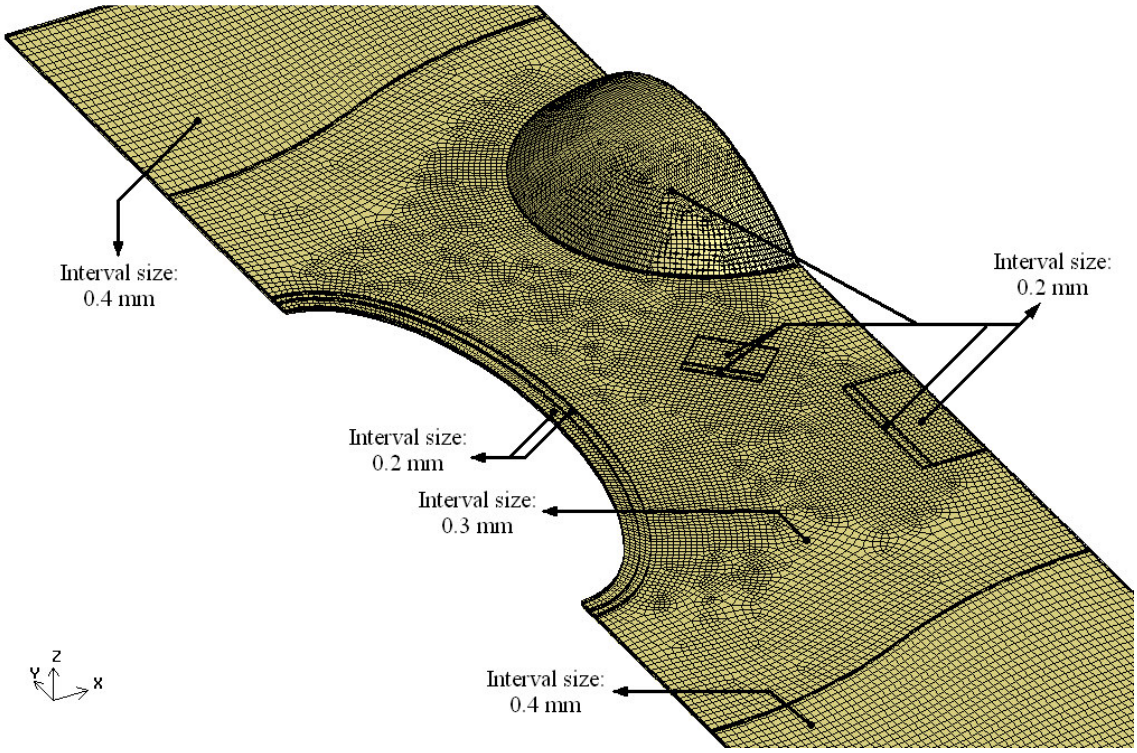

Figure 7.3. Interval size values used to create face meshes.

In order to determine the mesh number to be used along the gap between two fins, numerical analysis of a heat exchanger with plate fin is performed with different mesh numbers. It was found that the model, in which 20 elements along the gap between two fins are used, provides stable numerical solution in terms of heat transfer from the flue gas to the heating water and total pressure drop of flue gas across the heat exchanger as shown in Figures 7.4 and 7.5, respectively. It can be seen from Figures 7.4 and 7.5 that the use of lower mesh numbers than 20 along the gap between two fins leads to inaccurate heat transfer and total pressure drop values. However, when the

mesh number along this gap is increased beyond 20, it is observed that both heat transfer and total pressure drop values remain constant, which indicates that the use of 20 elements along the gap between two fins is appropriate to obtain realistic numerical solutions.

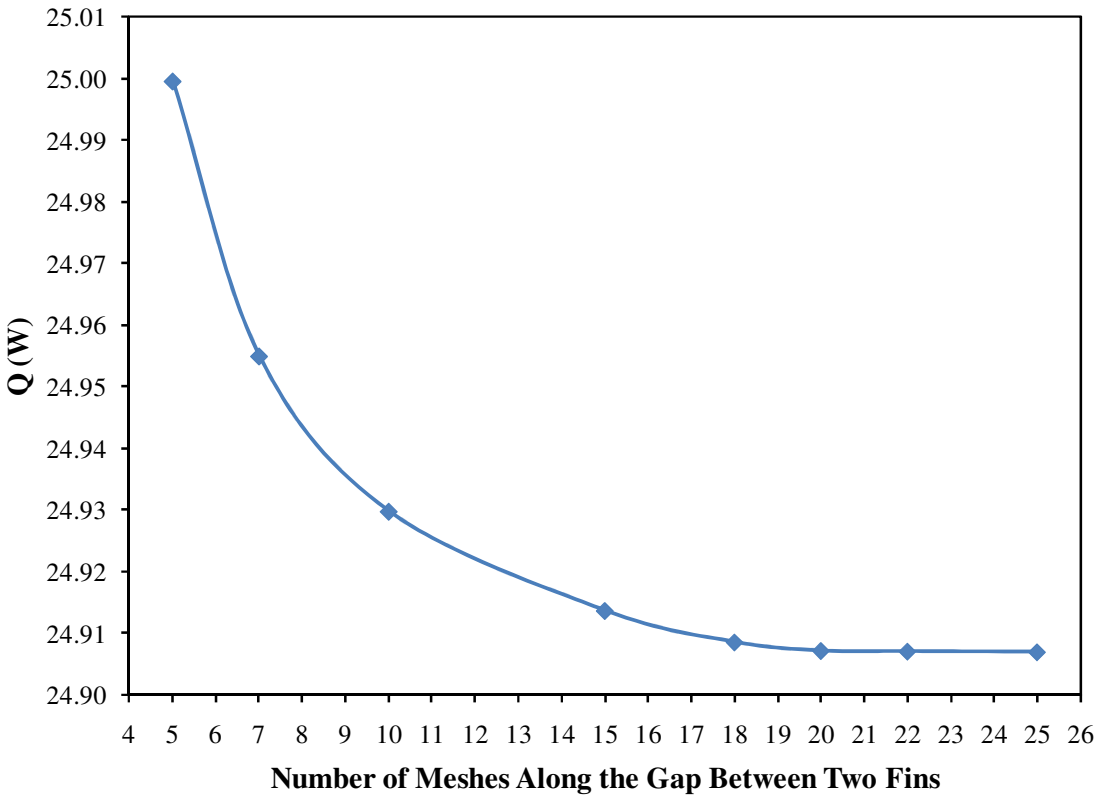

Figure 7.4. Heat transfer rate according to the number of meshes used along the gap between two fins.

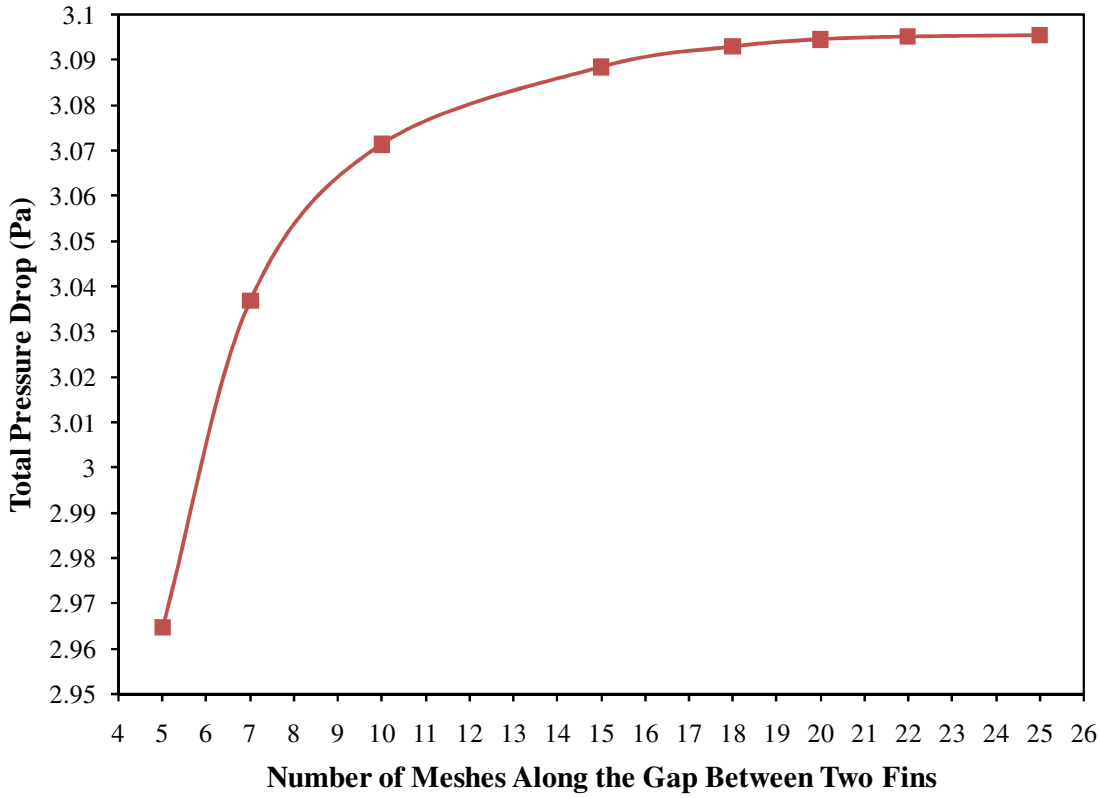

Figure 7.5. Total pressure drop across the heat exchanger according to the number of meshes used along the gap between two fins.

7.2. Meshing of the Models with Periodic Boundary Condition

The meshing operation for this case is similar to the case with symmetrical boundary condition. This time, the flue gas volume consists of two separate volumes. The mesh number created along the gap between two fins is also maintained as minimum 20. The meshes created for a heat exchanger are also shown in Figure 7.6.

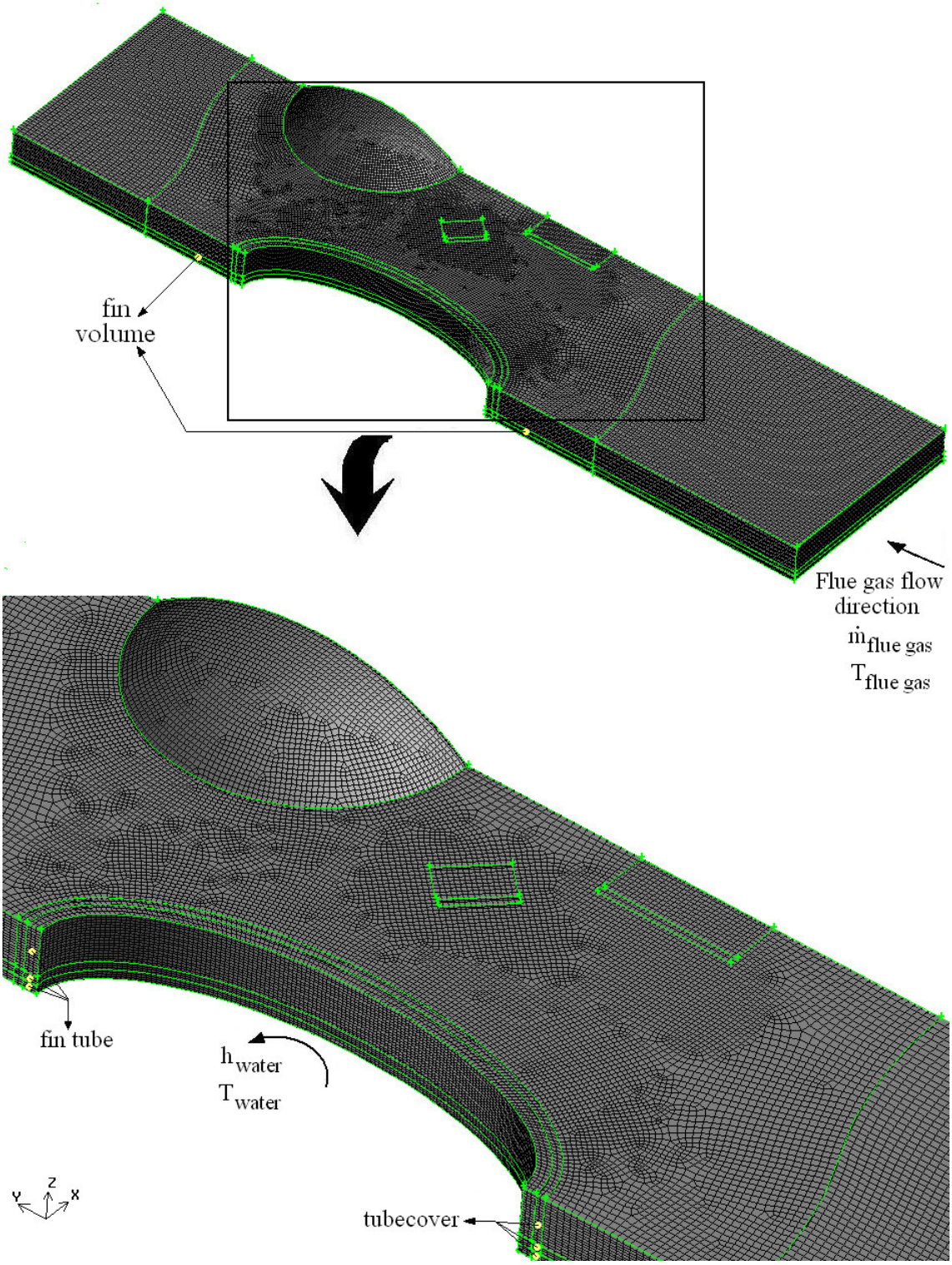

Figure 7.6. Meshes created for a heat exchanger model with periodic boundary condition.

7.3. Computational Details

7.3.1. Convergence of the Considered Problems

For the investigated heat exchanger problems, scaled residuals for velocities, continuity and energy equations are monitored during the iterative solutions and the following values are taken into consideration for the converged numerical results;

- Residual for continuity: $R^{c}_{scaled}=10^{-4}$
- Residuals for velocities in x, y and z directions: $R^{\Phi}_{scaled,velocity}=10^{-7}$
- Residual for energy: $R^{\Phi}_{scaled,energy}=10^{-7}$

The residual history of a heat exchanger model is illustrated in Figure 7.7. Similar residual histories are obtained for all of the investigated heat exchanger models.

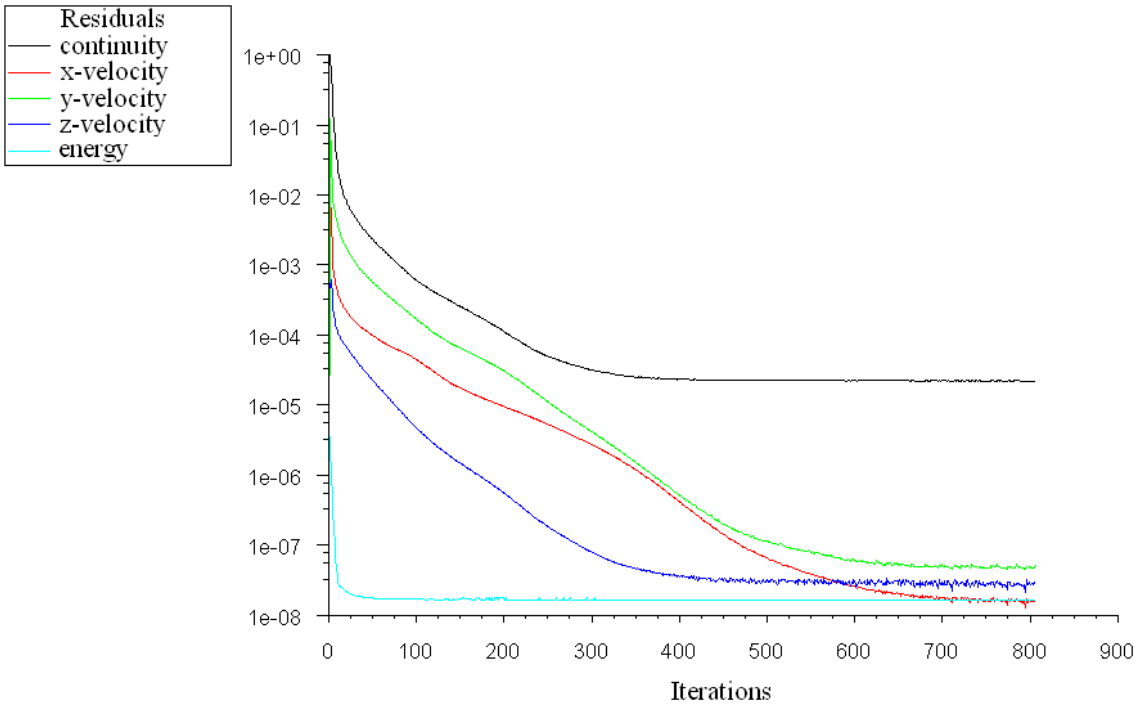

Figure 7.7. Residuals of a heat exchanger model solution.

However as it was mentioned previously, obtaining small residual values is not enough to obtain a converged solution in some cases. For this reason, the mass weighted average flue gas velocity and mass weighted average flue gas temperature at the outflow surface of the model are also monitored during the solutions and it was observed that

these two values also become constant after a certain number of iterations. The iterative solution procedure is not ended unless these two values become constant even if the residual values mentioned above are achieved. Consequently, lower residual values than the ones given above are achieved generally for the investigated problem solutions. The mass weighted average flue gas velocity and temperature at the outflow surface of a heat exchanger model are given in Figures 7.8 and 7.9 as an example. Similar results are obtained for all of the investigated models.

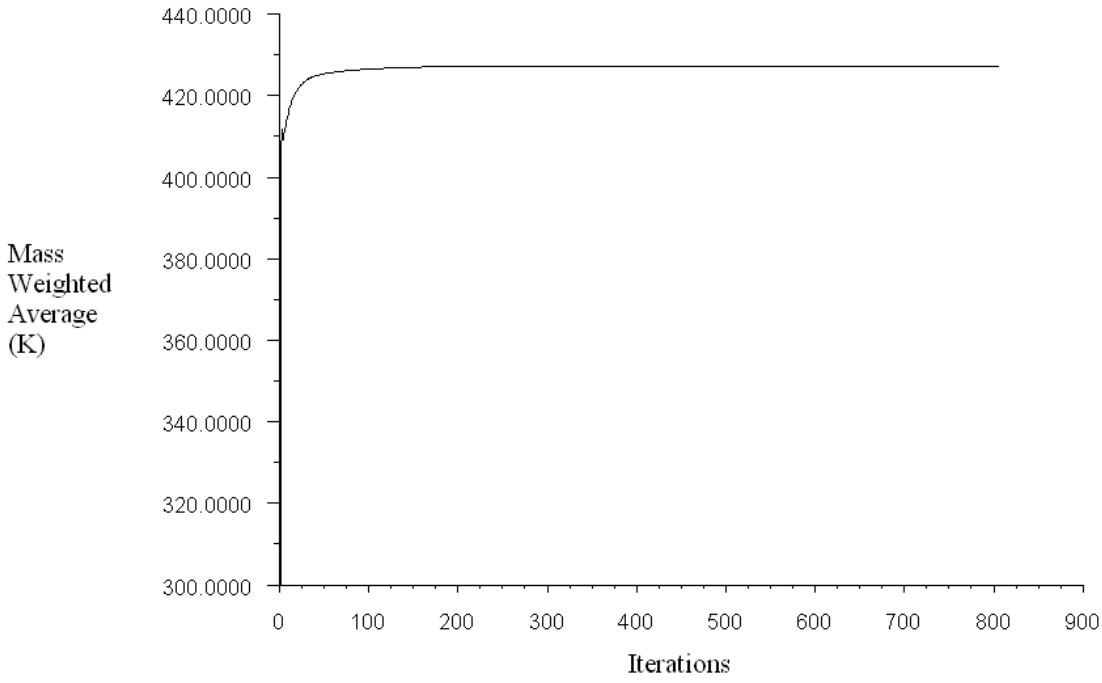

Figure 7.8. Mass weighted average flue gas temperature at the outflow surface of a heat exchanger model.

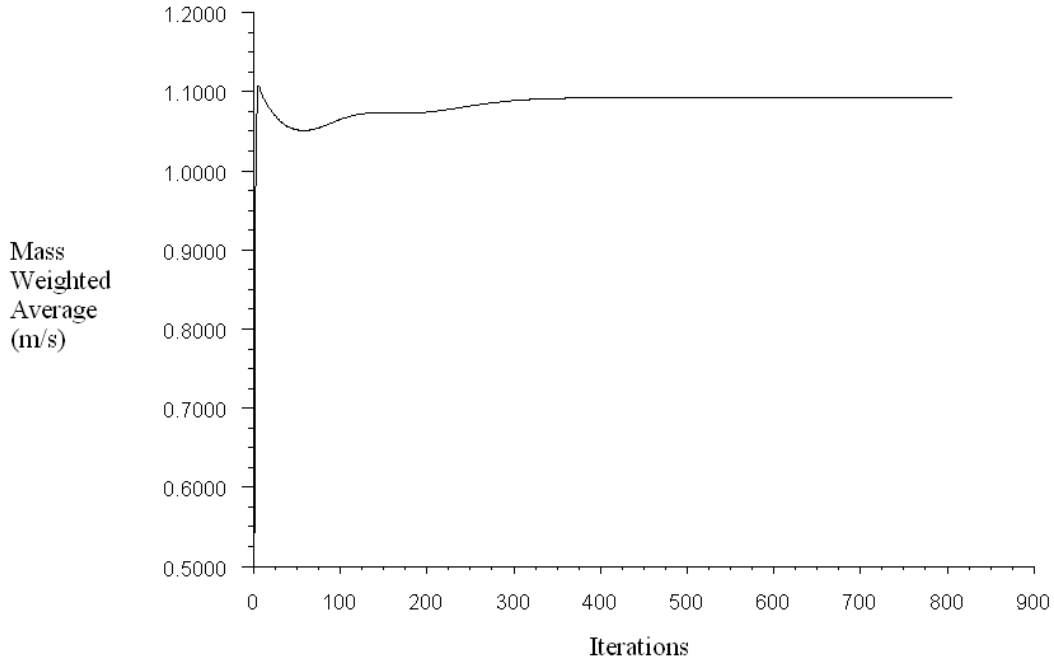

Figure 7.9. Mass weighted average flue gas velocity at the outflow surface of a heat exchanger model.

7.3.2. Under-Relaxation Factors for the Considered Problems

The constant under-relaxation factors (α) used in the solution of the present numerical problems can be listed as;

- Pressure: 0.3
- Momentum : 0.7
- Energy: 1

7.3.3. The Discretization Method for Convective Terms and the Used Pressure-Velocity Linkage Algorithm

First order convective discretization is selected for the numerical solution of the considered problems. Hexahedral meshes are generated for all of the volumes of the numerical models. In addition, the generated hexahedral meshes are mostly in the flow direction. Because of these reasons, the use of first order upwind scheme provides sufficient accuracy for the numerical solution. For the pressure-velocity coupling, SIMPLE algorithm is used for all of the investigated numerical problems.

CHAPTER 8

RESULTS AND DISCUSSION

The aim of this thesis is to determine the optimum fin and protrusion geometry of a finned tube gas to liquid heat exchanger. For this purpose, a combi boiler apparatus heat exchanger with actual operation conditions is investigated and several geometrical parameters are varied in order to find the optimum geometry. The cases summarized in chapter 3 are investigated step by step in this part of the study.

8.1. Comparison of the Numerical Models with an Experimental and Numerical Study

Before the numerical investigation of the fin parameters, a comparison with an experimental and numerical study available in literature is performed in order to test the reliability of the numerical models to be used in the optimization study. However, no other study, investigating fins with the same geometrical dimensions as the fins used in the present study, is encountered in the literature. So, the fins used in a similar study (Wu and Tao 2008b), in which the effects of a winglet pair on heat transfer are investigated numerically and experimentally, are analysed in order to accomplish validation of the current study. In addition to the lack of experimental study investigating the fins with the same geometrical dimensions, most of the studies available in literature do not provide clearly the experiment conditions or boundary conditions used in their investigation. Because of these reasons, the only study which provides the experimental conditions is decided to be used for comparison.

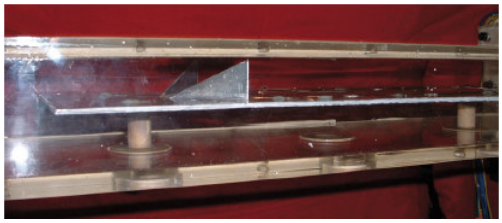

Figure 8.1. The experimental setup used in the study of Wu and Tao (2008b). (Source: Wu and Tao 2008b)

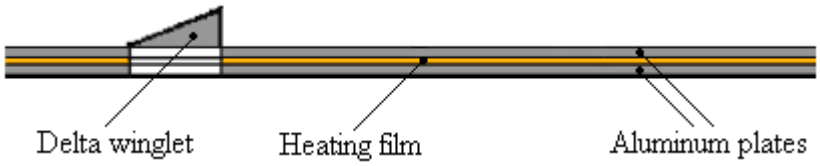

Figure 8.2. The fin used in the study of Wu and Tao (2008b).
(Source: Wu and Tao 2008b)

The view of the experimental setup used in Wu and Tao (2008b) and the fin used in experiments are given in Figures 8.1 and 8.2, respectively. The schematic view of the model to be used in numerical calculations in the present study is shown in Figure 8.3.

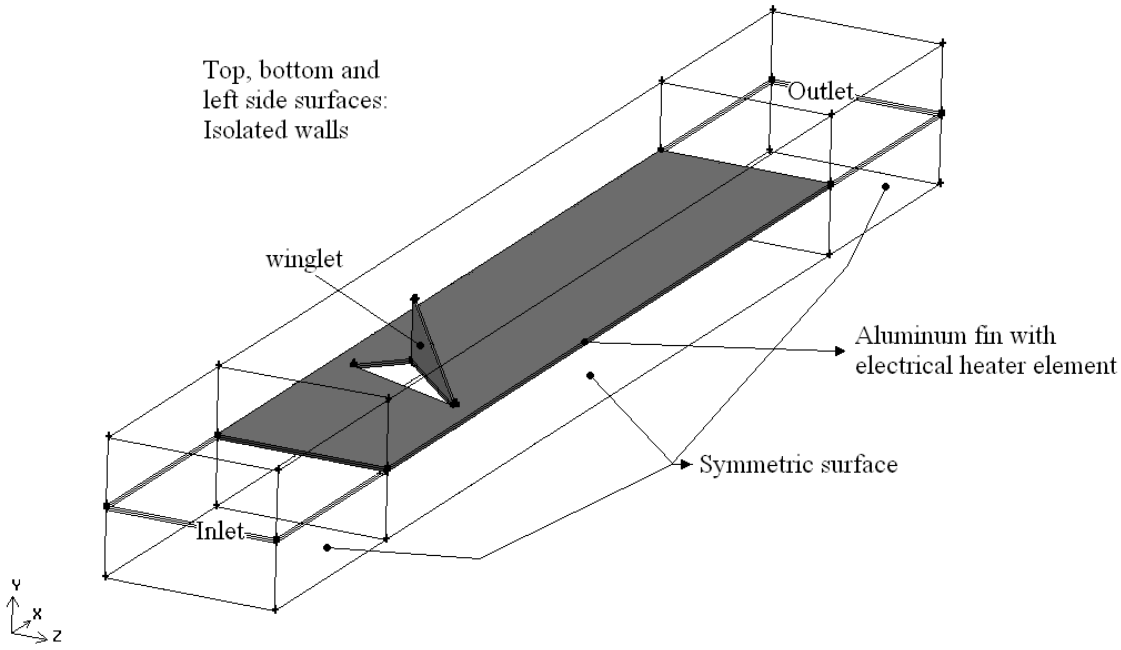

Figure 8.3. The schematic view of the computational model investigated in Wu and Tao (2008b).

The tests were conducted in a thermally isolated wind tunnel for different air velocity values in the study of Wu and Tao (2008b). The experimentally tested fins consisted of two aluminum layers with 1 mm thickness and an electrical heating element with 0.15 mm thickness in between the two aluminum layers as shown in Figure 8.2. As the fin is symmetric, half of the fin is considered for computational domain as shown in Figure 8.3. The dimensions of the air channel are 162 mm width and 62 mm height. The length of the fin is 400 mm and the delta winglet dimensions are 60 mm length and 27 mm height. A heating power of 35 W is supplied by the electrical

heater element and the average convective heat transfer coefficient over the upper and lower fin surfaces (h) was determined experimentally and numerically in Wu and Tao (2008b). The heating power given by the electrical heater element is considered as inner heat source for electrical heating element volume in the present model (7,291,667 W/m^3 for plate fin and 7,481,030 W/m^3 for the fin with winglet). The difference of the inner source values stems from the fact that there is a punched winglet hole in the model of the fin with winglet and this winglet hole changes the volume of the electrical heater element compared to the case of plate fin. Since the winglet angle of attack is taken as 45^o in the present study, the fin with the same winglet angle attack is taken into consideration for the comparison with the results of Wu and Tao (2008b). The models of the fins with the mentioned geometrical dimensions are created in the present study to accomplish the comparison of the numerical results obtained from Fluent software and the experimental and computational results of Wu and Tao (2008b). The meshes on the fin with winglet used in the present study for comparison purpose are given in Figure 8.4 and the complete model meshes are presented in Figure 8.5.

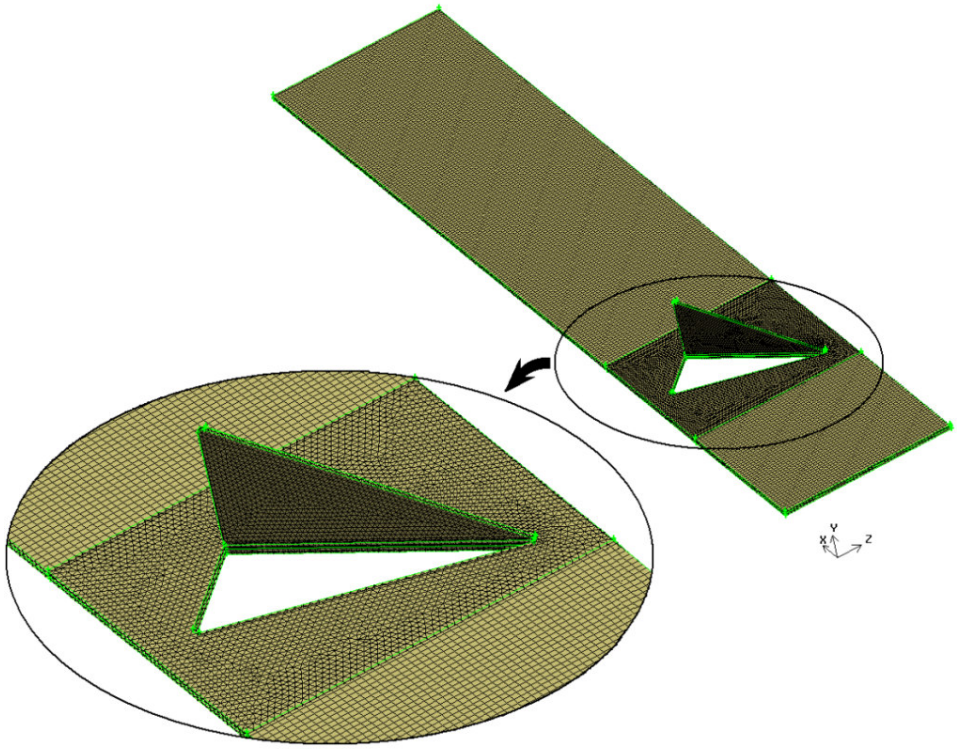

Figure 8.4. Meshes created on the fin surface investigated in Wu and Tao (2008b).

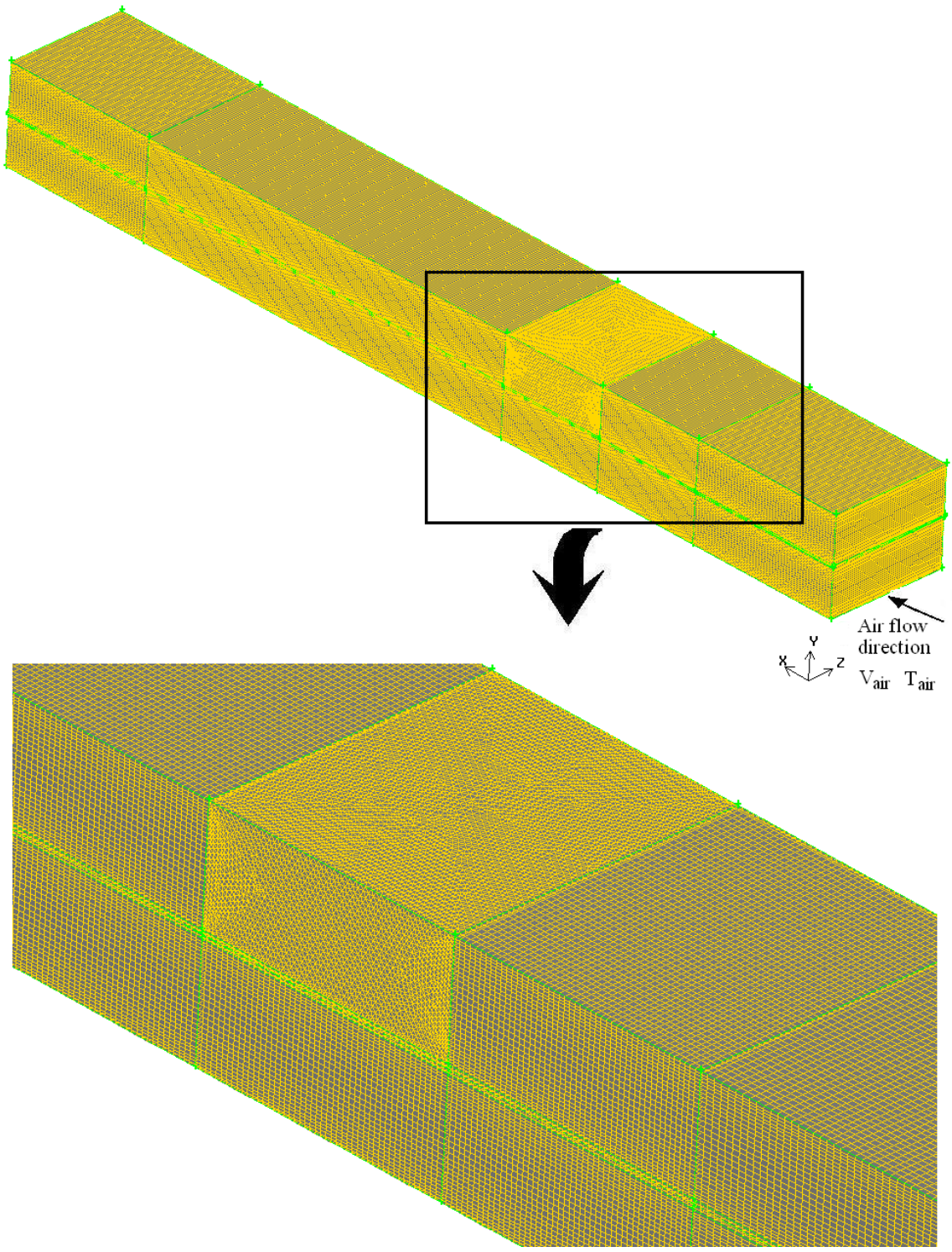

Figure 8.5. Meshes created for the heat exchanger model with winglet investigated in Wu and Tao (2008b).

As the number of control volumes is limited with the available computer source, approximately 1,200,000 control volume elements for plate fin and 1,760,000 control volume elements for the fin with winglet are used in the analysis. The total control volume elements used for the analysis of the fins investigated in the present study are less than the values of the models used for comparison purpose. However, since the geometrical dimensions of the fins investigated in Wu and Tao (2008b) are considerably greater than the ones of the fins examined in the present study and the wind tunnel channel height and width are significantly greater than the distance between the fins (2.6 mm) and the width of one tenth fin segment (17.5 mm) investigated in this study, the mesh quality for the fins investigated in the present study is noticeably finer.

The convective heat transfer coefficient results obtained from the numerical analysis for plate fin and for the fin with winglet are compared with the experimental and computational results of Wu and Tao (2008b) in Figures 8.6 and 8.7, respectively.

It can be seen that there is a good agreement between the results of present study and the ones of Wu and Tao (2008b) for both plate fin and fin with winglet cases. It is concluded that, since finer meshes are employed for the analysis of the fins in the present study and the use of coarser meshes in the comparison part of the study shows a satisfactory agreement with the results of Wu and Tao (2008b), the numerical results obtained for the analysis of the fins in the present study are reliable.

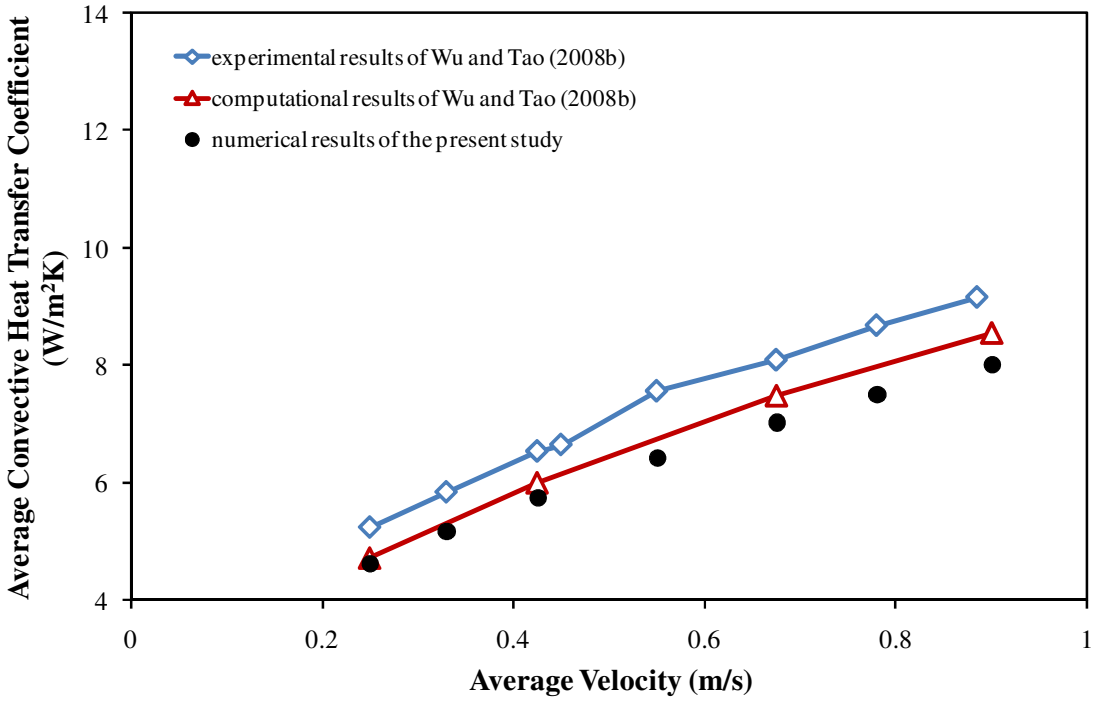

Figure 8.6. Comparison of the numerical results of the present study with the results of Wu and Tao (2008b) for the plate fin.

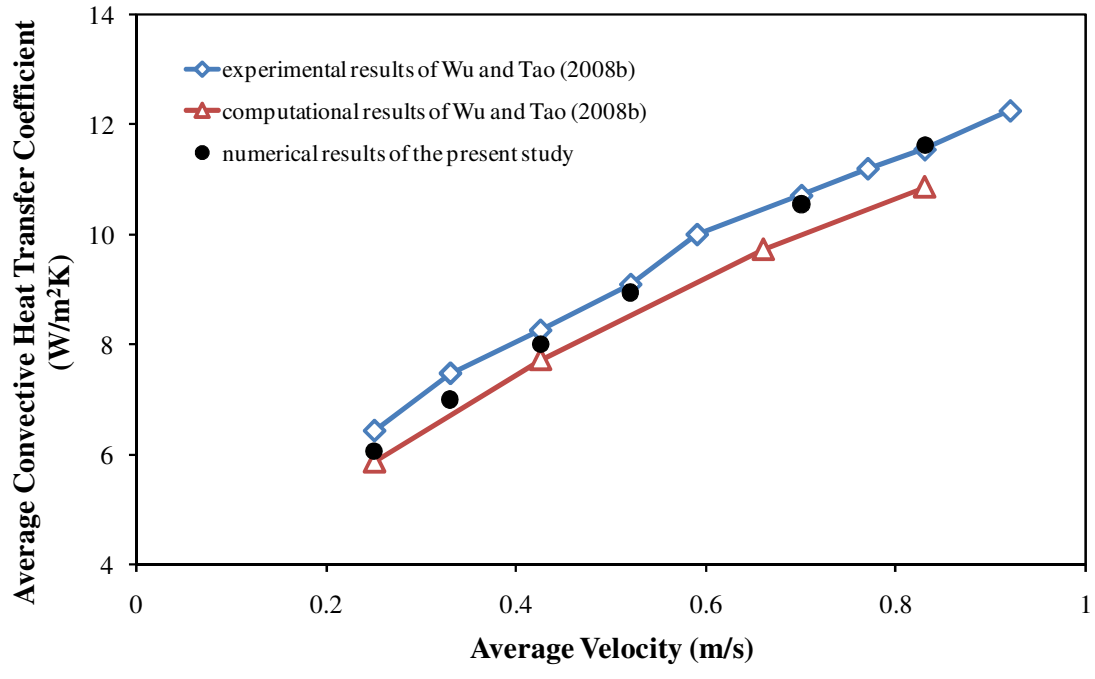

Figure 8.7. Comparison of the numerical results of the present study with the results of Wu and Tao (2008b) for the fin with a winglet with 45^{o} angle of attack.

8.2. Numerical Investigation with the Models with Symmetry Boundary Condition

The parametric study, conducted in order to determine the best fin and protrusion geometry, is accomplished with the models with symmetry boundary condition in this section. The comparison of the models with symmetry and periodic boundary conditions is also made after the determination of the best fin in this section.

8.2.1. The Effect of Fin Height and Fin Tube Thickness

The influence of plate fin height and fin tube thickness is examined firstly. The fin height (L) is varied between 35 mm and 40 mm while the ellipticity of the fin (b/a), location of fin tube (L_1) and fin tube thickness (t) are kept constant. In addition, the fin tube thickness value is also changed between 0.6 mm and 1.2 mm while the other parameters are constant. The schematic view of a plate fin and the investigated parameters are illustrated in Figure 8.8. The dimensions of the examined plate fins are given in Table 8.1 as well.

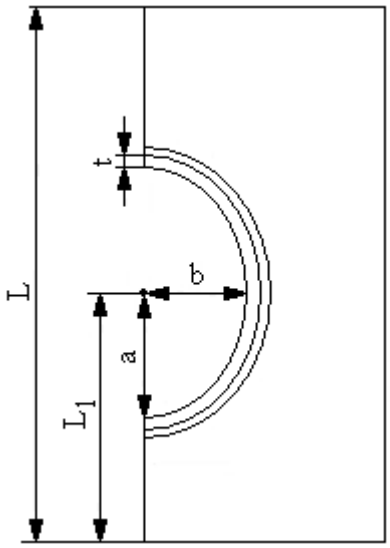

Figure 8.8. Schematic view of a plate fin.

Table 8.1. Dimensions of plate fins.

Model Name	L (mm)	t (mm)	L_1 (mm)	Ellipticity (b/a)
P-35mm-0.8mm	35	0.8	15.5	0.7345
P-35mm-0.6mm	35	0.6	15.5	0.7345
P-35mm-1.2mm	35	1.2	15.5	0.7345
P-38mm-0.8mm	38	0.8	15.5	0.7345
P-40mm-0.8mm	40	0.8	15.5	0.7345

The transferred heat from the flue gas to the heating water passing through the fin tube and the flue gas total pressure drop are calculated numerically using Fluent software with the boundary conditions explained in chapter 6 and the numerical results are presented in Table 8.2. Normalized heat transfer and total pressure drop values are also presented by taking the values of the model P-35mm-0.8mm as 100% in order to enable the comparison of the fins easier. The temperature distributions on the plate fins are also given in Figure 8.9. The effect of the changes in fin tube thickness is illustrated in Figure 8.10 and the fin length effect is illustrated in Figure 8.11.

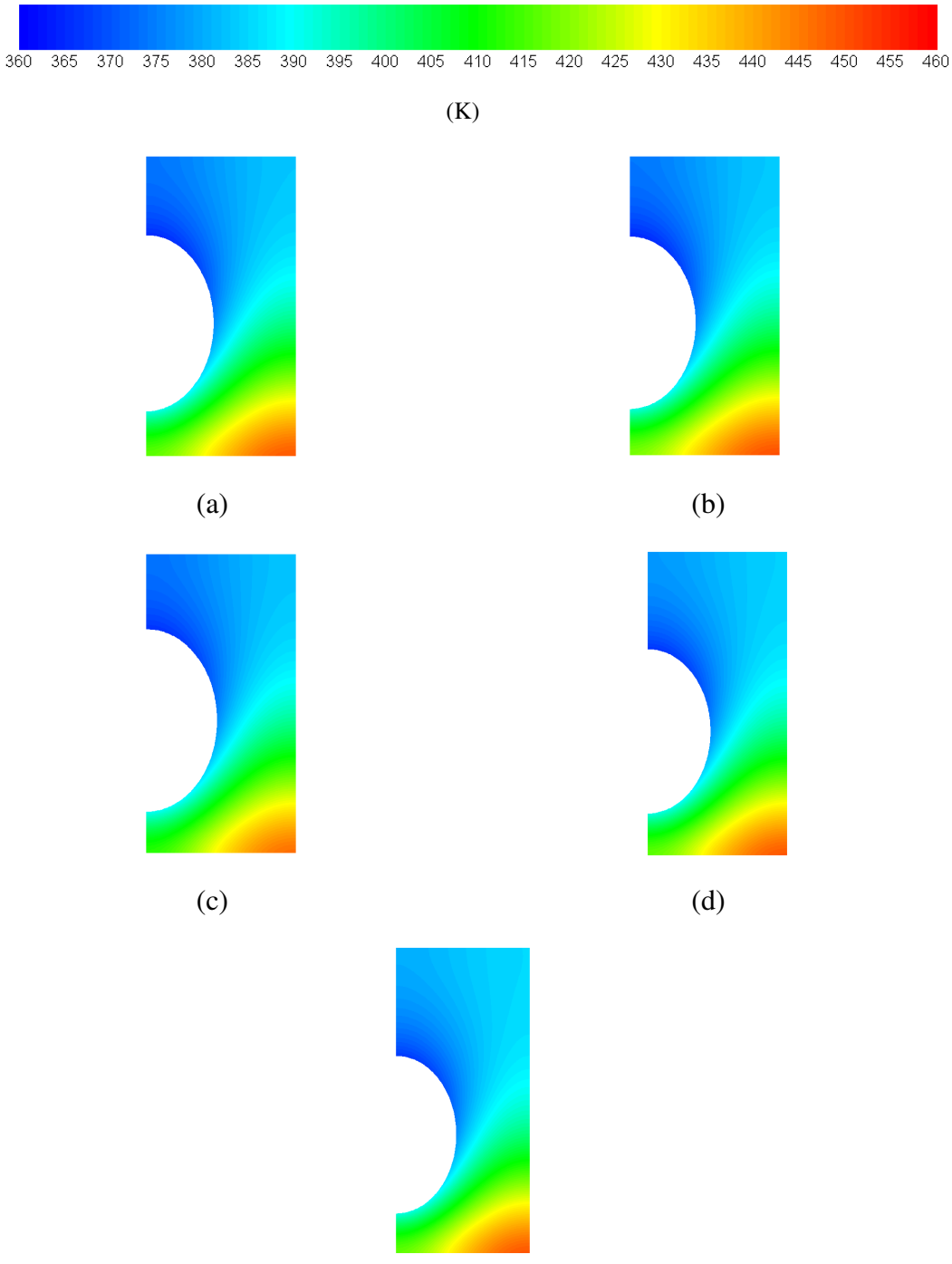

Figure 8.9. Temperature distribution on the plate fins (a) P-35mm-0.8mm (b) P-35mm-0.6mm (c) P-35mm-1.2mm (d) P-38mm-0.8mm (e) P-40mm-0.8mm.

It can be observed from Figures 8.9 (a), (b) and (c) that as the fin tube thickness is decreased, the hotter part on the fin (red part on the figures) enlarges, which indicates that higher heat is transferred from the flue gas to the heating water. This result can also be observed from the numerical results given in Table 8.2, as well as from Figure 8.10.

Table 8.2. Heat transfer and pressure drop values of plate fins.

Model Name	Q (per segment) (W)	Normalized Q (%)	Total Pressure Drop (Pa)	Normalized Total Pressure Drop (%)
P-35mm-0.8mm	24.0611	100	3.3649	100
P-35mm-0.6mm	24.1179	100.236	3.2894	97.756
P-35mm-1.2mm	23.9364	99.482	3.5294	104.889
P-38mm-0.8mm	24.3960	101.392	3.5024	104.086
P-40mm-0.8mm	24.5797	102.155	3.5915	106.734

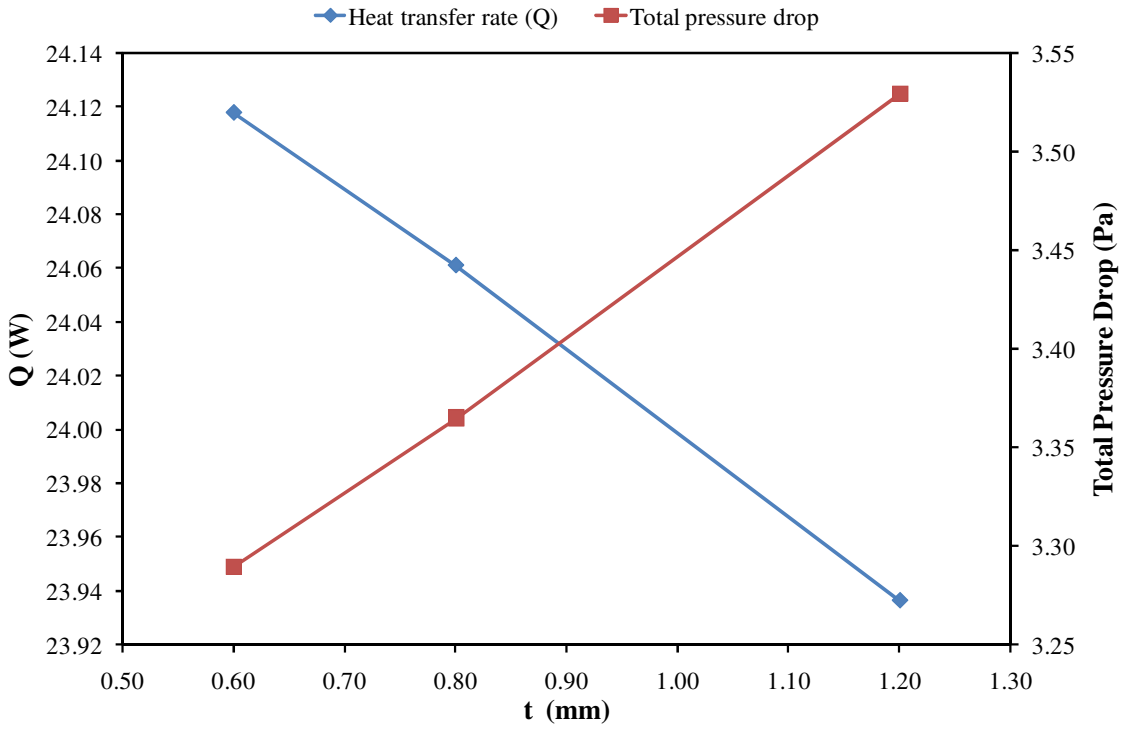

Figure 8.10. The effect of fin tube thickness on heat transfer and total pressure drop.

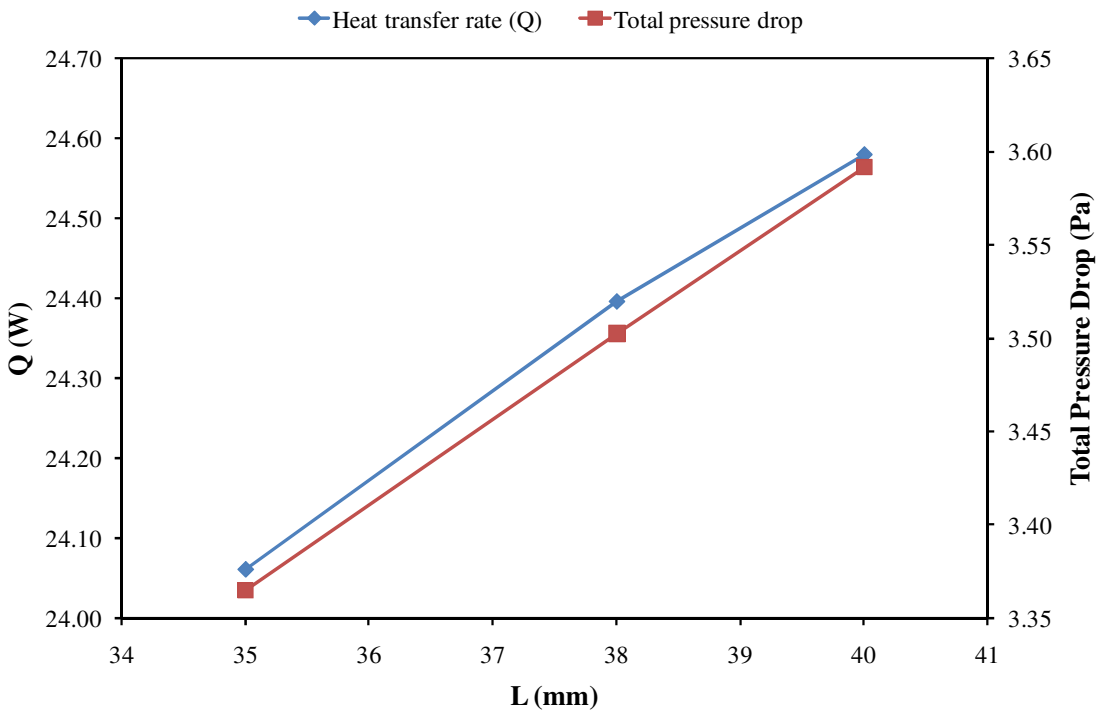

Figure 8.11. The effect of fin height on heat transfer and total pressure drop.

It can be seen from the results of this part of the study that the model P-40mm-0.8mm with a fin height of 40 mm is the best fin in terms of heat transfer performance, as expected. The higher fin heat transfer surface area of the model P-40mm-0.8mm provides the highest heat transfer rate from the flue gas to the heating water. It is also seen that the model P-40mm-0.8mm does not create an excessive pressure drop value when compared with the model P-35mm-0.8mm with a fin height value of 35 mm. Another conclusion of this part of the study is that the heat transfer and pressure drop performance of the fin with a thinnest fin tube (P-35mm-0.6mm), which has a 0.6 mm thick fin tube is the best compared to the fins P-35mm-0.8mm with a 0.8 mm thick fin tube and P-35mm-1.2mm with a 1.2 mm thick fin tube. The block effect of the fin tube and tubecover on the flue gas flow reduces when the fin tube thickness is decreased. Therefore, lower total pressure drop is created when the fin tube thickness is thinner.

As a result of these conclusions, it is decided to continue the optimization study with a plate fin with a fin height value of 40 mm and a fin tube thickness value of 0.6 mm.

8.2.2. The Effect of Fin Tube Location and Ellipticity

In order to determine the optimum fin tube shape and location, 16 different fins are investigated in this section of the study. These fins are grouped in 4 different types according to their fin tube ellipticity (b/a). One group consists of the fins with cylindrical fin tubes (b/a=1) while the other three groups have elliptical fin tubes. The fin tube ellipticity values are taken as 0.7345, 0.55 and 0.45. Since the ellipticity value of fin tube is different for each group, the convection coefficient of water flowing through the fin tube is also changed for each group in the numerical solution process. The same heat transfer area between the tubecover outer surface and flue gas flow is maintained while determining the dimensions of other fin tubes.

The perimeter of the elliptical tubecover outer surface which is in contact with the flue gas flow can be calculated as;

$$U = \pi \times (a' + b') \tag{8.1}$$

where, a' (= a + fin tube thickness (0.6 mm) + tubecover thickness (0.4 mm)) and

b'(= b + fin tube thickness (0.6 mm) + tubecover thickness (0.4 mm)) are the radii values of the tubecover ellipse.

As an example, for the fin tube with ellipticity value of 0.7345, U is calculated as 55.8685 mm (a'= 10.1 mm and b'=7.6835 mm). This value is used to calculate the a' and b' values of the fin tube with ellipticity value of 0.45. As a result, a is found as 10.885 mm and b is found as 4.9 mm for the fin tube with ellipticity value of 0.45. The same calculations are also conducted for the remaining two types and the following fin tube dimensions are determined.

Table 8.3. Dimensions of the fin tubes with different ellipticity values.

Fin tube ellipticity (b/a)	a	b
1	7.9	7.9
0.7345	9.1	6.6835
0.55	10.183	5.6
0.45	10.885	4.9

The velocity of water flow inside the fin tube is different for 4 different fin tubes since the mass flow rate of water is taken as constant 0.2866 kg/s and the cross sectional area of the fin tube is different for each type. So, the convective heat transfer coefficient, which will be the boundary condition for the models, will differ for each group with different fin tube ellipticity values. The convective heat transfer coefficient is calculated using Equation 6.19 and the following results are found for each group;

- For the fin tubes with ellipticity value of 1; h_{water} = 9870 W/m^{2}K
- For the fin tubes with ellipticity value of 0.7345; h_{water} = 10000 W/m^{2}K
- For the fin tubes with ellipticity value of 0.55; h_{water} = 10800 W/m^{2}K
- For the fin tubes with ellipticity value of 0.45; h_{water} = 11550 W/m^{2}K

Table 8.4. Dimensions of plate fins with different ellipticity values.

	Model Name	L (mm)	L_1 (mm)	Ellipticity (b/a)
Type 1	c-12.5mm	40	12.5	1
	c-15.5mm	40	15.5	1
	c-18.5mm	40	18.5	1
	c-21.5mm	40	21.5	1
Type 2	e0.7345-12.5mm	40	12.5	0.7345
	e0.7345-15.5mm	40	15.5	0.7345
	e0.7345-18.5mm	40	18.5	0.7345
	e0.7345-21.5mm	40	21.5	0.7345
Type 3	e0.55-12.5mm	40	12.5	0.55
	e0.55-15.5mm	40	15.5	0.55
	e0.55-18.5mm	40	18.5	0.55
	e0.55-21.5mm	40	21.5	0.55
Type 4	e0.45-12.5mm	40	12.5	0.45
	e0.45-15.5mm	40	15.5	0.45
	e0.45-18.5mm	40	18.5	0.45
	e0.45-21.5mm	40	21.5	0.45

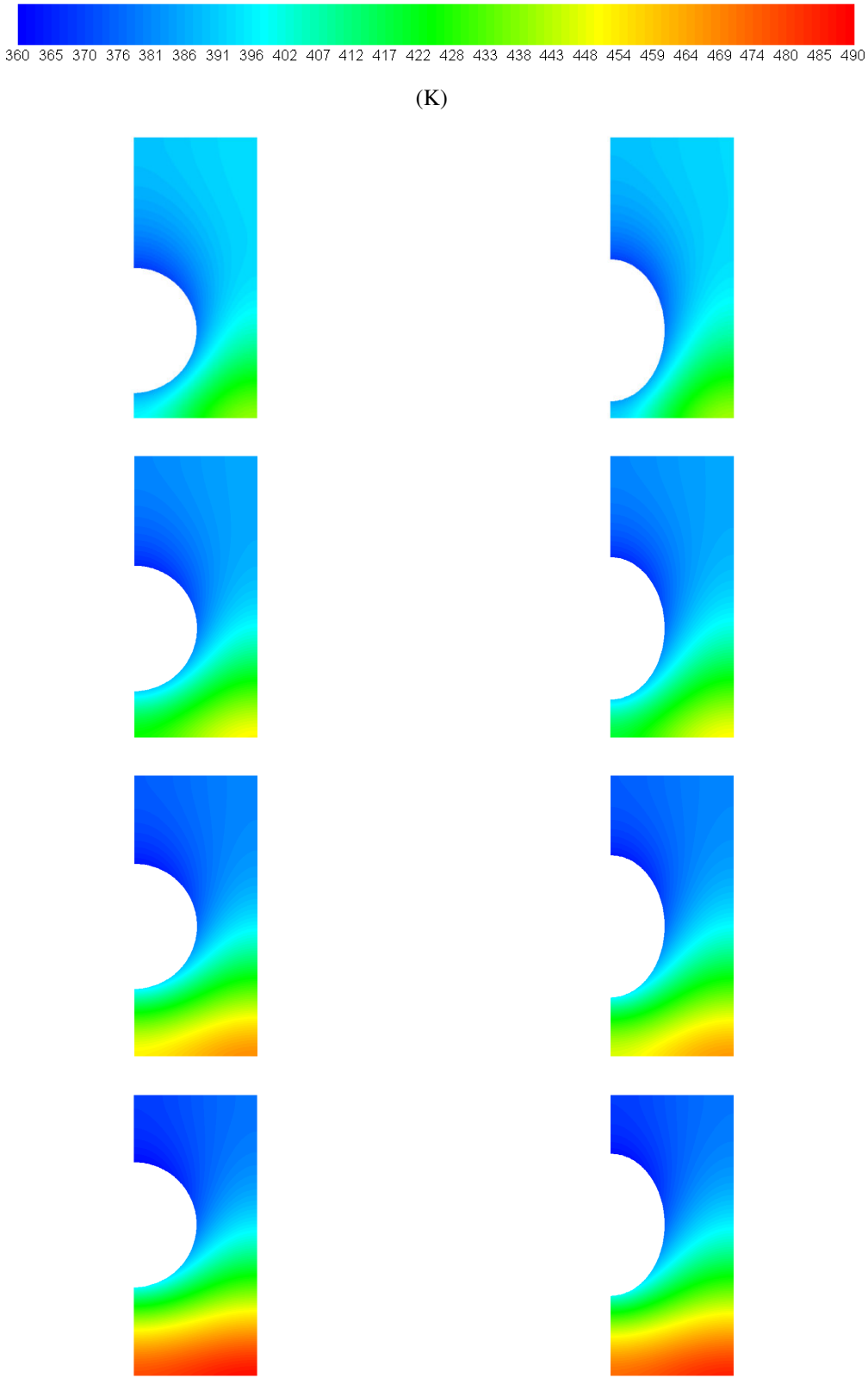

Figure 8.12. Temperature distribution on the plate fins with different fin tube ellipticity values (a) Ellipticity=1 (b) Ellipticity=0.7345 (c) Ellipticity=0.55 (d) Ellipticity=0.45. (cont. on next page)

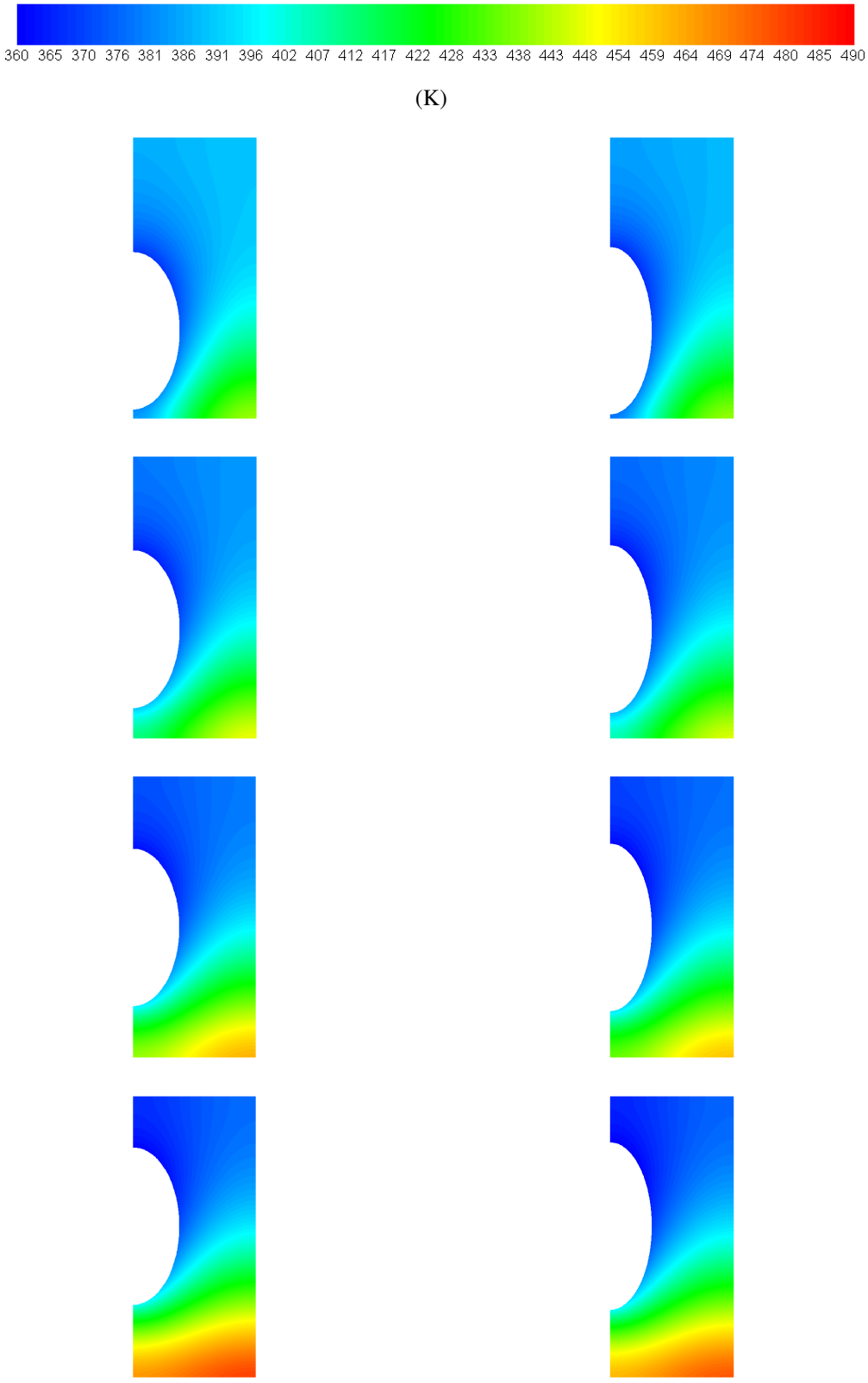

Figure 8.12. Temperature distribution on the plate fins with different fin tube ellipticity values. (a) Ellipticity=1 (b) Ellipticity=0.7345 (c) Ellipticity=0.55 (d) Ellipticity=0.45. (cont.)

Four different fin tube locations are investigated for each group. These locations are defined as 12.5 mm, 15.5 mm, 18.5 mm and 21.5 mm away from the bottom point of fin. The location of fin tube is shown as L_1 in Figure 8.8 and the dimensions used in this section are tabulated in Table 8.4.

The numerical results of heat transfer and pressure drop values for the plate fins with different ellipticity values are calculated using Fluent software and tabulated in Table 8.5. In this section, the normalized heat transfer and total pressure drop values are calculated by assuming the values of the model c-12.5mm as 100%. The temperature distributions on the fins investigated in this part of the thesis are given in Figure 8.12.

Table 8.5. Heat transfer and pressure drop values of plate fins with different fin tube ellipticity values.

	Model Name	Q (Per segment) (W)	Normalized Q (%)	Total Pressure Drop (Pa)	Normalized Total Pressure Drop (%)
Type 1	c-12.5mm	24.3610	100.000	3.9502	100.000
	c-15.5mm	24.4242	100.259	3.9015	98.767
	c-18.5mm	24.4551	100.386	3.8706	97.985
	c-21.5mm	24.4540	100.382	3.8489	97.436
Type 2	e0.7345-12.5mm	24.5508	100.779	3.5625	90.185
	e0.7345-15.5mm	24.6187	101.058	3.5165	89.021
	e0.7345-18.5mm	24.6425	101.156	3.4897	88.342
	e0.7345-21.5mm	24.6235	101.078	3.4793	88.079
Type 3	e0.55-12.5mm	24.7073	101.422	3.3023	83.598
	e0.55-15.5mm	24.7858	101.744	3.2598	82.522
	e0.55-18.5mm	24.8082	101.836	3.2351	81.897
	e0.55-21.5mm	24.7907	101.764	3.2280	81.717
Type 4	e0.45-12.5mm	24.8047	101.821	3.1573	79.928
	e0.45-15.5mm	24.8825	102.141	3.1172	78.912
	e0.45-18.5mm	24.9072	102.242	3.0939	78.323
	e0.45-21.5mm	24.8889	102.167	3.0883	78.181

The effects of the fin tube location and fin tube ellipticity are also illustrated in Figure 8.13. It can be observed from Figure 8.13 that as the ellipticity value of the fin tube is decreased (as more elliptical tube is used), the heat transferred across the heat exchanger increases. The increased ellipticity also affects pressure drop positively. This result stems from the increase in cross section of flue gas flow when more elliptical fin tube is used. Elliptical tube results less drag than the circular tube due to its better aerodynamic shape. This shape also causes better heat transfer characteristics.

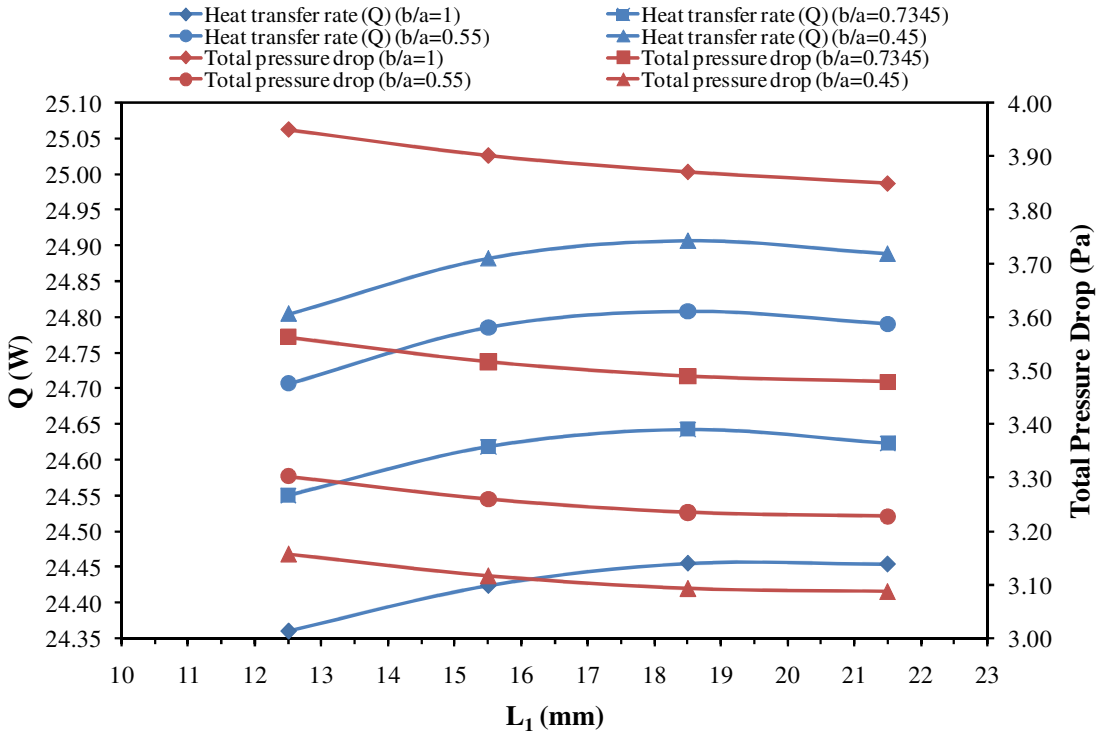

Figure 8.13. The effect of fin tube location and ellipticity on heat transfer and total pressure drop.

The second outcome is that when the fin tube is placed at downstream region, there is an increase in heat transfer while the flue gas total pressure drop decreases as can be observed from Figure 8.13. These results are consistent with the findings given in the studies of Kim and Song (2002) and Erek et al. (2005). However, the enhancement in heat transfer is found to be valid up to a certain value as can be seen from Table 8.5 and Figure 8.13. It is seen that the best fin tube position is at a distance of 18.5 mm away from the bottom of the fin since maximum heat transfer value is obtained at this location. The velocity contours of the models e0.45-18.5mm and e0.45-21.5mm at the middle surface of the gap between two fins are given in Figure 8.14. It

can be seen that flue gas accelerates earlier for the model e0.45-18.5mm because of the fin tube presence at upstream region compared to the model e0.45-21.5mm. It is also observed that the wake region of the model e0.45-21.5mm is larger than the one of the model e0.45-18.5mm. The heat transfer performance of all of the fins for which L_1=18.5 mm are better than the case of L_1=21.5 mm because of these reasons.

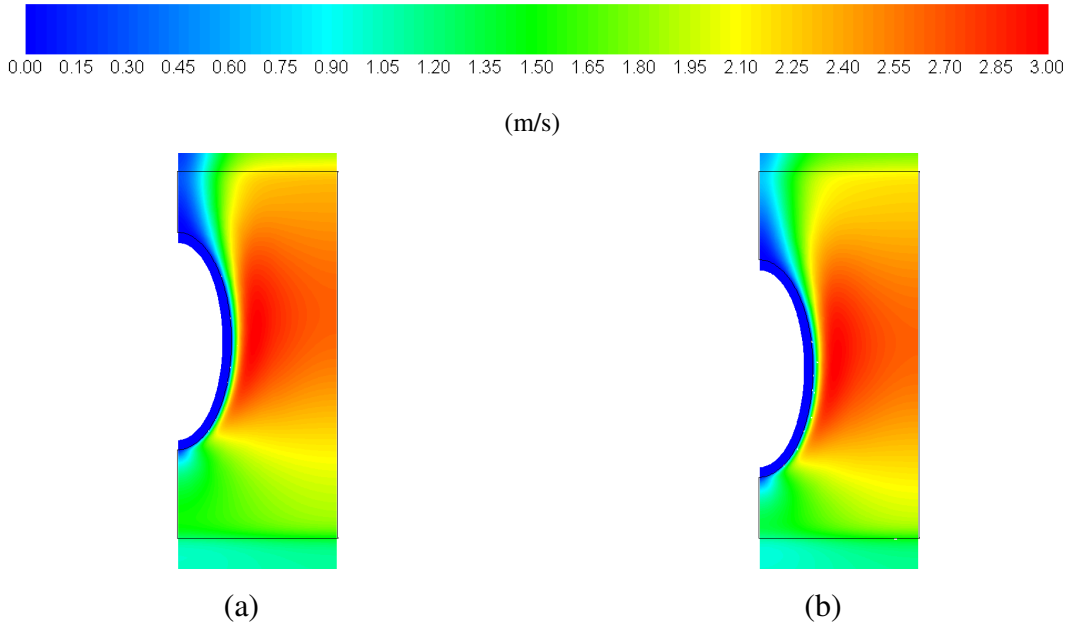

Figure 8.14. Velocity contours at the middle surface of the gap between two fins (a) for the model e0.45-21.5mm (b) for the model e0.45-18.5mm.

Additionally, the velocity vectors at the middle surface between two fins are given for the models c-18.5mm, e0.7345-18.5mm and e0.45-18.5mm in Figures 8.15, 8.16 and 8.17, respectively. The early flow separation and the rotating fluid at the wake region of the cylindrical fin tube are clearly seen from the Figure 8.15. This separation and fluid rotation also results in lower heat transfer value obtained by the use of cylindrical fin tube. The area, where the fluid is rotating, does not contribute to the heat transfer. The flow separation is encountered later as more elliptical tube is used, as can be observed from Figures 8.16 and 8.17. Moreover, the rotating fluid behind the cylindrical fin tube is not observed for elliptical tubes and as more elliptical tube is used, the flow becomes continuous at the wake region of the tube as illustrated in Figures 8.16 and 8.17.

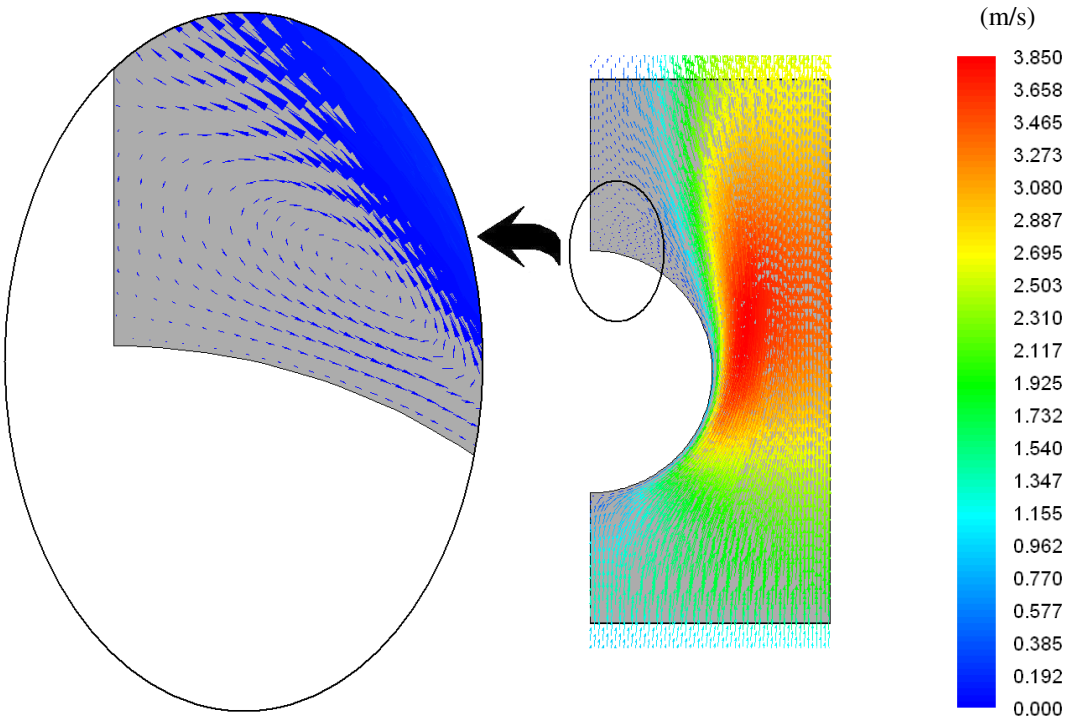

Figure 8.15. Velocity vectors at the middle plane between two fins for the model c-18.5mm.

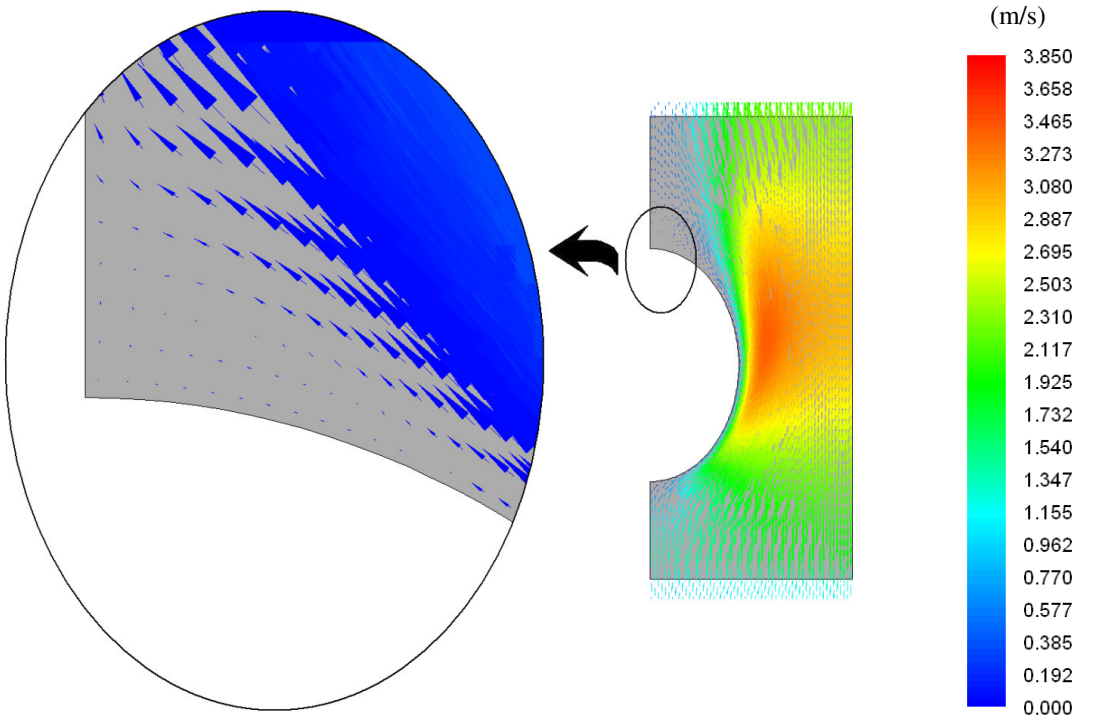

Figure 8.16. Velocity vectors at the middle plane between two fins for the model e0.7345-18.5mm.

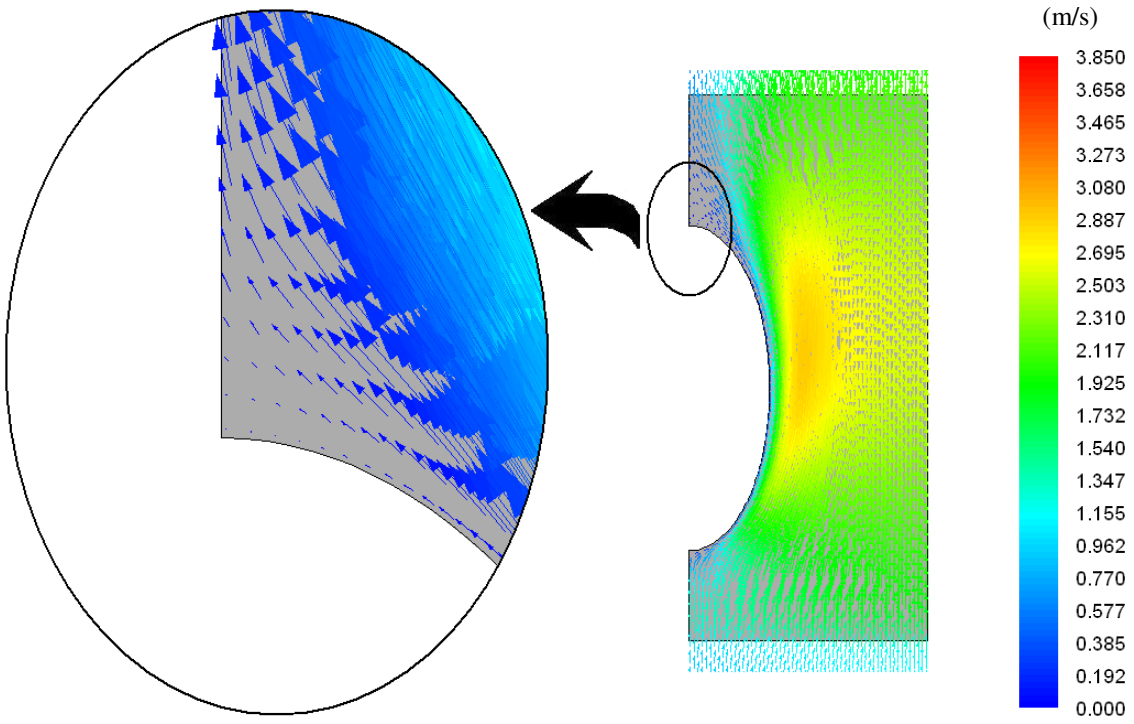

Figure 8.17. Velocity vectors at the middle plane between two fins for the model e0.45-18.5mm.

As a result, it is decided to continue the study with a fin having a fin tube with ellipticity value of 0.45. The location of fin tube is chosen at 18.5 mm away from the bottom point of the fin according to the results.

8.2.3. The Effect of Fin Shape

8.2.3.1. Fin Shape Study 1

In this part of the study, wavy fins are investigated. However, the wavy fin definition used before for corrugated fins does not define the fins under consideration in this thesis. The present wavy fins investigated in this study are also plate fins. However their upper and bottom parts are in wavy shape as illustrated in Figure 8.18. The fin heat transfer surface of wavy fins is kept the same as the plate fins in order to make the comparison between two fin types possible.

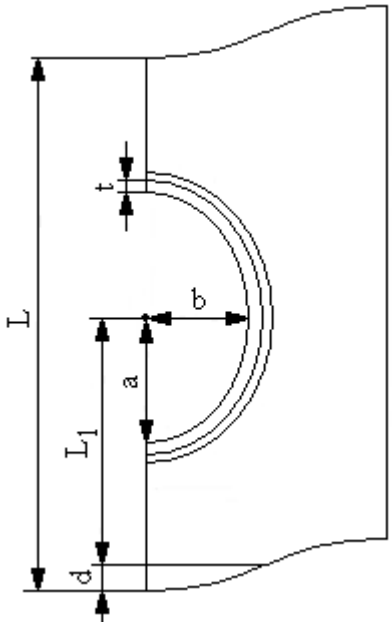

Figure 8.18. Schematic view of a wavy fin.

The wave height (d) is changed between 1 mm and 5 mm. Four different wave height values, namely 1, 2, 3 and 5 mm, are investigated. The dimensions used in this part of the study are summarized in Table 8.6.

Table 8.6. Dimensions of wavy fins.

Model Name	L (mm)	L_1 (mm)	Ellipticity (b/a)	d (mm)
wavy-d1mm	40	18.5	0.45	1
wavy-d2mm	40	18.5	0.45	2
wavy-d3mm	40	18.5	0.45	3
wavy-d5mm	40	18.5	0.45	5

The heat transfer and fluid flow problems are solved, numerically, to obtain the total heat transfer rate of the heat exchanger and the total pressure drop value of flue gas as it passes across the heat exchanger. In order to compare the wavy fins with plain fins, the values of the plain fin with the same geometrical dimensions (e0.45-18.5mm) are taken as 100% and normalized values of heat transfer and total pressure drop values are calculated with this assumption.

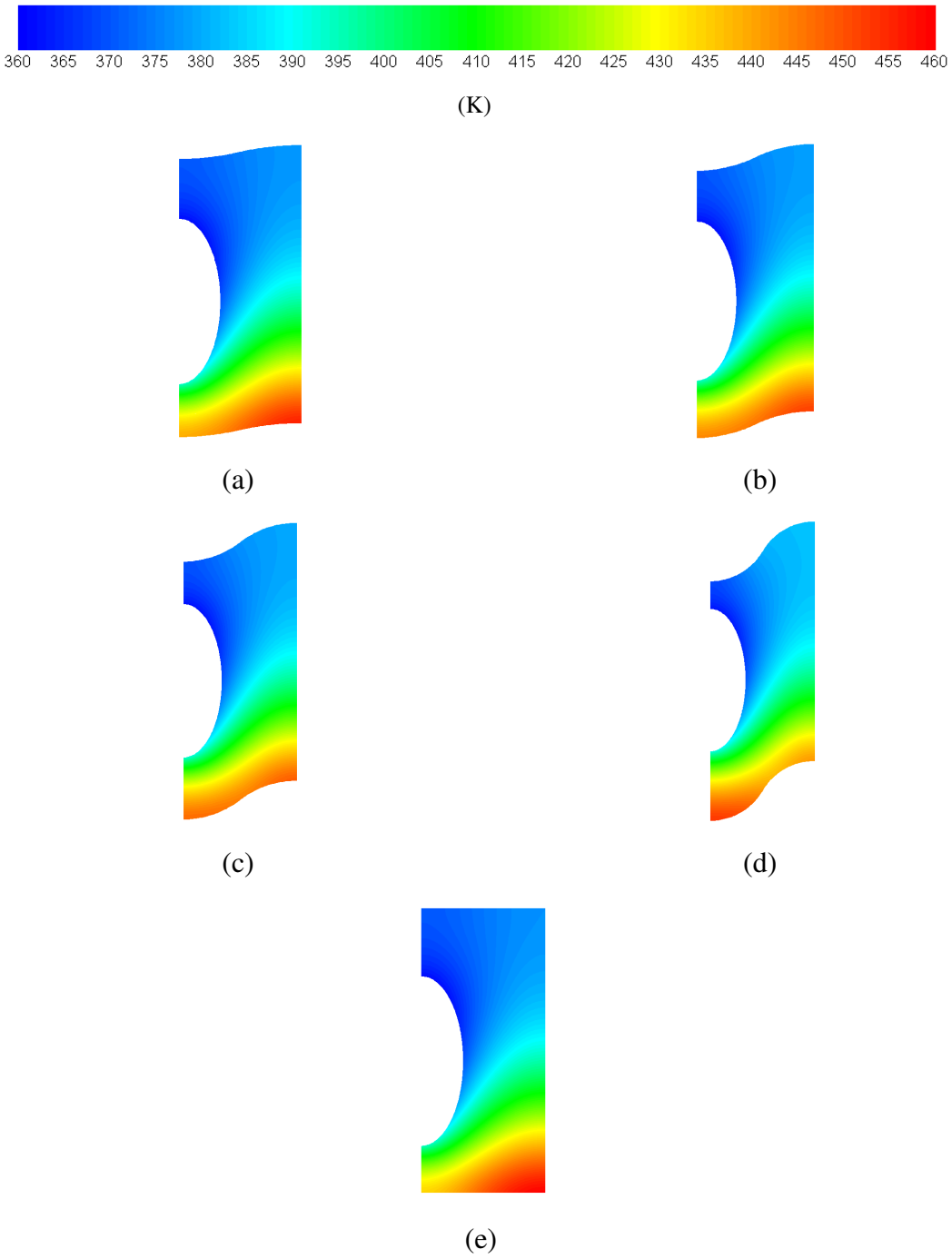

Figure 8.19. The temperature distribution on wavy fins (a) wavy-d1mm (b) wavy-d2mm (c) wavy-d3mm (d) wavy-d5mm (e) e0.45-18.5mm.

The temperature distributions on the wavy fins are illustrated in Figure 8.19 and the heat transfer and total pressure drop values are tabulated in Table 8.7. The effect of wave height is also illustrated in Figure 8.20.

Table 8.7. Heat transfer and pressure drop values of wavy fins.

Model Name	Q (Per segment) (W)	Normalized Q (%)	Total Pressure Drop (Pa)	Normalized Total Pressure Drop (%)
e-0.45-18.5mm	24.9072	100.000	3.0939	100.000
wavy-d1mm	24.9126	100.022	3.0930	99.971
wavy-d2mm	24.9176	100.042	3.0816	99.602
wavy-d3mm	24.9019	99.979	3.0631	99.004
wavy-d5mm	24.8530	99.782	3.0053	97.136

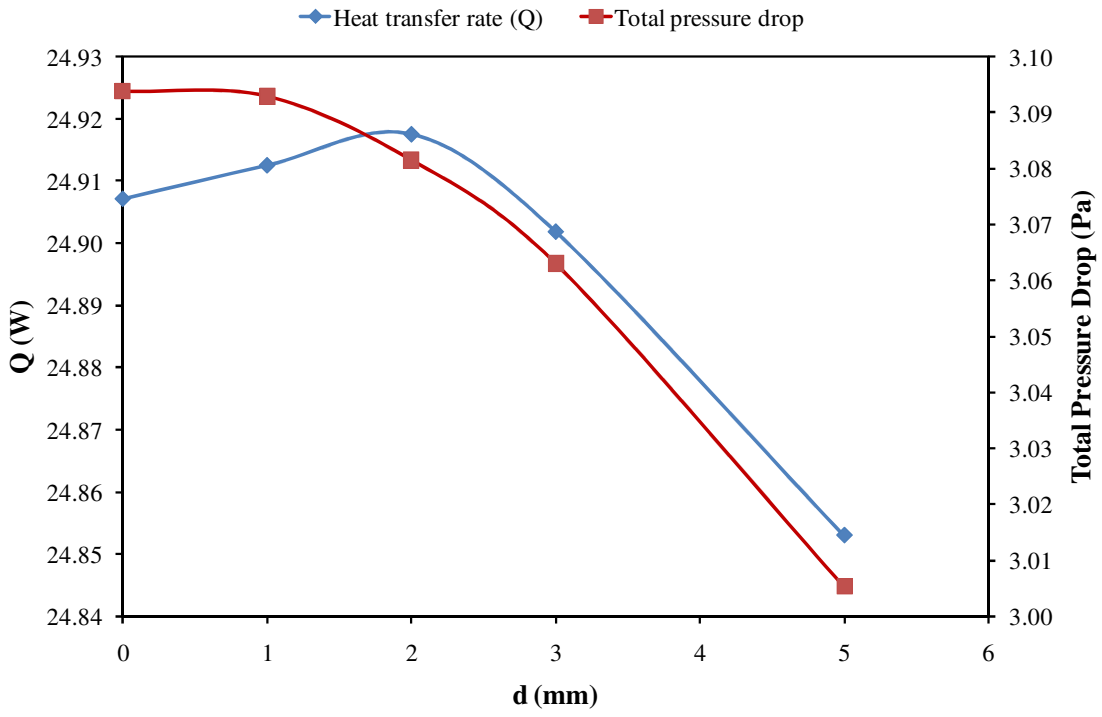

Figure 8.20. The effect of wave height on heat transfer and total pressure drop in fin shape study 1.

As can be seen from Table 8.7 and Figure 8.20, the use of wavy fins can be beneficial in some cases. The models with a wave height (d) of 1 mm and 2 mm show slightly better heat transfer performance compared to the plate fin. Furthermore, the wavy fin with a 2 mm wave value (d) is better than the one with a 1 mm wave value. It is also observed that as the wave height is increased the total pressure drop decreases.

8.2.3.2. Fin Shape Study 2

In fin shape study 1, the fin tube location (L_1) is not taken from the bottom point of the fin as can be seen in Figure 8.18, it is taken from the midpoint of the bottom line of the fin. However, the situation when it is determined according to the bottom fin point is also needed to be investigated. In this part of the study, this case is examined. The schematic view of the investigated fins in this part is given in Figure 8.21.

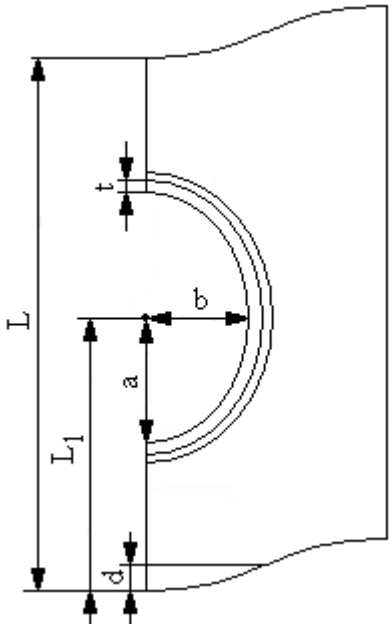

Figure 8.21. Schematic view of a wavy fin investigated in fin shape study 2.

In this section of the study, the wave height (d) is taken as 1, 2, 3 and 5 mm similar to the previous part of the investigation. The dimensions taken into consideration in this part are given in Table 8.8.

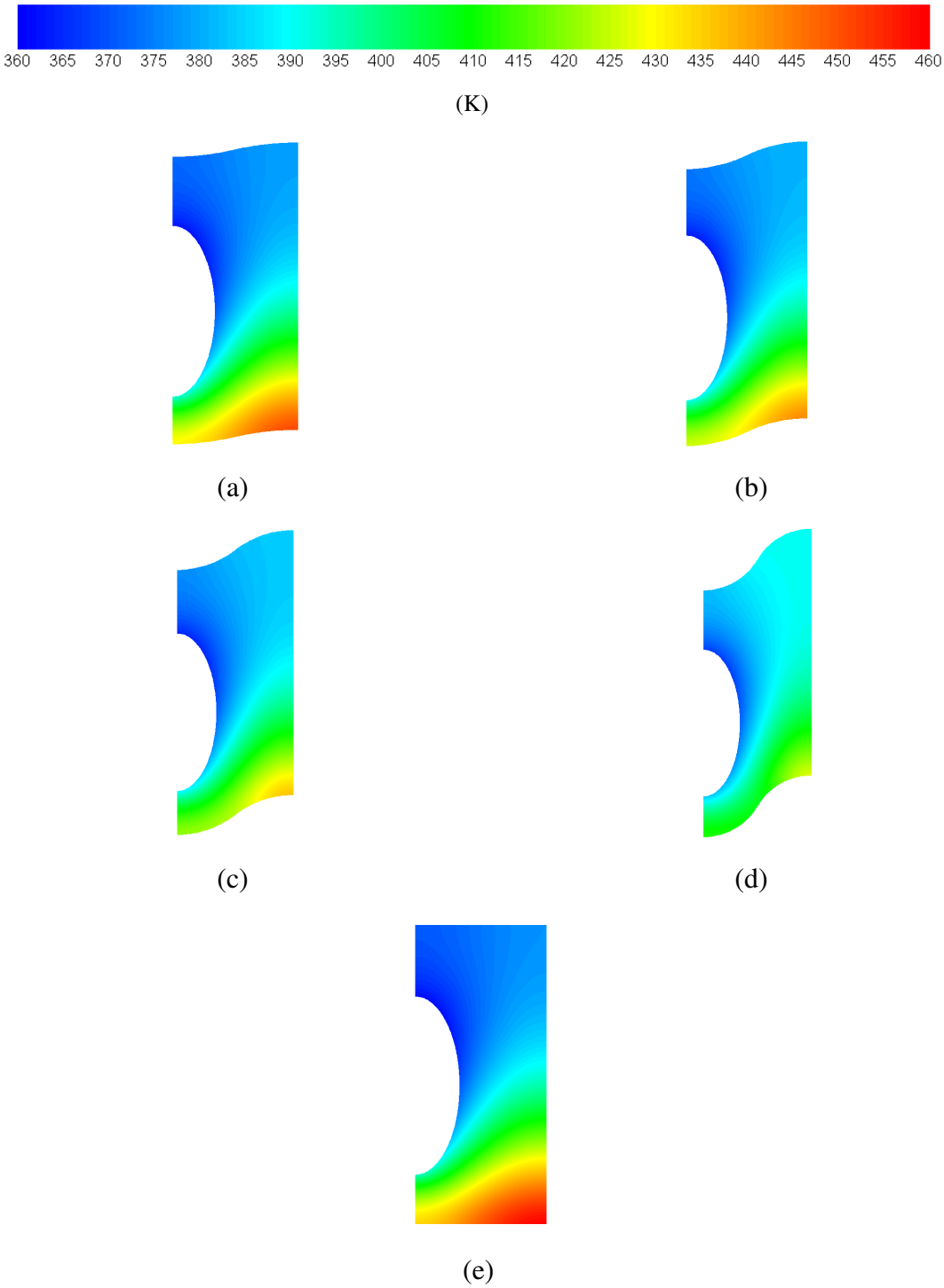

Figure 8.22. The temperature distribution on wavy fins investigated in fin shape study2 (a) wavy2-d1mm (b) wavy2-d2mm (c) wavy2-d3mm (d) wavy2-d5mm (e) e0.45-18.5mm.

Table 8.8. Dimensions of wavy fins investigated in fin shape study 2.

Model Name	L (mm)	L_1 (mm)	Ellipticity (b/a)	d (mm)
wavy2-d1mm	40	18.5	0.45	1
wavy2-d2mm	40	18.5	0.45	2
wavy2-d3mm	40	18.5	0.45	3
wavy2-d5mm	40	18.5	0.45	5

The numerical results obtained for this section of the study are tabulated in Table 8.9. The effect of wave height (d) is illustrated in Figure 8.23 as well. The comparison with corresponding plain fin (e0.45-18.5mm), for which the normalized heat transfer and total pressure drop values are taken as 100%, is also accomplished in this section of the study in order to show the effect of wave values. The temperature distributions on the wavy fins are also given in Figure 8.22.

Table 8.9. Heat transfer and pressure drop values of wavy fins investigated in fin shape study 2.

Model Name	Q (Per segment) (W)	Normalized Q (%)	Total Pressure Drop (Pa)	Normalized Total Pressure Drop (%)
e0.45-18.5mm	24.9072	100.000	3.0939	100.000
wavy2-d1mm	24.9026	99.982	3.0938	99.997
wavy2-d2mm	24.9011	99.976	3.0802	99.557
wavy2-d3mm	24.8662	99.835	3.0532	98.685
wavy2-d5mm	24.7607	99.412	2.9534	95.459

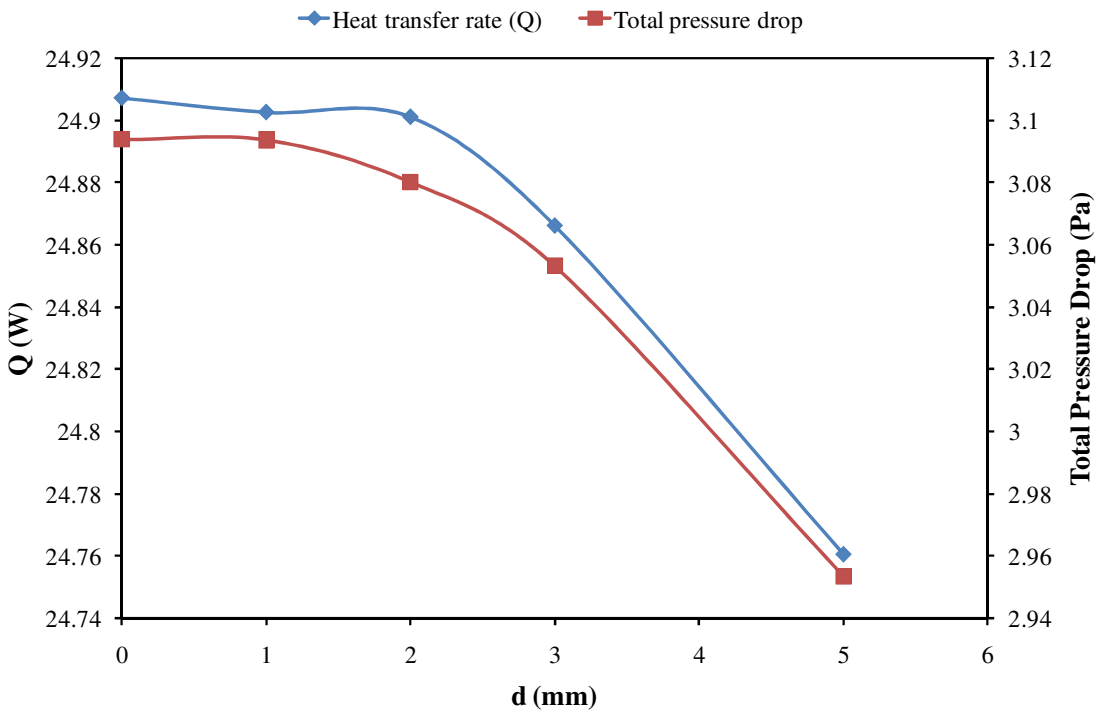

Figure 8.23. The effect of wave height on heat transfer and total pressure drop in fin shape study 2.

In this part of the study, it is found that the use of wavy fins with the chosen dimensions do not give better heat transfer value compared to plain fin. The total pressure drop value shows also a decreasing trend as the wave height is increased. However, in the previous section, it was found that the wavy fin with a wave value of 2 mm (model wavy-d2mm) is better than plain fin in terms of both pressure drop and heat transfer values. So, in the following sections of the study, it is decided to use the model wavy-d2mm for the fin optimization.

8.2.4. The Effect of Protrusion Dimensions

After the determination of the best plate fin, three different protrusions which are placed on the plate fin surface are taken into consideration. These protrusions disturb the flow and thus create a certain amount of heat transfer enhancement. However, since they block the flue gas flow passing through the gaps between fins, they also cause some pressure drop. In the present study, balcony, imprint and winglet type protrusions are investigated.

8.2.4.1. The Effect of Balcony Type Protrusion Height

Firstly, the use of balcony type protrusion is focused on. The schematic view of a plate fin with balcony type protrusion is given in Figure 8.24.

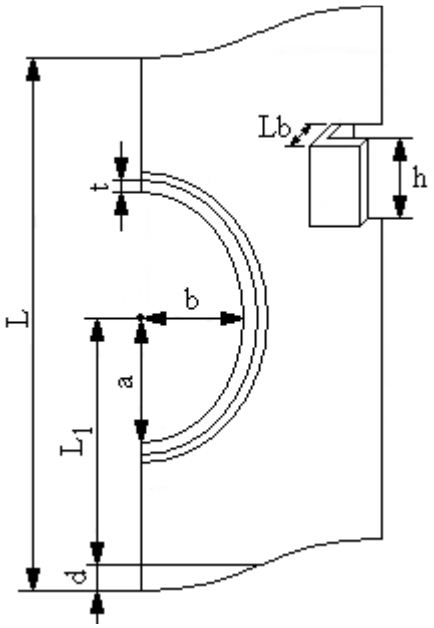

Figure 8.24. Schematic view of a plate fin with balcony.

Table 8.10. Dimensions of fins with different balcony heights.

Model Name	L (mm)	L_1 (mm)	Lb (mm)	Ellipticity (b/a)	d (mm)	h (mm)
Bh-2mm	40	18.5	2.425	0.45	2	2
Bh-3mm	40	18.5	2.425	0.45	2	3
Bh-4mm	40	18.5	2.425	0.45	2	4
Bh-6mm	40	18.5	2.425	0.45	2	6
Bh-8mm	40	18.5	2.425	0.45	2	8

The balcony type protrusion height (h) is varied between 2 mm and 8 mm while all the other dimensions shown in Figure 8.24 are kept constant. The dimensions are the same as those of the model wavy-d2mm, which is determined as the best plate fin in the previous parts of the investigation and the balcony length is maintained as 2.425 mm. The balcony heights used in the present part of the study are tabulated in Table 8.10.

The five fins with different balcony heights are modeled and numerical results of heat transfer and total pressure drop values for these fins are summarized in Table 8.11. In order to reveal the effect of balcony type protrusion usage, the results of plate fin with the same dimensions (wavy-d2mm) are also presented in this table. The results of the fin wavy-d2mm are assumed to be 100% in order to obtain normalized heat transfer and total pressure drop values. The effect of balcony height is also shown in Figure 8.25.

Table 8.11. Heat transfer and pressure drop values of fins with different balcony heights.

Model Name	Q (Per segment) (W)	Normalized Q (%)	Total Pressure Drop (Pa)	Normalized Total Pressure Drop (%)
wavy-d2mm	24.9176	100	3.0816	100
Bh-2mm	24.9703	100.211	3.1980	103.777
Bh-3mm	24.9717	100.217	3.2108	104.193
Bh-4mm	24.9689	100.206	3.2225	104.572
Bh-6mm	24.9639	100.186	3.2440	105.270
Bh-8mm	24.9587	100.165	3.2643	105.929

It is observed from Figure 8.25 that the heat transfer performance improves up to a balcony height value of 3 mm and after this value a decreasing trend is observed. However, the total pressure drop value increases as the balcony height value is increased. The reason of heat transfer enhancement due to the use of balcony type protrusion is the fact that the balcony type protrusion disturbs the flow and directs the flow to the fin tube as shown in Figure 8.27, where the velocity distribution of the model Bh-3mm is illustrated. Similar velocity distribution for the corresponding plate fin (wavy-d2mm) is also given in Figure 8.26. When the two figures are compared, the effect of balcony type protrusion on the flue gas flow is clearly observed. Nevertheless, since the balcony form an obstacle against the fluid flow, the total pressure drop values of the fins with balcony type protrusion are higher than the one of the corresponding plate fin.

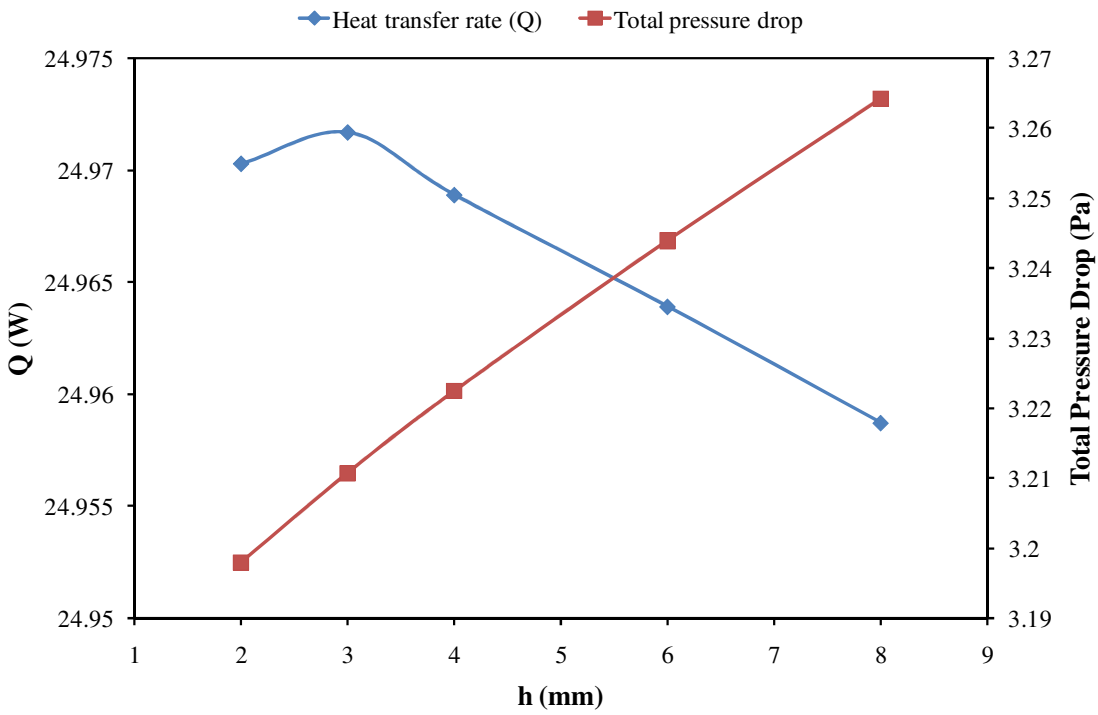

Figure 8.25. The effect of balcony height on heat transfer and total pressure drop.

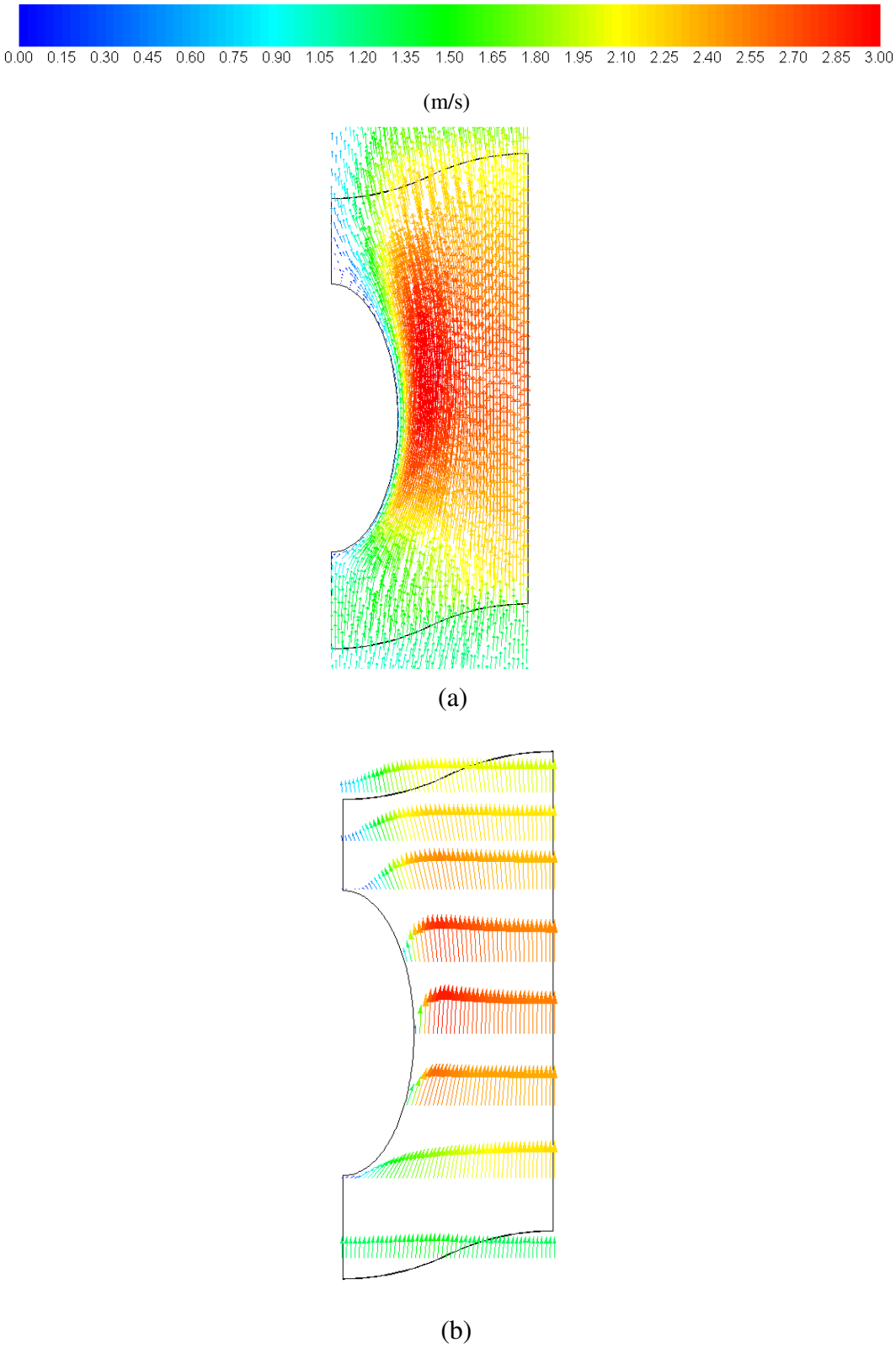

Figure 8.26. Velocity vectors for the model wavy-d2mm (a) at the middle plane of the gap between two fins (b) at various levels at the middle plane of the gap between two fins.

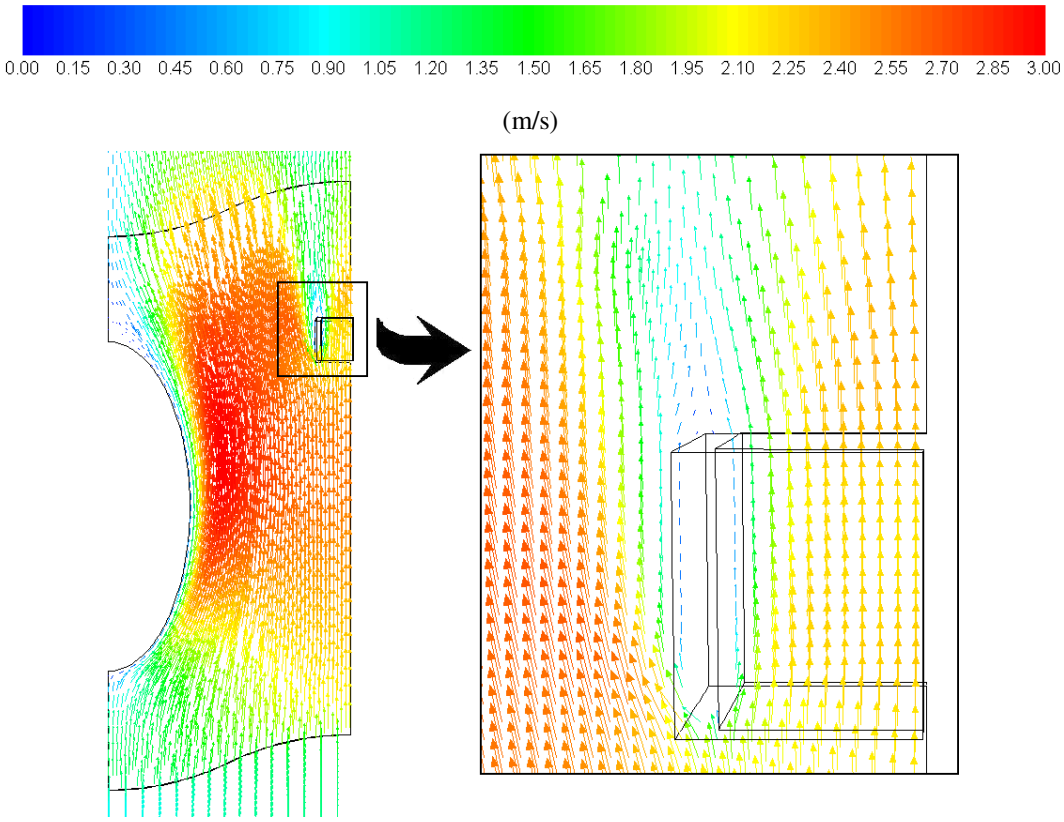

Figure 8.27. Velocity vectors for the model Bh-3mm (a) at the middle plane of the gap between two fins (b) at various levels at the middle plane of the gap between two fins.

As a result of this part of the study, it is found that that the fin with a balcony height of 3 mm (Bh-3mm) gives the best heat transfer performance. It can be also seen that the total pressure drop value increase due to the usage of balcony type protrusion do not reach an excessive value. So, it is decided to use the balcony dimensions of the model Bh-3mm in the next parts of the study.

8.2.4.2. The Effect of Winglet Type Protrusion Width

Similar to the balcony type protrusion, winglet type protrusion is also investigated in this study. The width of the winglet (w) is changed between 2 mm and 6 mm. The schematic view of a fin with winglet is shown in Figure 8.28.

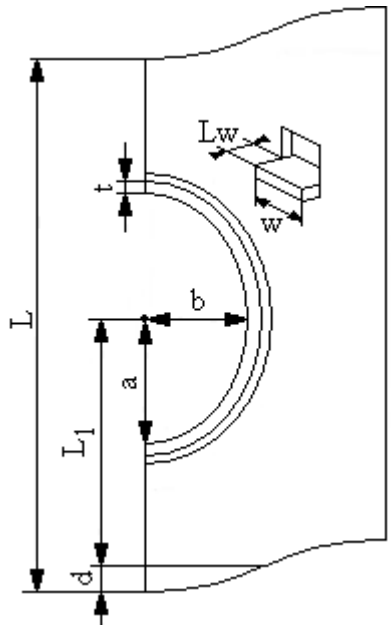

Figure 8.28. Schematic view of a plate fin with winglet.

The dimensions of the fins with winglet type protrusion are tabulated in Table 8.12. The dimensions other than winglet length in the gap between two fins (Lw) and winglet width (w) are again the same as those of the plate fin wavy-d2mm.

Table 8.12. Dimensions of fins with different winglet widths.

Model Name	L (mm)	L_1 (mm)	Lw (mm)	Ellipticity (b/a)	d (mm)	w (mm)
Ww-2mm	40	18.5	2.425	0.45	2	2
Ww-3mm	40	18.5	2.425	0.45	2	3
Ww-4mm	40	18.5	2.425	0.45	2	4
Ww-5mm	40	18.5	2.425	0.45	2	5
Ww-6mm	40	18.5	2.425	0.45	2	6

The heat transfer and fluid flow problems are solved, numerically, to obtain the total heat transfer rate of the heat exchanger and the pressure drop value of flue gas as it passes across the heat exchanger. Similar to the previous part of the study, the numerical results of the fins with winglets are compared with the plate fin wavy-d2mm, whose values are assumed to be 100 %. The numerical results are presented in Table 8.13 and Figure 8.29.

Table 8.13. Heat transfer and pressure drop values of fins with different winglet widths.

Model Name	Q (Per segment) (W)	Normalized Q (%)	Total Pressure Drop (Pa)	Normalized Total Pressure Drop (%)
wavy-d2mm	24.9176	100	3.0816	100
Ww-2mm	24.9674	100.200	3.2369	105.040
Ww-3mm	24.9686	100.205	3.3000	107.087
Ww-4mm	24.9528	100.141	3.3726	109.443
Ww-5mm	24.9399	100.089	3.4549	112.114
Ww-6mm	24.9253	100.031	3.5483	115.145

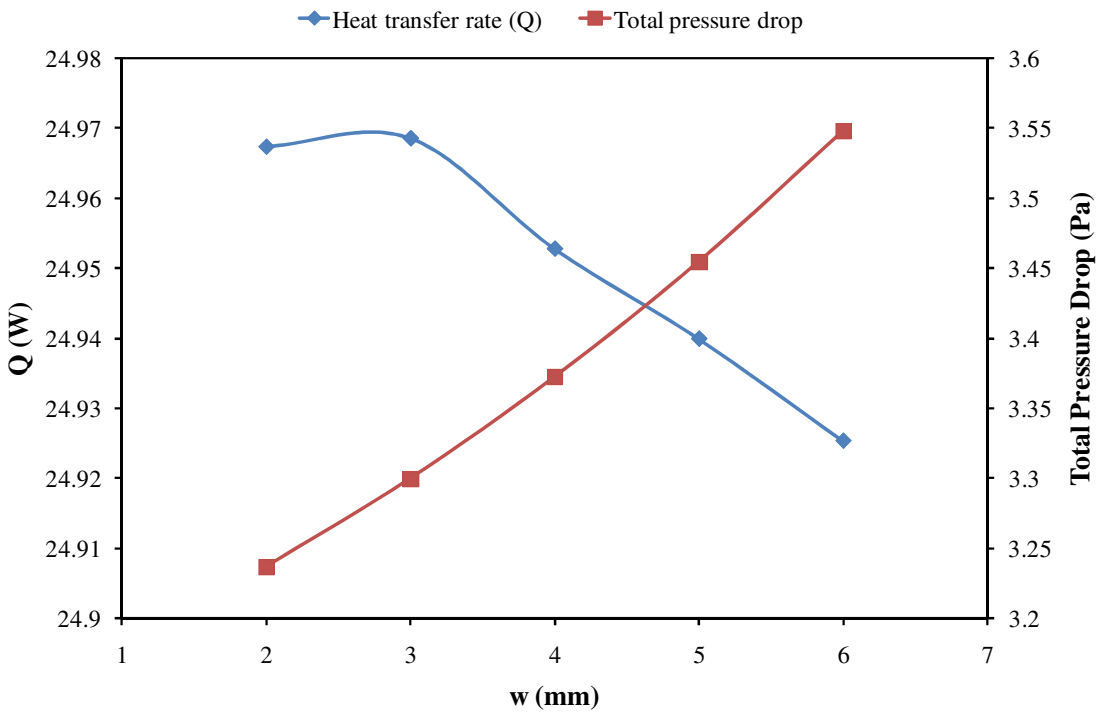

Figure 8.29. The effect of winglet width on heat transfer and total pressure drop.

The heat transfer rate of the fins with winglets is observed to be increased until the winglet width reaches 3 mm. Increasing the winglet width beyond this value leads to a lower heat transfer rate. It is also seen that wider winglets causes higher total pressure drop.

The velocity vectors at the middle plane of the gap between two fins for the fin Ww-3mm, which gives the maximum heat transfer value, is given in Figure 8.30 in order to show the effect of winglet on the flow. As it can be seen from Figure 8.30, the winglet directs the flow into the wake region of the tube. The mixing of the flue gas as it passes through the winglet and the resulting vortices can be observed clearly in Figure 8.31, in which the pathlines released from the inlet of the flue gas are presented. As a result of these influences, an increase in heat transfer is achieved by the use of the fins with winglets compared to the corresponding plate fin. However, higher total pressure drop values are also encountered due to the block effect created by the winglets on the flow.

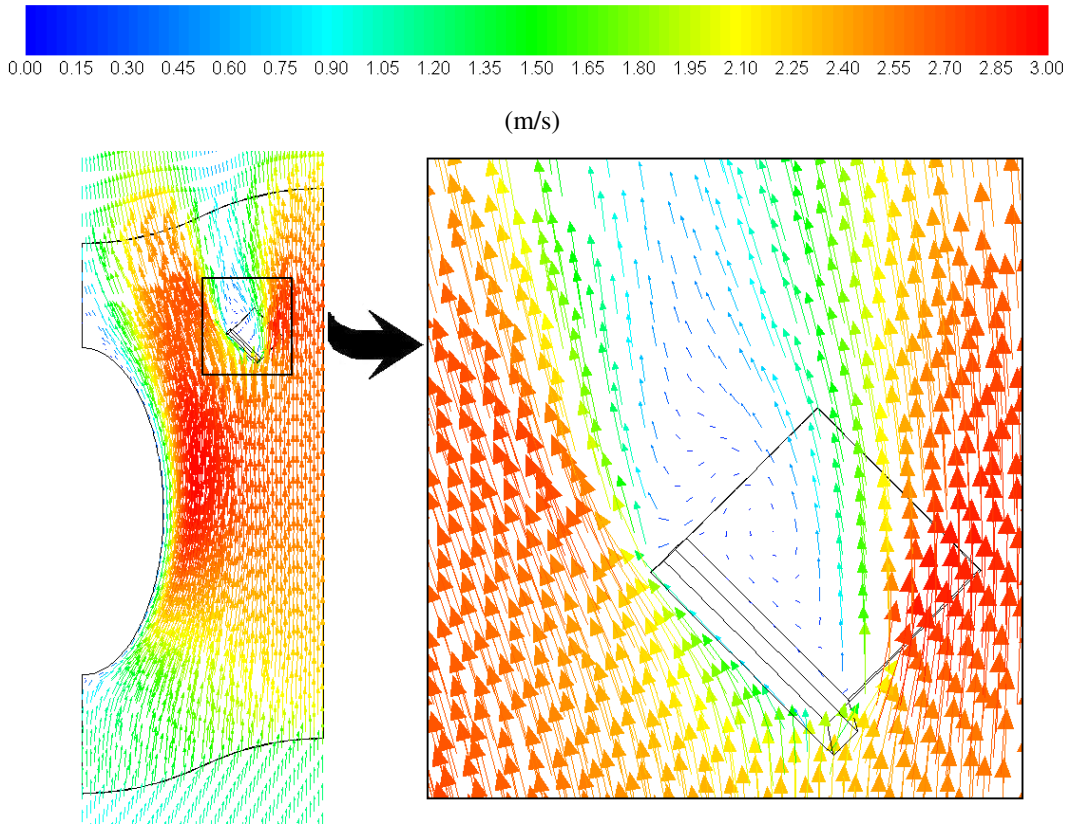

Figure 8.30. Velocity vectors for the model Ww-3mm (a) at the middle plane of the gap between two fins (b) at various levels at the middle plane of the gap between two fins.

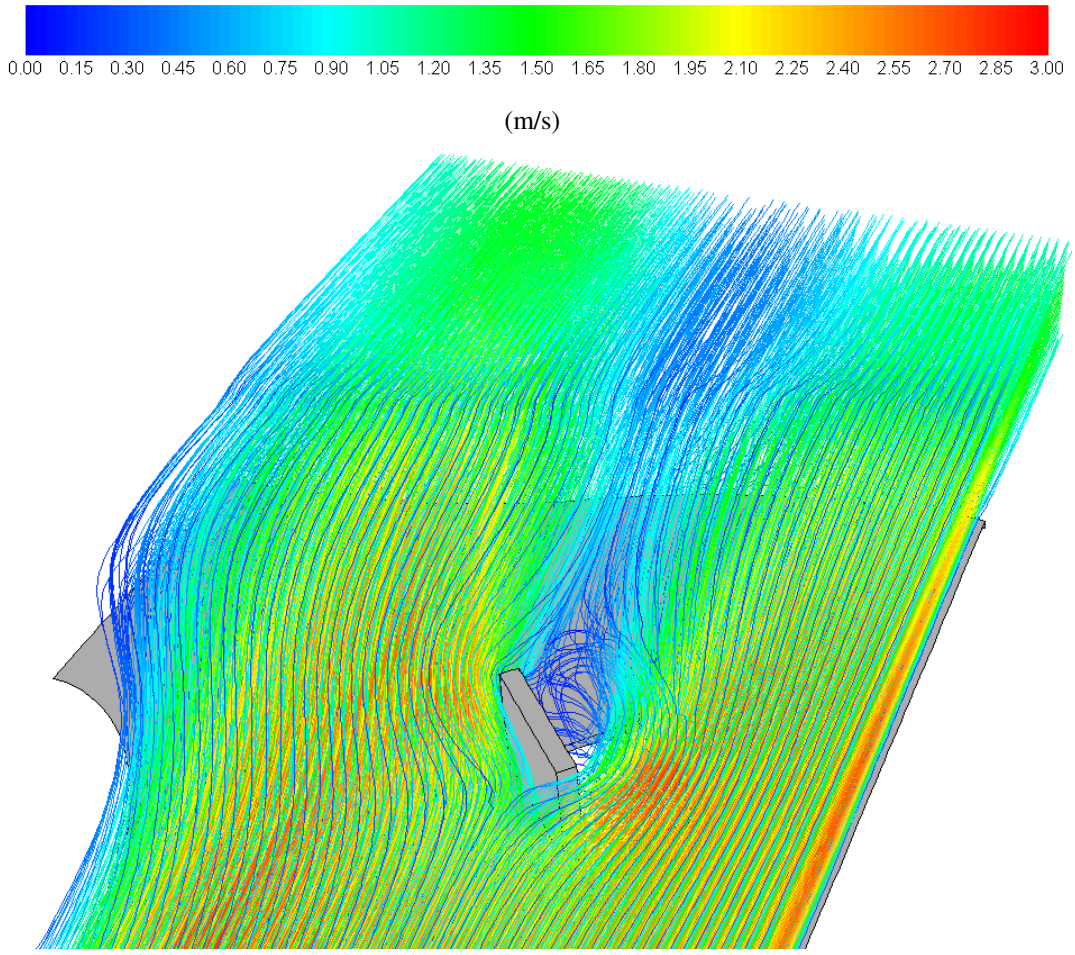

Figure 8.31. Pathlines released from the inlet of flue gas for the model Ww-3mm.

As the result of this part of the study, it is decided to continue the next parts using the winglet dimensions of the fin Ww-3mm because of its highest heat transfer rate and modest total pressure drop increase.

8.2.4.3. The Effect of Imprint Type Protrusion Radius

The effect of the imprint type protrusion radius is also investigated as a final part of this section of the study. The radius value is varied between 4 mm and 8 mm. The schematic view of a fin with imprint type protrusion can be seen in Figure 8.32.

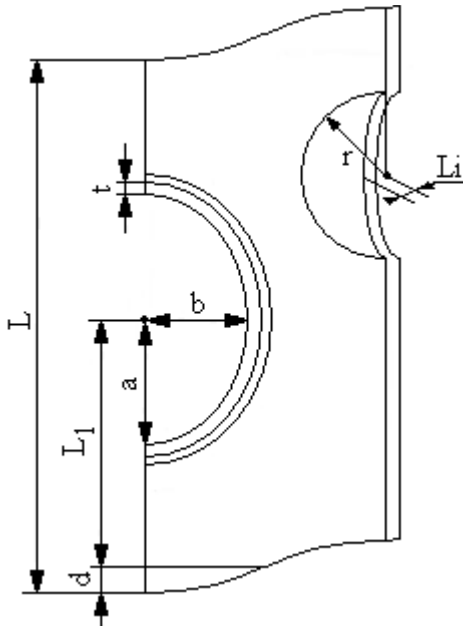

Figure 8.32. Schematic view of a plate fin with imprint.

All dimensions shown in Figure 8.32 (except the radius of the imprint (r) and imprint length (Li), which is taken as 2.425 mm) are kept constant as the dimensions of the plate fin wavy-d2mm. The radius values investigated in this part of the study are summarized in Table 8.14.

Table 8.14. Dimensions of fins with different imprint radii.

Model Name	L (mm)	L_1 (mm)	Li (mm)	Ellipticity (b/a)	d (mm)	r (mm)
Ir-4mm	40	18.5	2.425	0.45	2	4
Ir-5mm	40	18.5	2.425	0.45	2	5
Ir-6mm	40	18.5	2.425	0.45	2	6
Ir-7mm	40	18.5	2.425	0.45	2	7
Ir-8mm	40	18.5	2.425	0.45	2	8

The numerical heat transfer and pressure drop values obtained from Fluent software solution of these 5 different fins with imprint are summarized in Table 8.15 and Figure 8.33.

Similar to the previous two parts of the study, the values of the corresponding plate fin wavy-d2mm are taken as 100 % in order to make the comparison of the fins easier.

Table 8.15. Heat transfer and pressure drop values of fins with different imprint radii.

Model Name	Q (Per segment) (W)	Normalized Q (%)	Total Pressure Drop (Pa)	Normalized Total Pressure Drop (%)
wavy-d2mm	24.9176	100	3.0816	100
Ir-4mm	24.9982	100.323	3.2716	106.166
Ir-5mm	25.0210	100.415	3.2721	106.182
Ir-6mm	25.0403	100.492	3.2715	106.162
Ir-7mm	25.0476	100.522	3.2707	106.136
Ir-8mm	25.0442	100.508	3.2703	106.123

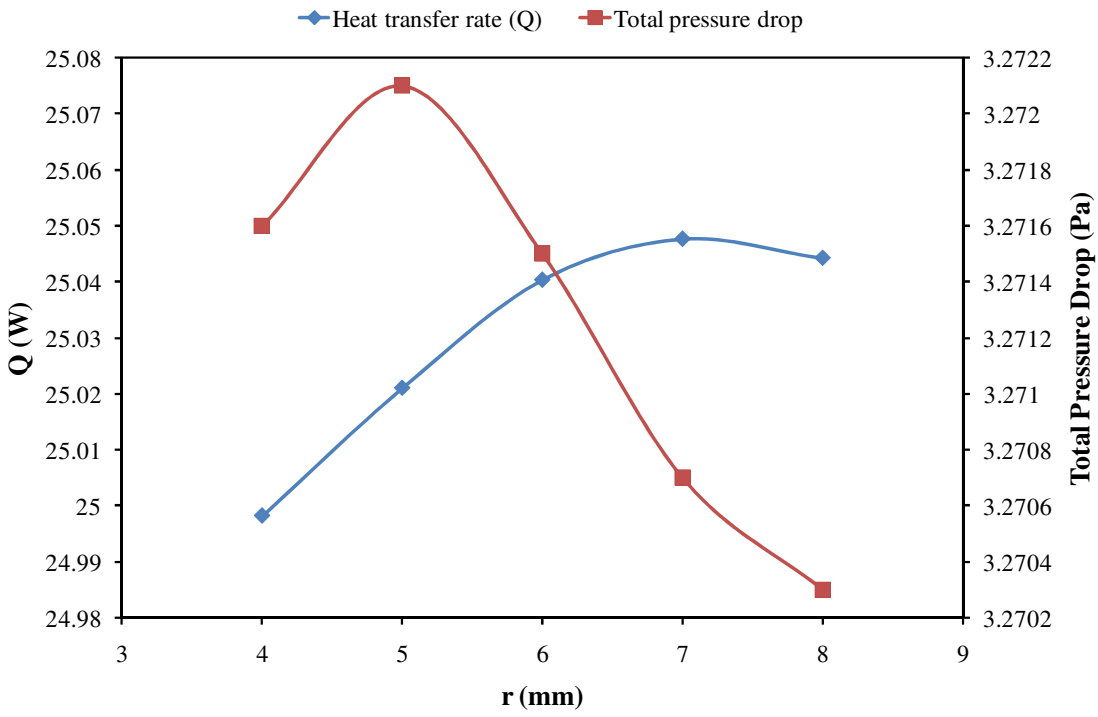

Figure 8.33. The effect of imprint radius on heat transfer and total pressure drop.

The heat transfer enhancement increases as the radius of imprint increases up to 7 mm. The total pressure drop value of the fins with imprint shows an increasing trend up to a radius value of 5 mm, after this value it starts to decrease. The reason of this pressure drop decrease can be explained with the fact that as the imprint radius value is decreased, more concave structure is obtained for the imprint. The concavity of the imprint leads to an increase in pressure drop penalty.

The effect of the imprint on the flow can be seen in Figure 8.34, which is for the fin with imprint radius of 7 mm (Ir-7mm). The flow directing effect of the imprint into the fin tube wake is clearly seen in Figure 8.34, which results in an increase in heat transfer.

According to the numerical results of this part of the study, it is decided to continue the following studies with the imprint dimensions of the fin Ir-7mm as its heat transfer value is the maximum among the investigated models and its total pressure drop increase compared to the corresponding plate fin is modest.

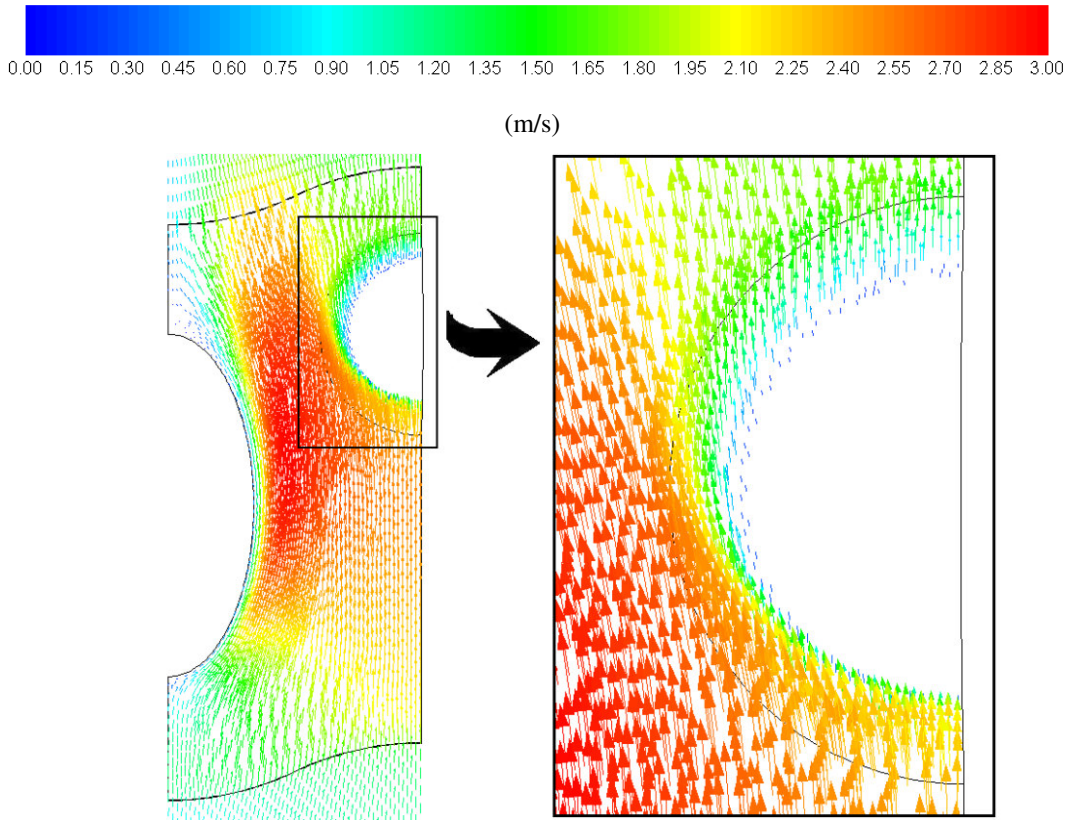

Figure 8.34. Velocity vectors for the model Ir-7mm (a) at the middle plane of the gap between two fins (b) at various levels at the middle plane of the gap between two fins.

8.2.5. The Effect of Protrusion Length Between Two Fins

The geometrical dimensions of protrusions which give the maximum heat transfer for fins with balcony, winglet and imprint are determined as the fins Bh-3mm, Ww-3mm and Ir-7mm, respectively in the previous parts. However, the length of protrusions between fins (Lb, Lw and Li) is taken as 2.425 mm for all of the fins investigated so far. In this section of the study the length of each type protrusion is changed and the effects on heat transfer and total pressure drop values are examined.

8.2.5.1. The Effect of Balcony Length

The length of balcony is given as Lb in Figure 8.24. This value is varied between 1 mm and 2.425 mm. The length values used in this part of investigation and the corresponding model names are summarized in Table 8.16. Since the numerical results of the previous parts indicates that the fin with a balcony height of 3 mm has the best performance, the geometrical dimensions (other than the length between two fins) of the fin Bh-3mm are maintained in this study.

The numerical analysis of the fins with 9 different balcony length values are obtained from the Fluent software as summarized in Table 8.17. The heat transfer and pressure drop values of the fin wavy-d2mm are taken as 100% in this section again since the corresponding plate fin is wavy-d2mm. The effect of balcony length on heat transfer and total pressure drop is also shown in Figure 8.35.

Table 8.16. Dimensions of fins with different balcony lengths.

Model Name	L (mm)	L_1 (mm)	h (mm)	Ellipticity (b/a)	d (mm)	Lb (mm)
Lb-2.425mm	40	18.5	3	0.45	2	2.425
Lb-2.2mm	40	18.5	3	0.45	2	2.2
Lb-2mm	40	18.5	3	0.45	2	2
Lb-1.8mm	40	18.5	3	0.45	2	1.8
Lb-1.6mm	40	18.5	3	0.45	2	1.6
Lb-1.5mm	40	18.5	3	0.45	2	1.5
Lb-1.4mm	40	18.5	3	0.45	2	1.4
Lb-1.2mm	40	18.5	3	0.45	2	1.2
Lb-1mm	40	18.5	3	0.45	2	1

Table 8.17. Heat transfer and pressure drop values of the fins with different balcony lengths.

Model Name	Q (Per segment) (W)	Normalized Q (%)	Total Pressure Drop (Pa)	Normalized Total Pressure Drop (%)
wavy-d2mm	24.9176	100	3.0816	100
Lb-2.425mm	24.9717	100.217	3.2108	104.193
Lb-2.2mm	24.9765	100.236	3.2303	104.825
Lb-2mm	24.9928	100.302	3.2442	105.276
Lb-1.8mm	25.0075	100.361	3.2494	105.445
Lb-1.6mm	25.0100	100.371	3.2442	105.276
Lb-1.5mm	25.0114	100.376	3.2376	105.062
Lb-1.4mm	25.0074	100.360	3.2299	104.812
Lb-1.2mm	24.9952	100.311	3.2080	104.102
Lb-1mm	24.9730	100.222	3.1829	103.287

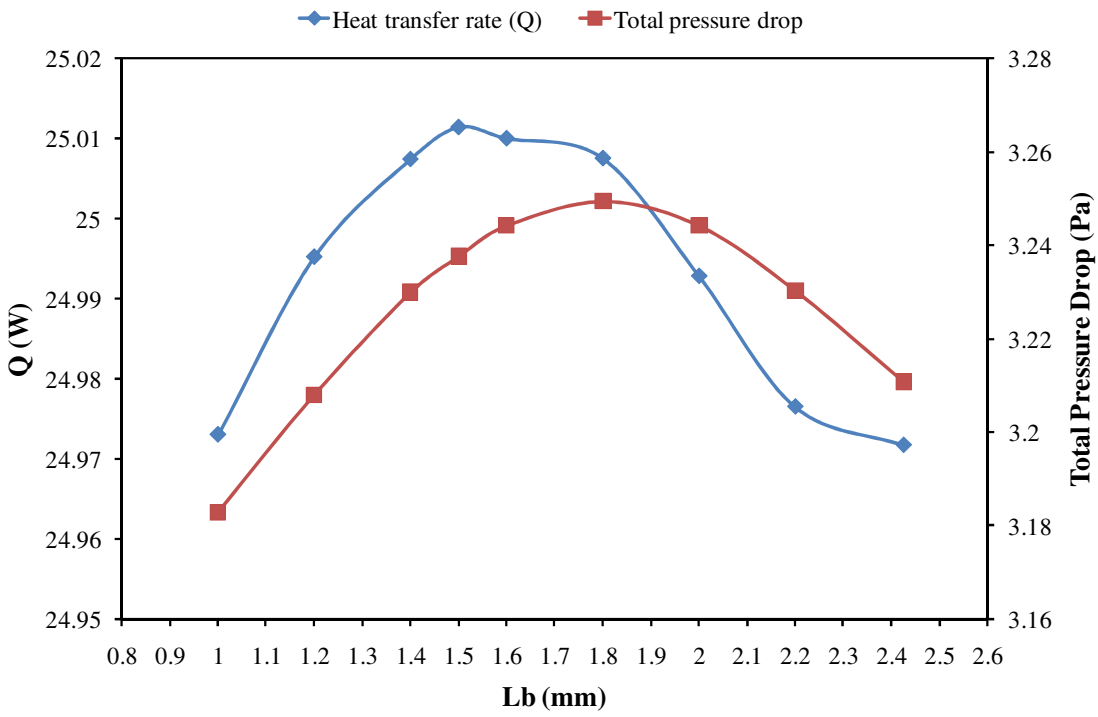

Figure 8.35. The effect of balcony length on heat transfer and total pressure drop.

It can be concluded from the numerical results of this part of the study that as the balcony length approaches to the midpoint of the gap between two fins, an increase in heat transfer value is obtained (the balcony of the model Lb-1.5mm is exactly placed at the middle point of the gap between two fins). It is also observed that pressure drop values of the fins with balconies, whose length is around the midpoint of the gap between two fins, are the highest. Since at the midpoint of the gap between two fins the flue gas velocity is higher, the block effect of the balconies placed around this point causes bigger pressure drop values.

The velocity vectors at the middle plane of the gap between two fins and at the plane which coincides to the midpoint of the balcony for the model Lb-1.5mm, which is the best in terms of heat transfer, are given in Figure 8.36. It can be observed that balcony type protrusion directs the flow into the fin tube and cause the flow to accelerate, which causes the heat transfer and pressure drop values to increase.

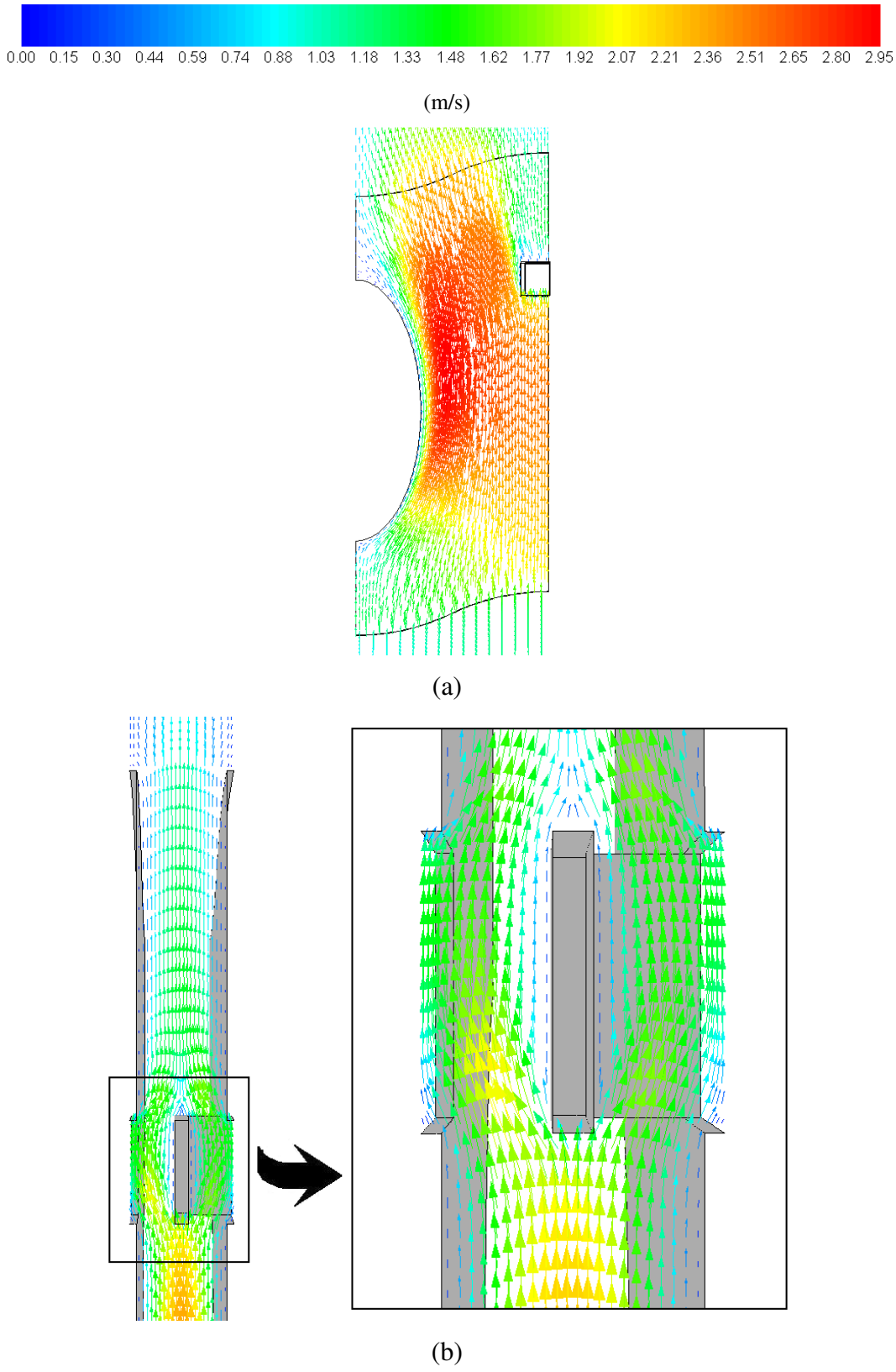

Figure 8.36. Velocity vectors for the model Lb-1.5mm (a) at the middle plane of the gap between two fins (b) at the plane which coincides to the midpoint of the balcony.

According to the results of this part of the study, it is decided to continue the following parts with the dimensions of the balcony of the fin Lb-1.5mm, which gives the maximum heat transfer and reasonable total pressure drop value.

8.2.5.2. The Effect of Winglet Length

The length of winglet type protrusion is notated as Lw in Figure 8.28. Similar to the balcony length, the winglet length is changed between 1.3 mm and 2.425 mm and the effects are observed. The fin with a winglet width of 3 mm is chosen according to the numerical results of the previous parts of the study. So, the geometrical dimensions (other than the length between two fins) of the fin Ww-3mm are kept constant in this section. The length values used in this section of the study are given in Table 8.18.

Table 8.18. Dimensions of fins with different winglet lengths.

Model Name	L (mm)	L_1 (mm)	w (mm)	Ellipticity (b/a)	d (mm)	Lw (mm)
Lw-2.425mm	40	18.5	3	0.45	2	2.425
Lw-2.2mm	40	18.5	3	0.45	2	2.2
Lw-2mm	40	18.5	3	0.45	2	2
Lw-1.8mm	40	18.5	3	0.45	2	1.8
Lw-1.6mm	40	18.5	3	0.45	2	1.6
Lw-1.4mm	40	18.5	3	0.45	2	1.4
Lw-1.3mm	40	18.5	3	0.45	2	1.3

The seven different fins with different winglet length values are modeled and numerical results of Fluent software are tabulated in Table 8.19. Similar to the previous cases, the results of the fin wavy-d2mm are also presented (as 100%) for comparison. The winglet length influence on the heat transfer and total pressure drop values are also shown in Figure 8.37.

Table 8.19. Heat transfer and pressure drop values of fins with different winglet lengths.

Model Name	Q (Per segment) (W)	Normalized Q (%)	Total Pressure Drop (Pa)	Normalized Total Pressure Drop (%)
wavy-d2mm	24.9176	100	3.0816	100
Lw-2.425mm	24.9686	100.205	3.3000	107.087
Lw-2.2mm	24.9747	100.229	3.2894	106.743
Lw-2mm	24.9860	100.275	3.2726	106.198
Lw-1.8mm	24.9964	100.316	3.2494	105.445
Lw-1.6mm	24.9948	100.310	3.2247	104.644
Lw-1.4mm	24.9860	100.275	3.1977	103.768
Lw-1.3mm	24.9781	100.243	3.1853	103.365

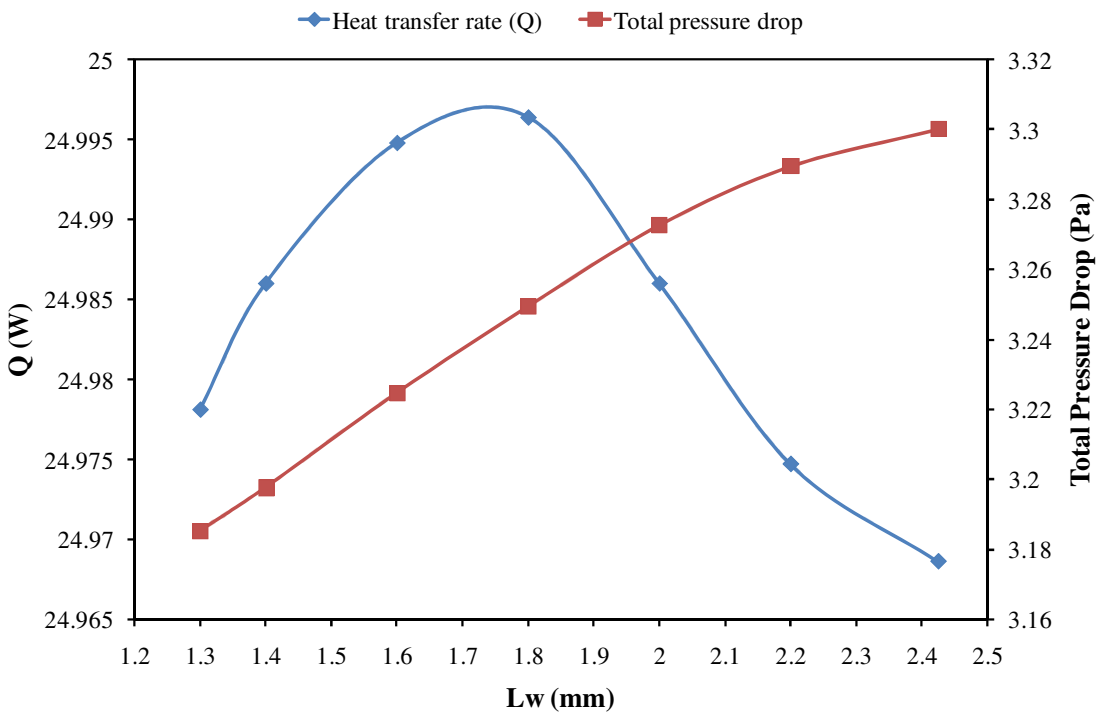

Figure 8.37. The effect of winglet length on heat transfer and total pressure drop.

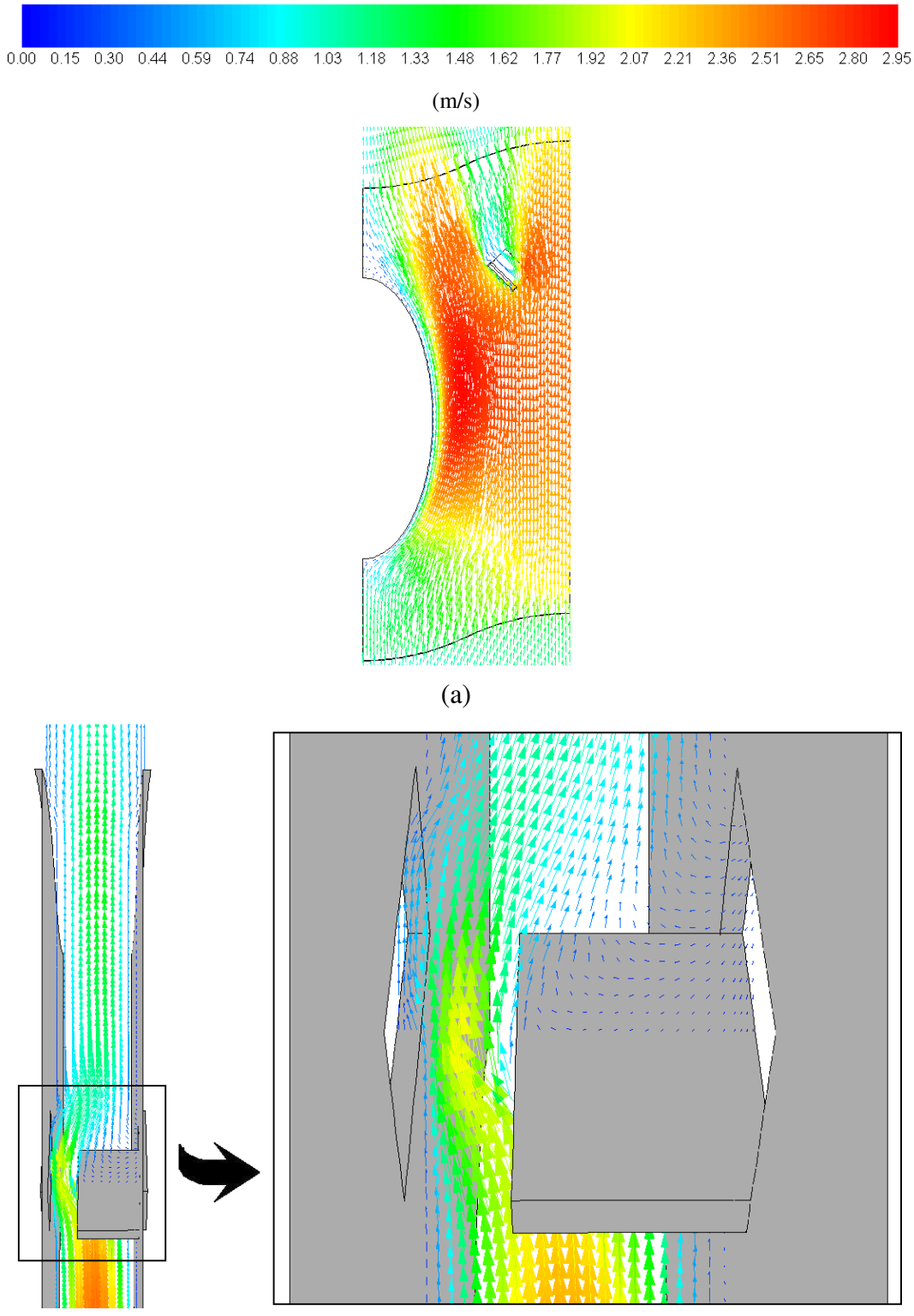

Figure 8.38. Velocity vectors for the model Lw-1.8mm (a) at the middle plane of the gap between two fins (b) at the plane which coincides to the midpoint of the winglet.

It is found in this part of the study that the fin with a winglet length value of 1.8 mm has the best heat transfer performance. Another conclusion is that as the winglet length is decreased it is observed a decrease in the pressure drop values. This result stems from the fact that as the winglet length is decreased, the flue gas flow area increases and less pressure drop values are encountered.

The velocity vectors of the fin Lw-1.8mm with a winglet length of 1.8 mm is presented in Figure 8.38 in order to present its effect on flue gas flow. Figure 8.38 (a) shows the velocity vectors on a plane placed at the midpoint of the gap between two fins, while Figure 8.38 (b) shows the velocity vectors on a plane which coincides to the midpoint of the winglet. In these figures, it is observed that, the flow path is directed to the tube wake zone similar to the previous cases. The fin Lw-1.8mm is chosen considering the numerical results of this part of the study for the following parts of the investigation.

8.2.5.3. The Effect of Imprint Length

Finally, the investigation of imprint length, which is given as Li in Figure 8.32, is performed. Li values, taken between 1.3 mm and 2.425 mm, are given in Table 8.20. The fin Ir-7mm, with an imprint radius of 7 mm, is taken as the base fin according to previous study results and its geometrical dimensions except the length of imprint are maintained throughout this part of the study.

Table 8.20. Dimensions of fins with different imprint lengths.

Model Name	L (mm)	L_1 (mm)	r (mm)	Ellipticity (b/a)	d (mm)	Li (mm)
Li-2.425mm	40	18.5	7	0.45	2	2.425
Li-2.2mm	40	18.5	7	0.45	2	2.2
Li-2mm	40	18.5	7	0.45	2	2
Li-1.8mm	40	18.5	7	0.45	2	1.8
Li-1.6mm	40	18.5	7	0.45	2	1.6
Li-1.4mm	40	18.5	7	0.45	2	1.4
Li-1.3mm	40	18.5	7	0.45	2	1.3

The heat transferred and total pressure drop values for seven fins are obtained numerically and given in Table 8.21. Similar to the previous parts of the study, the results of fin wavy-d2mm, which is the plate fin with the same geometrical dimensions, are also presented and comparisons are made by taking its results as 100%. The change in heat transfer and total pressure drop values of the investigated fins are also illustrated in Figure 8.39.

Table 8.21. Heat transfer and pressure drop values of fins with different imprint lengths.

Model Name	Q (Per segment) (W)	Normalized Q (%)	Total Pressure Drop (Pa)	Normalized Total Pressure Drop (%)
wavy-d2mm	24.9176	100	3.0816	100
Li-2.425mm	25.0476	100.522	3.2707	106.136
Li-2.2mm	25.0296	100.449	3.2395	105.124
Li-2mm	25.0163	100.396	3.2131	104.267
Li-1.8mm	25.0023	100.340	3.1897	103.508
Li-1.6mm	24.9872	100.279	3.1691	102.839
Li-1.4mm	24.9738	100.226	3.1499	102.216
Li-1.3mm	24.9654	100.192	3.1415	101.944

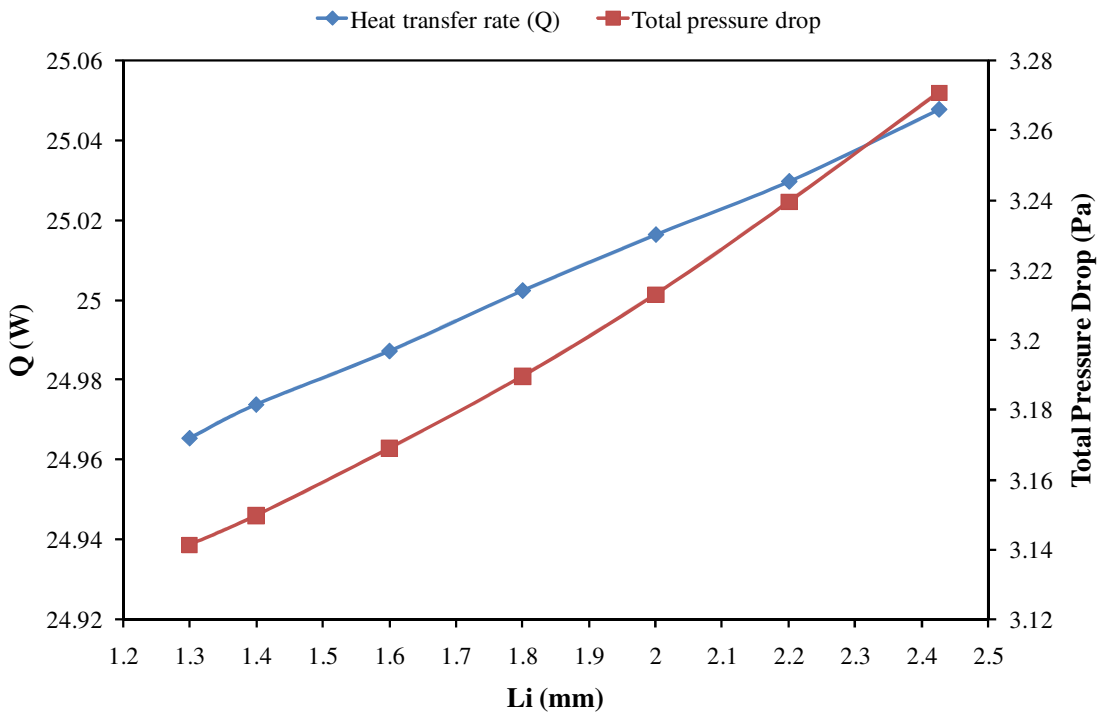

Figure 8.39. The effect of imprint length on heat transfer and total pressure drop.

The velocity vectors of the fin Li-2.425mm, which has the best heat transfer performance, are presented in Figure 8.40. The results of this part of the study indicate that the decrease in imprint length results in reduction in both heat transfer and pressure drop values. This is an expected result, because when the imprint length is increased the flue gas flow path is lengthened and greater obstacle against the flue gas flow is created as can be observed from Figure 8.40 (b). Consequently, higher heat transfer and total pressured drop characteristics are observed with increasing imprint length. According to the obtained numerical results, it is decided to use the dimensions of the model Li-2.425mm in the following parts of the study.

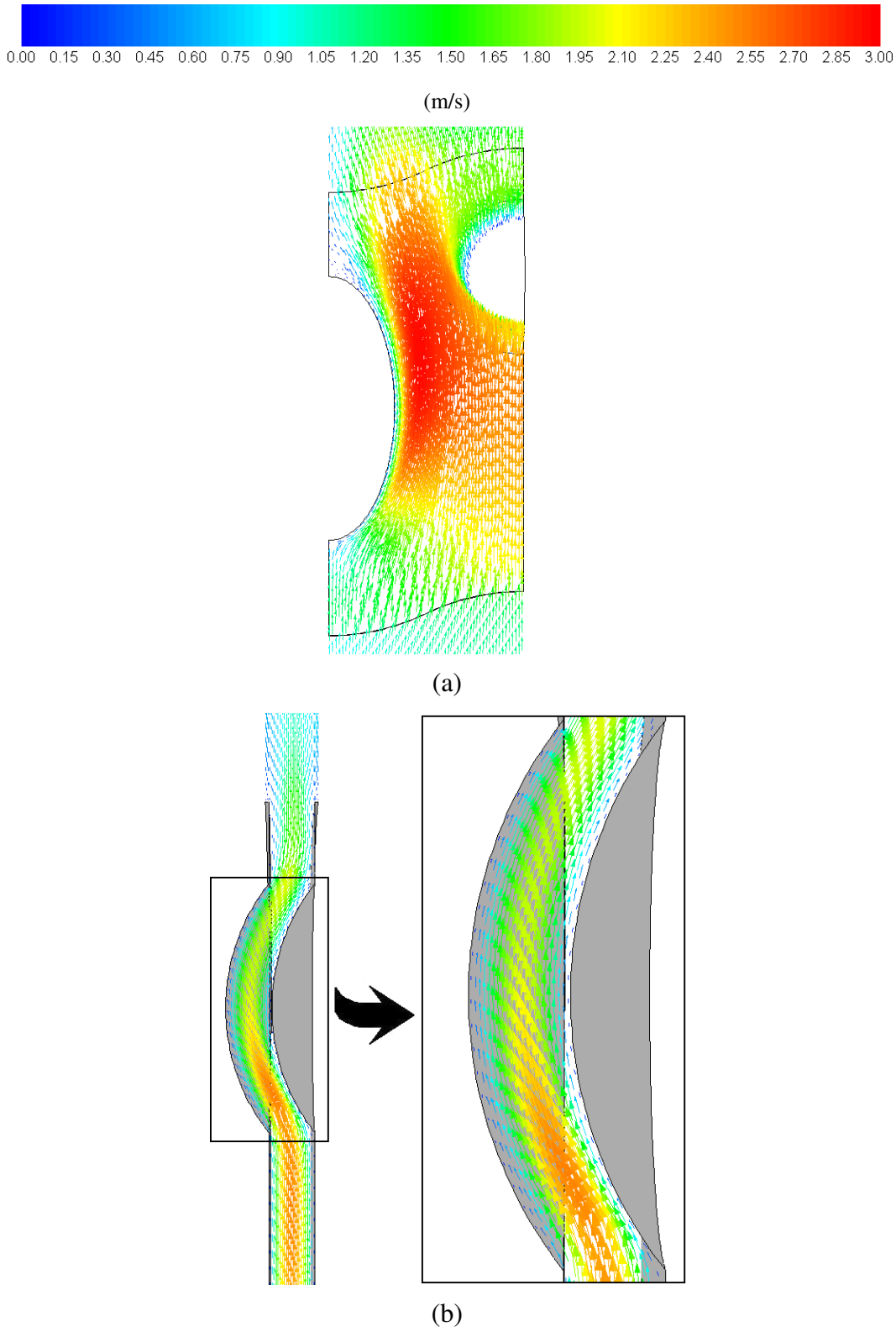

Figure 8.40. Velocity vectors for the model Li-2.425mm (a) at the middle plane of the gap between two fins (b) at the plane which coincides to the midpoint of the imprint.

8.2.6. The Effect of Protrusion Location on Fin

The geometrical dimensions of fin and three different protrusions are determined using the numerical heat transfer and total pressure drop values obtained from Fluent software in the previous studies. However, the protrusions are always placed at location 5. The location of the protrusions on the plate fin has also an influence on heat transfer and pressure drop characteristics. So, in this section the best location of the balcony, winglet and imprint type protrusions will be determined. Seven different locations are defined as illustrated in Figure 8.41.

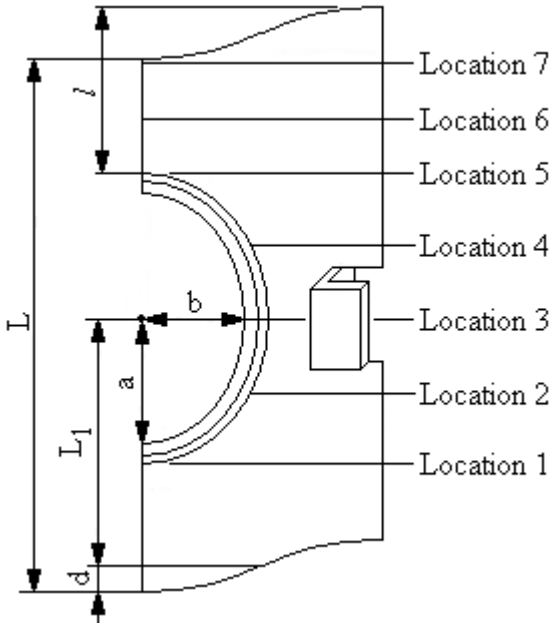

Figure 8.41. Different protrusion locations on fin.

These seven different locations are defined as;

- Location 1: corresponds to the bottom point of tube cover
- Location 2: midpoint of locations 1 and 3
- Location 3: corresponds to the center of fintube
- Location 4; midpoint of location 3 and 5
- Location 5: corresponds to the upper point of tubecover
- Location 6: placed at $l/3$ upper than the upper point of tubecover
- Location 7: placed at $2l/3$ upper than the upper point of tubecover

The models used in this study are summarized in Table 8.22. The dimensions of the models Lb-1.5mm, Lw-1.8 mm and Li-2.425 mm are used in this part since they are determined as the best in the previous sections of the study. Imprint type protrusion cannot be placed at locations 1 and 7 because of its greater radius value than the distances between the location 1 and lower point of the fin and location 7 and the upper point of the fin.

Table 8.22. Fins with protrusions placed at different locations.

Model Name							
with Balcony	with Winglet	with Imprint	Location	L (mm)	L_1 (mm)	Ellipticity (b/a)	d (mm)
B1	W1	-	1	40	18.5	0.45	2
B2	W2	I2	2	40	18.5	0.45	2
B3	W3	I3	3	40	18.5	0.45	2
B4	W4	I4	4	40	18.5	0.45	2
B5	W5	I5	5	40	18.5	0.45	2
B6	W6	I6	6	40	18.5	0.45	2
B7	W7	-	7	40	18.5	0.45	2

A total of 19 different fins are analyzed numerically in this part of the study and the numerical results are tabulated in Table 8.23. Here also the fin wavy-d2mm represents the corresponding plate fin and its heat transfer and total pressure drop values are assumed as 100% for the calculation of normalized values of the other fin models. The heat transfer and total pressure drop values of the examined cases are also summarized is Figure 8.42, 8.43 and 8.44, for the fins with balcony, winglet and imprint, respectively.

Table 8.23. Heat transfer and pressure drop values of fins with protrusions placed at different locations.

	Model Name	Q (Per segment) (W)	Normalized Q (%)	Total Pressure Drop (Pa)	Normalized Total Pressure Drop (%)
	wavy-d2mm	24.9176	100	3.0816	100
Fins with balcony	B1	24.9897	100.289	3.2742	106.250
	B2	25.0042	100.348	3.3224	107.814
	B3	25.0121	100.379	3.3450	108.548
	B4	25.0136	100.385	3.3060	107.282
	B5	25.0114	100.376	3.2376	105.062
	B6	25.0084	100.364	3.1973	103.755
	B7	25.0029	100.342	3.1655	102.723
Fins with winglet	W1	24.9672	100.199	3.3086	107.366
	W2	24.9767	100.237	3.4191	110.952
	W3	24.9912	100.295	3.4521	112.023
	W4	25.0004	100.332	3.3588	108.995
	W5	24.9951	100.311	3.2494	105.445
	W6	24.9904	100.292	3.2063	104.047
	W7	24.9731	100.223	3.1751	103.034
Fins with imprint	I2	25.0339	100.467	3.3565	108.921
	I3	25.0496	100.530	3.3799	109.680
	I4	25.0527	100.542	3.3438	108.509
	I5	25.0476	100.522	3.2707	106.136
	I6	25.0346	100.470	3.2269	104.715

The best protrusion location for all protrusion types is determined as location 4 in terms of heat transfer performance since the maximum heat transfer value can be obtained when protrusion is placed at location 4. This result stems from the fact that the flue gas is better directed to the fin tube when the protrusion is present at this location. Another conclusion is that fins with imprint type protrusion give better heat transfer performance than the fins with balcony or imprint type protrusions. It is also observed that the pressure drop values are the highest when protrusions are placed at location 3, which coincides to the center of fin tube. At location 3, the flue gas flow area takes its minimum value, so the pressure drop value increase can be explained with this flow area reduction.

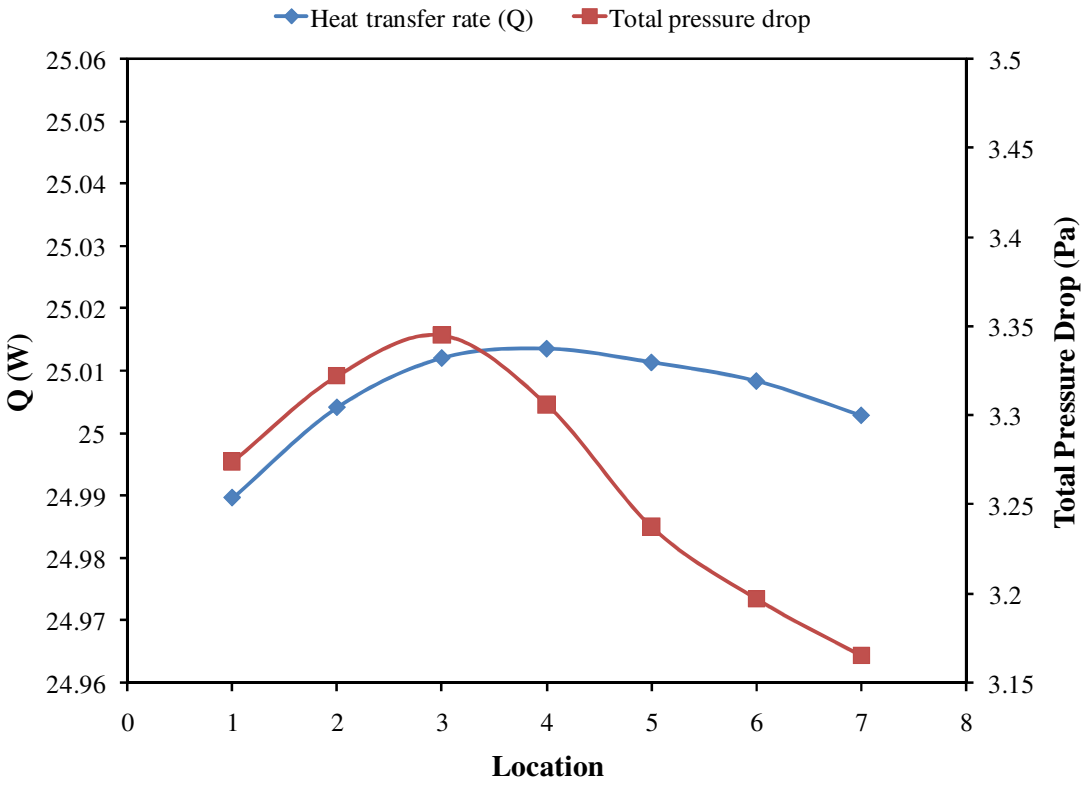

Figure 8.42. The effect of balcony location on heat transfer and total pressure drop.

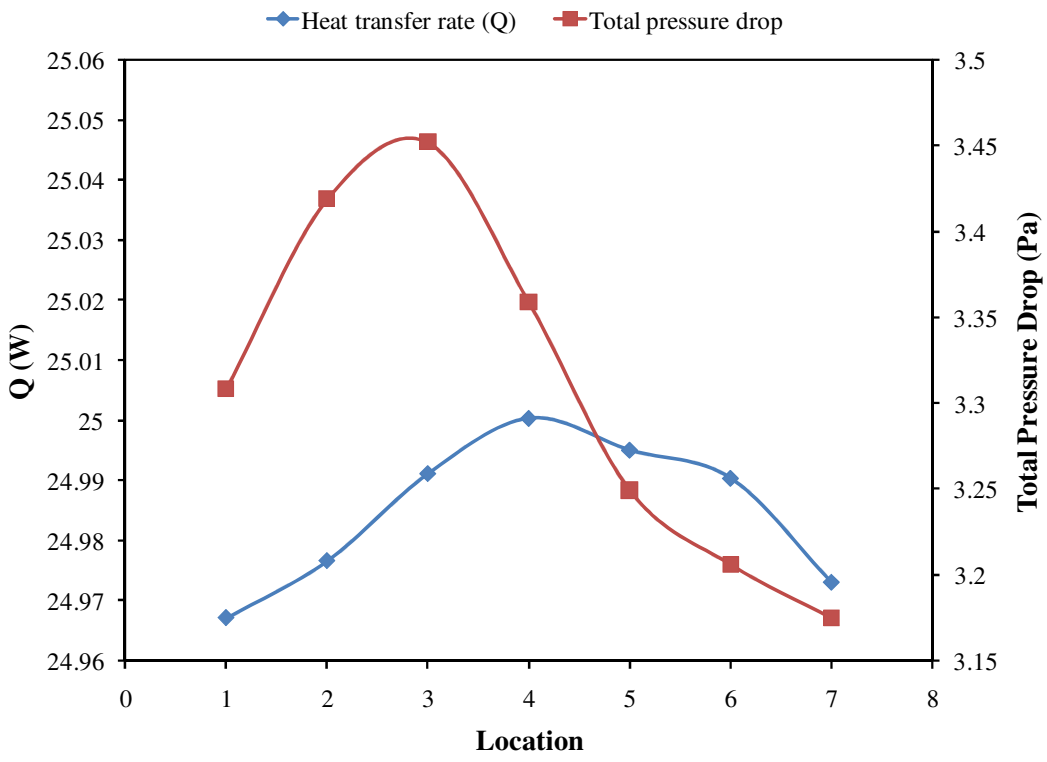

Figure 8.43. The effect of winglet location on heat transfer and total pressure drop.

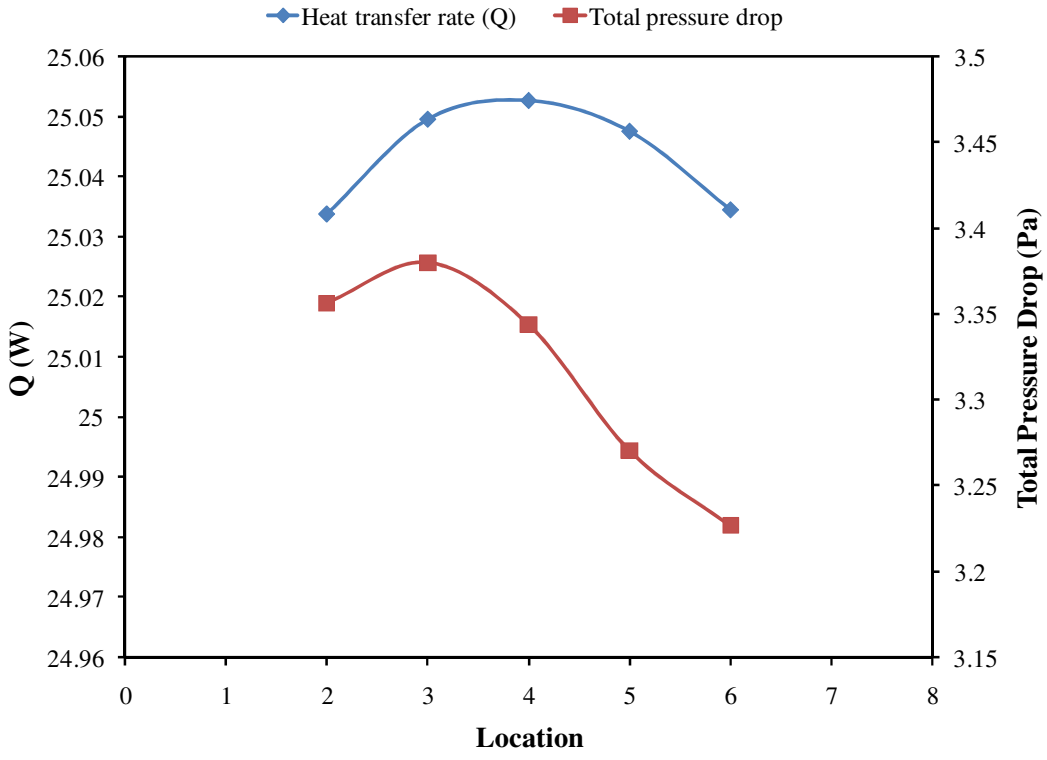

Figure 8.44. The effect of imprint location on heat transfer and total pressure drop.

8.2.7. Use of Three Different Protrusions Together

The individual effects of plate fin geometry and protrusion dimensions and location on fin are analyzed step by step in the above sections of the study. The best fin found in the previous section is used to continue the next step of the study. Finally, the best fins with only one protrusion are determined as the fins B4, W4 and I4. However, the case for which the three protrusions are placed on the plane fin surface at the same time needs also to be investigated. In this way, the cumulative effect of three protrusions will be revealed. So, it is decided to try some combinations of protrusion placement on the plate fin. Since the biggest increase for heat transfer is obtained from the imprint type protrusion, the cases when it is placed at location 2,3,4,5 and 6 are investigated. The placement of the other protrusions is decided according to the results obtained in the previous sections. The fins with three different protrusions investigated in this part of the study are presented in Table 8.24 and a view of the fin I5B2W3 is given in Figure 8.45 as an illustration.

Table 8.24. Protrusion placement on the fins with three different protrusions.

Model Name	Balcony Location	Winglet Location	Imprint Location
I2B4W5	4	5	2
I2W4B5	5	4	2
I3B5W6	5	6	3
I3W5B6	6	5	3
I4B2W6	2	6	4
I4W2B7	7	2	4
I5B2W3	2	3	5
I5W2B3	3	2	5
I6B3W4	3	4	6
I6W3B4	4	3	6

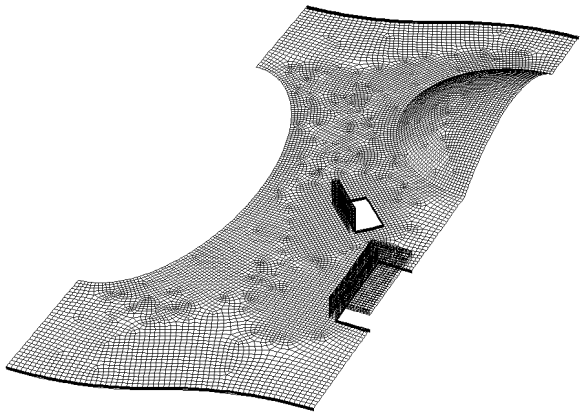

Figure 8.45. A view of the fin I5B2W3.

The ten different fins with three different types of protrusions are modeled and numerical solution of heat transfer and fluid flow problems are obtained using Fluent software. The results of numerical analysis are given in Table 8.25. The comparison with the plate fin wavy-d2mm is also made in this section.

Table 8.25. Heat transfer and pressure drop values of fins with three different protrusions.

Model Name	Q (Per segment) (W)	Normalized Q (%)	Total Pressure Drop (Pa)	Normalized Total Pressure Drop (%)
wavy-d2mm	24.9176	100	3.0816	100
I2B4W5	25.1973	101.122	3.7878	122.917
I2W4B5	25.2284	101.247	3.8385	124.562
I3B5W6	25.1806	101.055	3.6812	119.457
I3W5B6	25.1982	101.126	3.6804	119.431
I4B2W6	25.1570	100.961	3.7099	120.389
I4W2B7	25.1922	101.102	3.7642	122.151
I5B2W3	25.2396	101.292	3.9971	129.709
I5W2B3	25.1987	101.128	3.9220	127.272
I6B3W4	25.2212	101.218	3.8469	124.835
I6W3B4	25.1900	101.093	3.8907	126.256

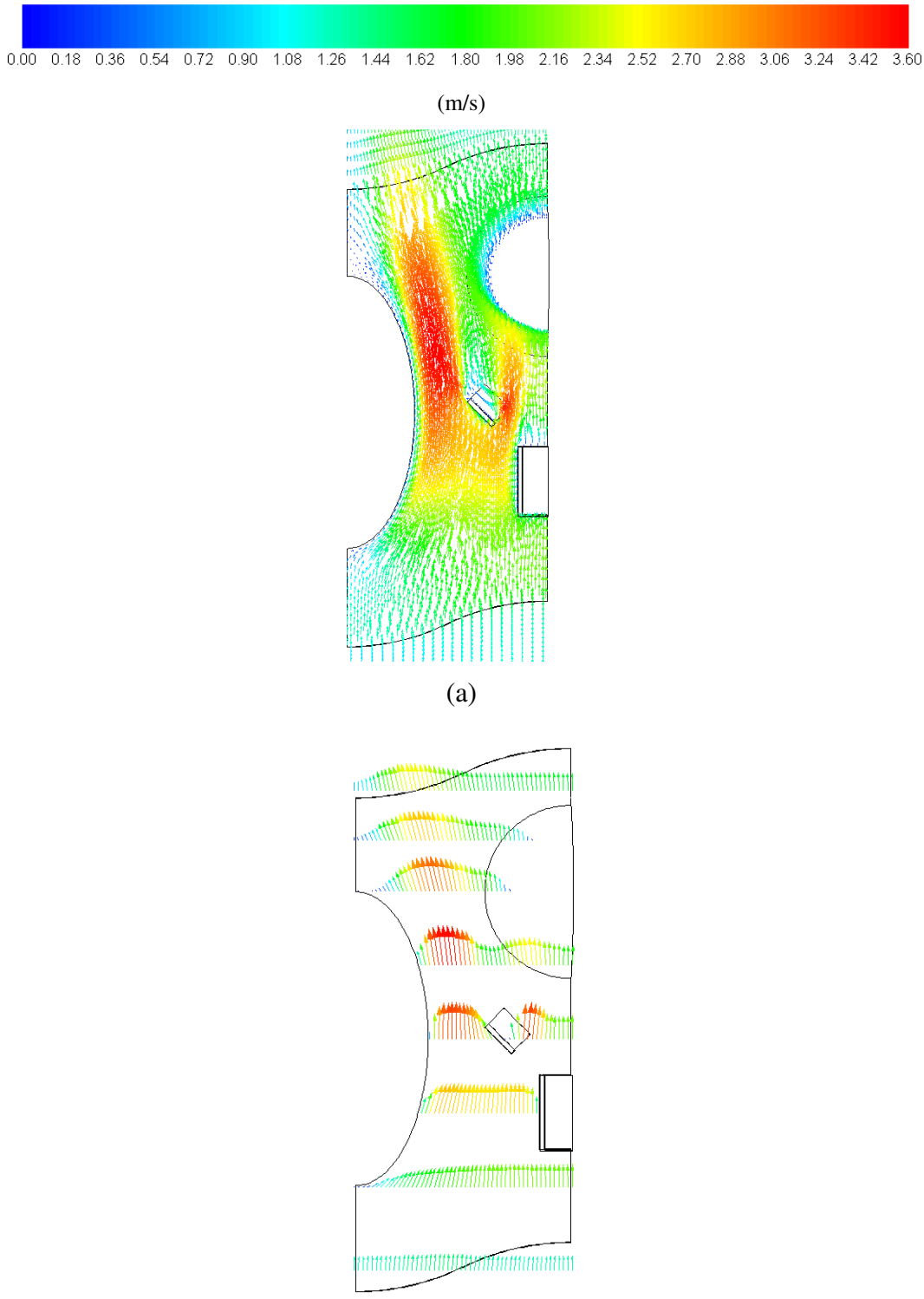

Figure 8.46. Velocity vectors for the model I5B2W3 (a) at the middle plane of the gap between two fins (b) at various levels at the middle plane of the gap between two fins.

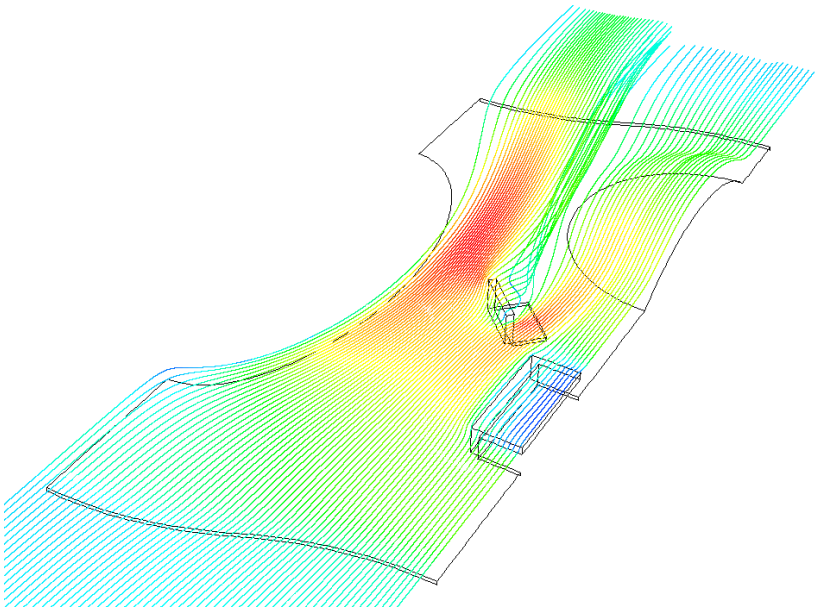

Figure 8.47. Pathlines released from the inlet of the flue gas at the middle plane of the gap between two fins for the model I5B2W3.

The velocity vectors and the pathlines released from the inlet of flue gas at the middle plane of the gap between two fins for the model I5B2W3, which gives the best heat transfer performance, is presented in Figure 8.46 and 8.47, respectively.

It can be observed from Figure 8.46 that the flue gas flow acceleration with the use of three protrusions together is higher compared to the case of only one protrusion usage. In addition, the flue gas flow path is longer. Consequently, higher heat transfer results are obtained when three protrusions are placed on the plate fin at the same time.

When the numerical results of the final section of the study are investigated, it is seen that the placement of balcony at location 2, imprint at location 3 and imprint at location 5 is the best combination in terms of heat transfer performance. This configuration gives 1.292 % more heat transfer value compared to the plate fin with the same geometrical dimensions (wavy-d2mm). Besides this increase in heat transfer, the fin I5B2W3 also causes a 29.709% higher total pressure drop compared to the fin wavy-d2mm. If we compare the fin I5B2W3 with the fin whose heat transfer performance is the worst (the fin c-12.5mm, with a cylindrical fin tube, L= 40 mm and L_1=12.5 mm), it is seen that the fin I5B2W3 provides a heat transfer increase of 3.607 % and a total pressure increase of 1.012 %. The numerical optimization of a fin-tube type heat exchanger in the chosen geometrical ranges is completed with this final study and the best fin is determined as the fin I5B2W3 with the following geometrical dimensions.

Table 8.26. The geometrical dimensions of the fin I5B2W3.

Fin height (L)	40 mm	Balcony length (Lb)	1.5 mm
Fin tube location (L_1)	18.5 mm	Winglet length (Lw)	1.8 mm
Fin tube ellipticity (b/a)	0.45	Imprint length (Li)	2.425 mm
Wave height (d)	2 mm	Balcony location	2
Balcony height (h)	3 mm	Winglet Location	3
Winglet width (w)	3 mm	Imprint Location	5
Imprint radius (r)	7 mm		

8.3. Numerical Investigation with the Models with Periodic Boundary Condition

After the completion of the numerical investigation with the models with symmetry boundary condition, the comparison of the models with symmetry and periodic boundary conditions is accomplished. For this purpose the numerical results obtained from Fluent software for the models I5B2W3, I2W4B5 and I6B3W4 are compared for the two cases. These three models are selected for comparison, because they are the best three fins according to the results obtained for the case with symmetry boundary condition. The results are tabulated in Table 8.27.

It can be seen from Table 8.27 that the results of the models with both boundary conditions are very close. The difference for heat transfer is observed as about 0.05 % maximum, and the difference for total pressure drop values is about 0.23 % maximum. It is concluded that the modeling using either boundary condition do not affect the numerical results significantly and the results obtained in the previous sections are reliable.

Table 8.27. Comparison of the models with symmetry and periodic boundary conditions.

	Symmetry Boundary Condition	Periodic Boundary Condition		Symmetry Boundary Condition	Periodic Boundary Condition	
Model Name	Q (Per segment) (W)		Difference (%)	Total Pressure Drop (Pa)		Difference (%)
I2W4B5	25.2284	25.2198	0.0341	3.8385	3.8429	0.1146
I5B2W3	25.2396	25.2270	0.0499	3.9971	4.0062	0.2277
I6B3W4	25.2212	25.2111	0.0400	3.8469	3.8549	0.2080

CHAPTER 9

CONCLUSIONS

In this thesis, the optimization of the fin and protrusion geometries of a finned tube heat exchanger is performed. Additionally, the best location of the protrusions on the plate fin surface is determined. The heat transfer and pressure drop performances of heat exchangers with different fins are determined numerically using Fluent computational fluid dynamics software. The fin dimensions used in the study are selected in the range of practical application values. For this purpose, the dimensions used for a commercial combi boiler heat exchanger are taken as the basic dimensions and changes are made in the practical application ranges. The investigated parameters of the plate fin geometry are; fin height and fin tube thickness, fin tube location and ellipticity, fin shape (waviness). Furthermore, three different protrusions are examined in the study. These are balcony, winglet and imprint type protrusions. The individual as well as cumulative effects of these three different protrusions on the heat transfer and pressure drop characteristics of the finned tube heat exchanger are also investigated numerically. The parameters examined for protrusions can be summarized as; protrusion height, width and radius, protrusion length between two fins and protrusion location on fin. The numerical analyses are performed using boundary conditions which are taken from the actual operating conditions of the combi boiler heater taken as the practical model for the present study. The use of the actual operating conditions for the present study and the investigation of three different protrusions on a plate fin are the novelties of this thesis. A comparison of the computational models used for the numerical investigations of various fins is also made with a computational and experimental study available in literature. Since no other study investigating fins with the same geometrical dimensions as the fins used in the present study is encountered in the literature, and most of the studies do not provide their boundary or experimental conditions clearly, a similar study performed by Wu and Tao (2008b) is used for comparison. The fins of the study of Wu and Tao (2008b), in which the effects of a winglet pair on heat transfer are investigated numerically and experimentally, are analysed numerically in order to accomplish validation of the current study. As a result, good agreement between the results obtained from Fluent software and the

computational and experimental results reported in Wu and Tao (2008b) is observed. It is concluded that, since in the present parametric study finer meshes than the ones used in the comparison part with the study of Wu and Tao (2008b), are employed, the results obtained from the computational models used in the numerical analyses of the fins in the present study are reliable.

The results of the parametric study about plate fin geometry indicate that a plate fin with a fin height value of 40 mm, a fin tube thickness value of 0.6 mm, a fin tube, placed at a 18.5 mm away from the bottom point of the fin, with an ellipticity value of 0.45 and a wave height of 2 mm provides the best performance. The parametric study about the protrusions reveals that the balcony with a 3 mm height and a 1.5 mm length in the gap between two fins, the winglet with a 3 mm width and a 1.8 mm length in the gap between two fins and the imprint with a 7 mm radius and a 2.425 mm length in the gap between two fins are the best ones among the investigated cases. The best location of each protrusion on the fin surface is found as location 4 shown in Figure 3.6. Finally, the investigation of the cumulative effect of three protrusions shows that the use of three protrusions provides better heat transfer performance compared to the case with only one protrusion. However, a pressure drop increase is also observed with the use of three protrusions together. The best fin is determined as I5B2W3 according to the obtained numerical results and the optimization study is concluded with this outcome.

The two modeling alternative for the numerical analyses are also compared. Symmetrical boundary condition is used for one of the alternatives while periodic boundary condition is used for the other alternative. The models of three different fins with three protrusions (I2W4B5, I5B2W3 and I6B3W4) are created for these two alternatives and the numerical results are compared. The selection of these three fins is made according to the results found from the models created with symmetrical boundary condition. The mentioned three fins are the best three fins among the investigated ones according to the numerical results. It is observed that the heat transfer value difference between the models of two alternatives is 0.05 % maximum and the total pressure drop value difference reaches at 0.23 % maximum. It is concluded that the two modeling alternatives lead to very close results and the results obtained with the models with symmetrical boundary condition are reliable.

REFERENCES

Abu Madi, M., Johns, R.A., Heikal, M.R. 1998. Performance characteristics correlation for round tube and plate finned heat exchangers. *International Journal of Refrigeration* 21 (7) : 507-517.

Allison, C.B. and Dally, B.B. 2007. Effect of a delta-winglet vortex pair on the performance of a tube-fin heat exchanger. *International Journal of Heat and Mass Transfer* 50 : 5065-5072.

Alpha Heat Transfer & Allied Services. 2008. http://alphaheatspares.com/ images/pro_PHE1.gif. (accessed July 23, 2008).

Ay, H., Jang, J.Y., Yeh, J.-N. 2002. Local heat transfer measurements of plate finned-tube heat exchangers by infrared thermography. *International Journal of Heat and Mass Transfer* 45 : 4069-4078.

Bird R.B., Stewart W.E., Lightfoot E.N., eds. 1960. *Transport Phenomena*. New York: John Wiley & Sons Inc.

Burr Oak Tool Incorporation. 2008. http://www.burroak.com/files/images/Die_06.jpg (accessed August 7, 2008).

Chen, Y., Fiebig, M., Mitra, N.K. 1998. Heat transfer enhancement of a finned oval tube with punched longitudinal vortex generators in-line. *International Journal of Heat and Mass Transfer* 41: 4151-4166.

Chen, Y., Fiebig, M., Mitra, N.K. 2000. Heat transfer enhancement of finned oval tubes with staggered punched longitudinal vortex generators. *International Journal of Heat and Mass Transfer* 43 : 417-435.

Chen, T.Y. and Shu, H.T. 2004. Flow structures and heat transfer characteristics in fan flows with and without delta-wing vortex generators. *Experimental Thermal and Fluid Science* 28 : 273-282.

Chen, H.-T., Song, J.-P., Wang, Y.-T. 2005. Prediction of heat transfer coefficient on the fin inside one-tube plate finned-tube heat exchangers. *International Journal of Heat and Mass Transfer* 48 : 2697-2707.

Chu, P., He, Y.L., Lei, Y.G., Tian, L.T., Li, R. 2008. Three-dimensional numerical study on fin-and-oval-tube heat exchanger with longitudinal vortex generators. *Applied Thermal Engineering* doi: 10.1016/j.applthermaleng.2008.04.021.

Chung, T.J. 2002. *Computational fluid dynamics.* Cambridge: Cambridge University Press.

Date, A.W. 2005. *Introduction to computational fluid dynamics.* New York: Cambridge University Press.

Elyyan, M.A., Rozati, A., Tafti, D.K. 2008. Investigation of dimpled fins for heat transfer enhancement in compact heat exchangers. *International Journal of Heat and Mass Transfer* 51 : 2950-2966.

Erek, A., Özerdem, B., Bilir, L., İlken, Z. 2005. Effect of geometrical parameters on heat transfer and pressure drop characteristics of plate fin and tube heat exchangers. *Applied Thermal Engineering* 25 : 2421-2431.

Fluent Incorporation, 2006. *Fluent 6.3. User's Guide*. Canterra Resource Park 10 Cavendish Court Lebanon: Fluent Inc.

GB Coil Incorporation. 2008. http://www.gbcoil.com/images/12%20fin%20copy.JPG (accessed August 7, 2008)

Gentry, M.C. and Jacobi A.M. 1997. Heat transfer enhancement by delta-wing vortex generators on a flat plate: vortex interactions with the boundary layer. *Experimental Thermal and Fluid Science* 14 : 231-242.

Hesselgreaves, J.E. 2001. *Compact heat exchangers. Selection, design and operation.* Oxford: Pergamon, Elsevier Science Ltd.

Hiravennar, S.R., Tulapurkara, E.G., Biswas, G. 2007. A note on the flow and heat transfer enhancement in a channel with built-in winglet pair. *International Journal of Heat and Fluid Flow* 28 : 299-305.

Joardar, A. and Jacobi, A.M. 2005. Impact of leading edge delta-wing vortex generators on the thermal performance of a flat tube, louvered-fin compact heat exchanger. *International Journal of Heat and Mass Transfer* 48 : 1480-1493.

Joardar, A. and Jacobi, A.M. 2008. Heat transfer enhancement by winglet-type vortex generator arrays in compact plain-fin-and-tube heat exchangers. *International Journal of Refrigeration* 31 : 87-97.

Kakaç S. and Yener Y., eds. 1995. *Convective Heat Transfer*. Boca Raton, Florida, USA: CRC Press, Begell House.

Kakaç, Sadık and Liu, Hongtan, eds. 2002. *Heat exchangers selection, rating and thermal design.* Boca Raton, Florida: CRC Press.

Kim, E. and Yang, J.S. 2002. An experimental study of heat transfer characteristics of a pair of longitudinal vortices using color capturing technique. *International Journal of Heat and Mass Transfer* 45 : 3349-3356.

Kim., J.-Y. and Song, T.-H. 2002. Microscopic phenomena and macroscopic evaluation of heat transfer from plate fins/circular tube assembly using naphthalene sublimation technique. *International Journal of Heat and Mass Transfer* 45 : 3397-3404.

Kim, M.-H. and Bullard, C.W. 2002. Air-side thermal hydraulic performance of multi-louvered fin aluminum heat exchangers. *International Journal of Refrigeration* 25 : 390-400.

Kim, K.-Y. and Shin, D.-Y. 2007. Optimization of a staggered dimpled surface in a cooling channel using Kriging model. *International Journal of Thermal Sciences* doi:10.1016/ j.ijthermalsci.2007.12.011.

Kundu, B. and Das, P.K. 1997. Optimum dimensions of plate fins for fin-tube heat exchangers. *International Journal of Heat and Fluid Flow* 18 : 530-537.

Kwak, K.M., Torii, K., Nishino, K. 2003. Heat transfer and pressure loss penalty for the number of tube rows of staggered finned-tube bundles with a transverse row of winglets. *International Journal of Heat and Mass Transfer* 46 : 175-180.

Kwak, K.M., Torii, K., Nishino, K. 2005. Simultaneous heat transfer enhancement and pressure loss reduction for finned-tube bundles with the first or two transverse rows of built-in winglets. *Experimental Thermal and Fluid Science* 29 : 625-632.

Lawson M.J. and Thole K.A. 2008. Heat transfer augmentation along the tube wall of a louvered fin heat exchanger using practical delta winglets. *International Journal of Heat and Mass Transfer* 51 : 2346-2360.

Leu, J.-S., Wu, Y.-H., Jang, J.-Y. 2004. Heat transfer and fluid flow analysis in plate-fin and tube heat exchangers with a pair of block shape vortex generators. *International Journal of Heat and Mass Transfer* 47 : 4327-4338.

Lienhart, H., Breuer, M., Köksoy, C. 2008. Drag reduction by dimples? – A complementary experimental/numerical investigation. *International Journal of Heat and Fluid Flow* 29 : 783-791.

Ligrani, P.M., Mahmood, G.I., Harrison, J.L., Clayton, C.M., Nelson, D.L. 2001. Flow structure and local Nusselt number variations in a channel with dimples and protrusions on opposite walls. *International Journal of Heat and Mass Transfer* 44 : 4413-4425.

Lomax, H., Pulliam, T.H., Zingg, D.W., eds. 1999. *Fundamentals of computational fluid dynamics.* Nasa Ames Research Center.

Lozza, G. and Merlo, U. 2001. An experimental investigation of heat transfer and friction losses of interrupted and wavy fins for fin-and-tube heat exchangers. *International Journal of Refrigeration* 24 : 409-416.

Löhner, R. 2008. *Applied computational fluid dynamics techniques. An introduction based on finite element methods.* Chichester, West Sussex: John Wiley&Sons Inc.

Mahmood, G.I. and Ligrani, P.M. 2002. Heat transfer in a dimpled channel: combined influences of aspect ratio, Reynolds number, and flow structure. *International Journal of Heat and Mass Transfer* 45 : 2011-2020.

Matos, R.S., Vargas, J.V.C., Laursen, T.A., Saboya, F.E.M. 2001. Optimization study and heat transfer comparison of staggered circular and elliptic tubes in forced convection. *International Journal of Heat and Mass Transfer* 44 : 3953-3961.

Mendez, R.R., Sen, M., Yang, K.T., McClain, R. 2000. Effect of fin spacing on convection in a plate fin and tube heat exchanger. *International Journal of Heat and Mass Transfer* 43 : 39-51.

Pesteei, S.M., Subbararo, P.M.V., Agarwal, R.S. 2005. Experimental study of the effect of winglet location on heat transfer enhancement and pressure drop in fin-tube heat exchangers. *Applied Thermal Engineering* 25 : 1684-1696.

Pirompugd, W., Wongwises, S., Wang, C.-C. 2006. Simultaneous heat and mass transfer characteristics for wavy fin-and-tube heat exchangers under dehumidifying conditions. *International Journal of Heat and Mass Transfer* 49 : 132-143.

Rocha, L.A.O., Saboya, F.E.M., Vargas, J.V.C. 1997. A comparative study of elliptical and circular sections in one- and twrow tubes and plate fin heat exchangers. *International Journal of Heat and Fluid Flow* 18 : 247-252.

Saboya, S. and Saboya, F.E.M. 2001. Experiments on elliptic sections in one- and two-row arrangements of plate fin and tube heat exchangers. *Experimental Thermal and Fluid Science* 24 : 67-75.

SEC Heat Exchangers. 2008. http://www.secshellandtube.com/ images/st-pic2x400-index.jpg. (accessed July 23, 2008).

Shah, Ramesh K. and Sekulic, Dusan P., eds. 2003. *Fundamentals of heat exchanger design.* New Jersey: John Wiley & Sons Inc.

Shaw, C.T. 1992. *Using computational fluid dynamics.* New York: Prentice Hall.

Sohankar, A. 2007. Heat transfer augmentation in a rectangular channel with a vee-shaped vortex generator. *International Journal of Heat and Fluid Flow* 28 : 306-317.

Sommers, A.D. and Jacobi, A.M. 2005. Air-side heat transfer enhancement of a refrigerator evaporator using vortex generation. *International Journal of Refrigeration* 28 : 1006-1017.

Tiwari, S., Maurya, D., Biswas, G., Eswaran, V. 2003. Heat transfer enhancement in cross-flow heat exchangers using oval tubes and multiple delta winglets. *International Journal of Heat and Mass Transfer* 46 : 2841-2856.

Torii, K., Kwak, K.M., Nishino, K. 2002. Heat transfer enhancement accompanying pressure-loss reduction with winglet-type vortex generators for fin-tube heat exchangers. *International Journal of Heat and Mass Transfer* 45 : 3795-3801.

Tutar, M. and Akkoca, A. 2004. Numerical analysis of fluid flow and heat transfer characteristics in three-dimensional plate fin-and-tube heat exchangers. *Numerical Heat Transfer, Part A* 46 : 301-321.

Versteeg, H.K. and Malalasekera, W., eds. 1995. *An introduction to computational fluid dynamics The finite volume method.* London: Longman Group Ltd.

Wang, C.C., Fu, W.L., Chang, C.T. 1997. Heat transfer and friction characteristics of typical wavy fin-and-tube heat exchangers. *Experimental Thermal and Fluid Science* 14 : 174-186.

Wang, C.-C. and Chi, K.-Y. 2000. Heat transfer and friction characteristics of plain fin-and-tube heat exchangers, part I: new experimental data. *International Journal of Heat and Mass Transfer* 43 : 2681-2691.

Wang, C.-C., Chi, K.-Y., Chang, C.-J. 2000. Heat transfer and friction characteristics of plain fin-and-tube heat exchangers, part II: correlation. *International Journal of Heat and Mass Transfer* 43 : 2693-2700.

Wang, C.-C., Lo, J., Lin, Y.-T., Liu, M.-S. 2002a. Flow visualization of wave-type vortex generator having inline fin-tube arrangement. *International Journal of Heat and Mass Transfer* 45 : 1933-1944.

Wang, C.-C., Lo, J., Lin, Y.-T., Wei, C.-S. 2002b. Flow visualization of annular and delta winlet vortex generators in fin-and-tube heat exchanger application. *International Journal of Heat and Mass Transfer* 45 : 3803-3815.

White F.M., eds. 1999. *Fluid Mechanics*. Singapore, WCB/McGraw-Hill.

Wikimedia. 2008a. http://upload.wikimedia.org/wikipedia/commons/5/59/ Straight-tube_heat_exchanger_2-pass.PNG. (accessed July 23, 2008)

Wikimedia.2008b.http://images.google.com.tr/imgres?imgurl=http://upload.wikimedia.org/wikipedia/commons/7/79/Rotary_heat_exchanger.png&imgrefurl=http://commons.wikimedia.org/wiki/Image:Rotary_heat_exchanger.png&h=1150&w=1080&sz=45&hl=tr&start=3&um=1&usg=__6rdt3DmHM3KWfJyVdKcQGuJuO3Q=&tbnid=9yxnAU1N84Mv4M:&tbnh=150&tbnw=141&prev=/images%3Fq%3D%2522rotary%2522%252B%2522heat%2Bexchanger%2522%26ndsp%3D20%26um%3D1%26hl%3Dtr%26safe%3Doff%26sa%3DN. (accessed August 7, 2008)

Wu, J.M. and Tao W.Q. 2008a. Numerical study on laminar convective heat transfer in a channel with longitudinal vortex generator. Part A: Verification of field synergy principle. *International Journal of Heat and Mass Transfer* 51 : 1179-1191.

Wu, J.M. and Tao W.Q. 2008b. Numerical study on laminar convective heat transfer in a channel with longitudinal vortex generator. Part B: Parametric study of major influence factors. *International Journal of Heat and Mass Transfer* 51 : 3683-3692.

Yan, W.-M. and Sheen, P.-J. 2000. Heat transfer and friction characteristics of fin-and-tube heat exchangers. *International Journal of Heat and Mass Transfer* 43 : 1651-1659.

VITA

Levent BİLİR

Date and Place of Birth: 22/01/1977, İzmir

Research Areas:
- Computational Fluid Dynamics
- Heat Energy Storage (Heat Transfer with Phase Change)
- Numerical Methods in Heat Transfer

Education:
- **Ph.D.** (2003 – 2009)
  İzmir Institute of Technology, Mechanical Engineering Department
- **M. Sc.** (2000 – 2003)
  İzmir Institute of Technology, Mechanical Engineering Department
  M. Sc. Thesis Title: Estimation of the Total Solidification Time of a Liquid Phase Change Material Enclosed in Cylindrical and Spherical Containers
- **B. Sc.** (1995 – 1999)
  Dokuz Eylül University, Mechanical Engineering Department (finished in second place among the graduates)
  B. Sc. Thesis Title: Buz Pateni Sahalarının Soğutma Yükü Hesabı ve Soğutma Tesisatının Tasarlanması, in Turkish

Experience:
- Research Assistant (2000 – 2009), İzmir Institute of Technology, Mechanical Engineering Department, Urla- İZMİR

Publications:
- **International Journal Papers**

1) **Bilir**, **L.**, İlken, Z. 2005. Total solidification time of a liquid phase change material enclosed in cylindrical/spherical containers. *Applied Thermal Engineering* 25 : 1488-1502.
2) Erek, A., Özerdem, B., **Bilir**, **L.**, İlken, Z. 2005. Effect of geometrical parameters on heat transfer and pressure drop characteristics of plate fin and tube heat exchangers. *Applied Thermal Engineering* 25 : 2421-2431.
3) Alpay, S.**, Bilir, L.**, Ozdemir, S., Ozerdem, B. 2006. Wind speed time series characterization by Hilbert transform. *International Journal of Energy Research* 30 (5) : 359-364.

- **International Conference and Symposium Papers**

1) Alpay, S., **Bilir**, **L.**, Ozdemir, S., Ozerdem, B. 14-16 July 2004 (Nevşehir, Turkey). Estimation of wind speed in Urla district via Hilbert transforms. *1st Cappadocia International Mechanical Engineering Symposium Book* 244-247.
2) **Bilir**, **L.**, Alpay, S., Ozdemir, S. 6-8 September 2004 (Sakarya, Turkey). Study of population of heterogeneous individuals. *4th International Symposium on Intelligent Manufacturing Systems (IMS'2004), Symposium Book.*
3) **Bilir L.**, Ozerdem B., İlken Z. 22-24 June 2005 (Budapest, Hungary). The effect of tube location and ellipticity in plate fin-tube heat exchangers. *14th Conference on Thermal Engineering and Thermogrammetry (THERMO) Conference Book.*